Department of Geography
University of Zurich

GEO 511 Master Thesis

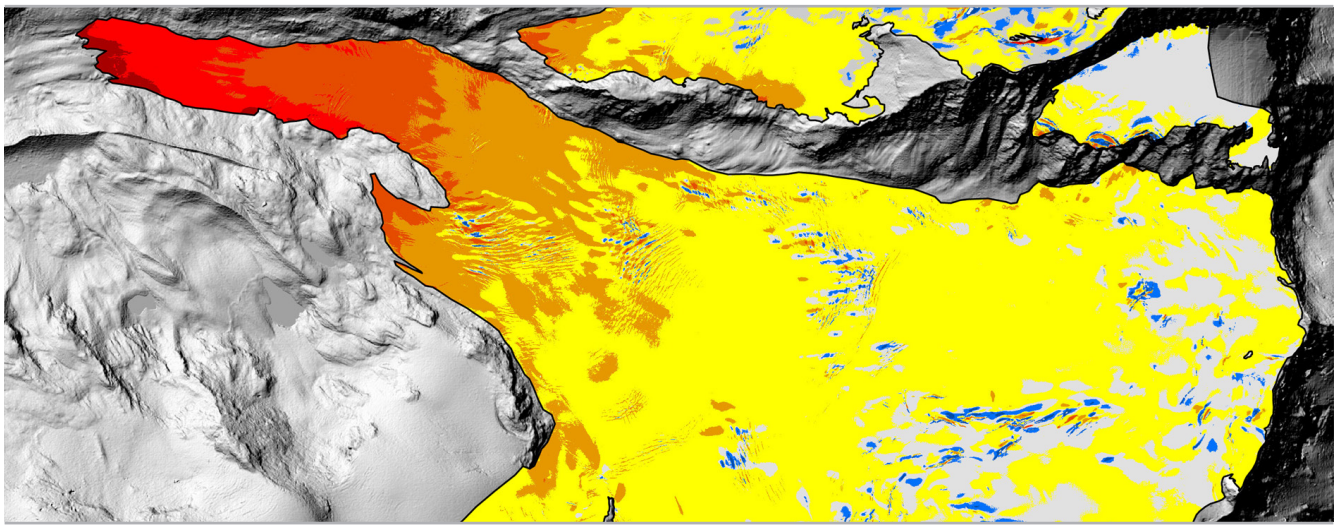

Evaluation of swissALTI^{3D} with airborne laser scanning data for applications in glaciology

A case study on glaciers in the upper Mattertal, Switzerland

Thierry Bossard
07-704-224

Advisor:	PD Dr. Michael Zemp[1]
Co-Advisor:	Philip Claudio Joerg[1]
Co-Advisor:	Roberto Artuso[2]
Co-Advisor:	Dr. Tobias Kellenberger[2]
Faculty Member:	Prof. Dr. Andreas Vieli[1]
Submission Date:	30. April 2014

[1] Department of Geography, University of Zurich
[2] Federal Office of Topography swisstopo, Seftigenstrasse 264, 3084 Wabern (roberto.artuso@swisstopo.ch / tobias.kellenberger@swisstopo.ch)

Acknowledgement

First of all, I would like to thank my advisors without whom this master's thesis would not have been realized. Michael Zemp and Philip Claudio Joerg always provided me with valuable support concerning conceptual and technical issues. Thereby, they formed a much appreciated first point of contact with numerous precious inputs and advices.

Cordial thanks also go to Roberto Artuso and Tobias Kellenberger for the confidence and effort from the side of swisstopo. Without the generation of the photogrammetrical digital elevation model from September 29, 2010 by Roberto Artuso, this thesis would not have been possible to the same extent.

In addition I would like to thank Ronald Schmidt, for his effort and the useful suggestions to deal with digital elevation models, and Philipp Rastner for the dissemination of the co-registration file and tutorial.

My thanks also go to Prof. Dr. Andreas Vieli, for the faculty representation and the initial acceptance of the topic of this master's thesis.

My academic studies at the University of Zurich would not be imaginable without the support of my parents. Thank you for the generosity and patience you have shown throughout all of these years. Thank you KaLö for proofreading my thesis.

Last but not least, I thank my girlfriend for her dedicated engagement.

Summary

By means of the geodetic method, glaciological changes from the differencing of multi-temporal digital elevation models (DEMs) can be calculated. Widely used techniques to derive DEMs are the stereo correlation of photogrammetrically recorded aerial images and airborne laser scanning. Photogrammetrically derived DEMs have limitations in areas of shadow and low contrast (e.g. snow), where less corresponding points for the cross-correlation calculations are availabe, which leads to a reduction of the elevation data accuracy.

The present master's thesis validates DEMs of high-alpine regions in the upper Mattertal, Switzerland, which were measured with the above mentioned acquisition methods. The objective of this master's thesis is the quantification of the glaciological changes in the upper Mattertal from 2005 to 2009 with the main focus on the uncertainty assessment of the compared DEMs. Additionally, the suitability of swissALTI^{3D}, the new reference DEM of Switzerland, for applications in glaciology is evaluated.

Since the data source of this master's thesis consists of DEMs from exactly the same day, a direct comparison of the performance of the two acquisition techniques not only over unglaciated but also over glaciated terrain is enabled. In order to reduce horizontal shifts between the DEMs and to estimate the systematic uncertainties, a co-registration (Nuth and Kääb, 2011) is performed. After that, the elevation data accuracies of areas with snow and shadow are compared between the photogrammetrical and the laser scaning DEMs. For the estimation of the zonal, stochastic uncertainties a new method is presented in this thesis, which considers the influence of shadow on the elevation data accuracy. From the differencing of the DEMs, the glaciological changes are then calculated.

The results of the present master's thesis indicate a glacier retreat from 2005 to 2009 in the upper Mattertal. The glacier area decreased on average by -5.56% per glacier. The average thickness change of all investigated glaciers in the upper Mattertal amounts to -3.17 $\pm$0.037 m and the total volume loss to -351.09 $\pm$0.144 mio m^3. The co-registration proves to be a useful method to detect horizontal shifts and to estimate systematic elevation biases between DEMs. Without taking account of these, the glaciological changes would be considerably overestimated. The evaluation of the simultaneously measured DEMs yields that photogrammetry still has limitations in areas of shadow and low contrast. It can be shown that areas under cast shadow have larger elevation differences between photogrammetry and laser scanning than non-shady areas.

In comparison with other studies, the glacier changes derived from swissALTI^{3D}, show under consideration of systematic and stochastic uncertainties, good agreement with the glaciological changes derived from airborne laser scanning.

swissALTI^{3D} with its high resolution and the continuous updates, is therefore very well suited for applications in glaciology.

Zusammenfassung

Mittels geodätischer Methode lassen sich Gletscheränderungen aus der Differenz von digitalen Höhenmodellen (DHMs) von verschiedenen Zeitpunkten berechnen. Die am meisten verwendeten Techniken zur Erstellung von DHMs sind die Stereokorrelation von photogrammetrisch erzeugten Luftbildern und das flugzeuggetragene Laserscanning. Photogrammetrisch erzeugte DHMs haben den Nachteil, dass in Gebieten mit Schatten und vermindertem Kontrast (z.B. Schnee) weniger korrespondierende Bildpunkte für die Stereokorrelation vorhanden sind, was zu einer Abnahme der Höhengenauigkeit führt.

Die vorliegende Masterarbeit validiert DHMs in hochalpinen Gebieten im oberen Mattertal, Schweiz, welche mit den obengenannten Aufnahmesystemen gemessen wurden. Das Ziel dieser Masterarbeit ist die Quantifizierung der Gletscheränderungen im oberen Mattertal von 2005 bis 2009 mit dem Hauptfokus auf der Unsicherheitsanalyse der verglichenen DHMs. Zudem wird die Eignung von swissALTI^{3D}, dem neuen Referenzhöhenmodell der Schweiz, für glaziologische Anwendungen abgeklärt.

Da die Datengrundlage dieser Masterarbeit aus DHMs vom exakt gleichen Tag besteht, ist ein direkter Vergleich der beiden Aufnahmemethoden nicht nur über unvergletscherten sondern auch über vergletscherten Gebieten möglich. Um horizontale Verschiebungen zwischen den DHMs zu vermindern und die systematischen Unsicherheiten der Höhendaten abzuschätzen, wird vorweg eine Co-registrierung nach Nuth and Kääb (2011) durchgeführt. Danach werden die Höhengenauigkeiten von Gebieten mit Schnee und Schatten zwischen dem photogrammetrischen und dem Laserscanning DHM verglichen. Für die Abschätzung der zonalen, stochastischen Unsicherheiten wird hier eine neue Methode vorgestellt, welche den Einfluss von Schatten auf die Höhengenauigkeit berücksichtigt. Aus den Differenzen der DHMs wurden dann die Gletscheränderungen berechnet.

Die Resultate dieser Masterarbeit zeigen einen Gletscherrückgang von 2005 bis 2009 im oberen Mattertal. Die Gletscherfläche nahm im Mittel um -5.56% pro Gletscher ab. Die mittlere Dickenänderung aller im oberen Mattertal untersuchten Gletscher liegt bei -3.17 $\pm$0.037 m und die totale Volumenabnahme bei -351.09 $\pm$0.144 mio m^3. Die Co-registrierung erwies sich als sehr nützliche Methode zur Erkennung von horizontalen Verschiebungen und zur Abschätzung von sytematischen Höhenfehlern zwischen DHMs. Ohne Berücksichtigung dieser, würden die Gletscheränderungen massgeblich überschätzt. Aus der Evaluierung der simultan aufgenommenen DHMs geht hervor, dass die Photogrammetrie nach wie vor Limitierungen in Gebieten mit vermindertem Kontrast aufweist. Es konnte gezeigt werden, dass schattige Gebiete grössere Höhenunterschiede zwischen mit Photogrammetrie und Laserscanning aufgenommenen DHMs aufweisen, als nicht schattige Gebiete.

Im Vergleich mit anderen Studien, zeigen die mit swissALTI^{3D} berechneten glaziologischen Änderungen, unter Berücksichtigung der systematischen und stochastischen Unsicherheiten, eine gute Übereinstimmung mit berechneten Gletscheränderungen aus Laserscanning Daten.

swissALTI^{3D}, als hoch aufgelöstes und kontinuierlich aktualisiertes DHM, eignet sich foglich sehr gut für Anwendungen in der Gletscherforschung.

Contents

List of Figures

List of Tables

Abbreviations

Table 1: Abbreviations

Abbreviation	Meaning
AAR	Accumulation Area Ratio
ADP	Airborne Digital Photogrammetry
ALS	Airborne Laser Scanning
CCD	Charge-Coupled Devices
DEM	Digital Elevation Model
DTM	Digital Terrain Model
DGNSS	Differential Global Navigation Satellite System
ELA	Equilibrium Line Altitude
FME	Feature Manipulation Engine
FOM	Figure of Merit
GCP	Ground Control Point
GLAXPO	Glacier Laserscanning Experiment Oberwallis
GNSS	Global Navigation Satellite System
INS	Inertial Navigation System
LiDAR	Light Detection and Ranging
NGATE	Next Generation Automatic Terrain Extraction
NIR	Near-infrared
PAN	Panchromatic
POS	Positioning and Orientation System
PSR	Potential Solar Radiation
RGB	Red, Green, Blue
RMSE	Root Mean Square Error
SAR	Synthetic Aperture Radar
SE	Standard Error
SGI	Swiss Glacier Inventory
STDV	Standard Deviation
TIN	Triangular Irregular Network
UTC	Coordinated Universal Time
UZH	University of Zurich
VAW	Versuchsanstalt für Wasserbau, Hydrologie und Glaziologie
WGMS	World Glacier Monitoring Service

Chapter 1

Introduction

1.1 State of the Art

Glaciers and ice caps provide among the most visible indications of the effects of climate change (IPCC, 2007). The study of these effects on glaciological changes has become important (Koblet et al., 2010), in particular, as glaciers have a large influence on natural hazards, the regional water cycle and the global sea level (WGMS, 2008).

With the geodetic method, glaciological changes can be quantified by a differencing of multi-temporal digital elevation models (DEMs). The two most widely used acquisition methods to generate elevation data products are airborne digital photogrammetry (ADP) and airborne laser scanning (ALS) (Schenk, 1999).

The DEM generation from photogrammetric sources shows limited accuracy in areas of shadow and low contrast (e.g. snow) often found in high-alpine environments (Rolstad et al., 2009). Airborne laser scanning, on the contrary, is not depending on these characteristics since it directly measures the surface elevations (Joerg et al., 2012).

Glaciological changes were in recent years extensively studied for arctic and high-alpine environments with DEMs from ADP and ALS. Since the first applications of ADP and ALS in the 1970s (Sandau, 2005), the quality of the elevation data products improved over the years to the extent, that today, highly accurate DEMs for glaciological research are available.

Nevertheless, these DEMs are only digital representations of the Earth's surface and contain errors and uncertainties due to different reasons (Fisher and Tate, 2006). In order to extract considerable and representative glaciological changes, the DEMs have to be homogenized and their systematic and stochastic uncertainties need to be assessed.

In this thesis, this is done in a statistical approach, since the conversion procedures between original data acquisition and final elevation data is difficult to access and thus errors can not be physically determined anymore (Nuth and Kääb, 2011).

1.2 Motivation

The extensive data source for this master's thesis consists of six DEMs from three different years (2005, 2009, 2010), which were either derived from airborne digital photogrammetry or airborne laser scanning. These DEMs cover the area of and around Findelengletscher (2009, 2010) and the upper Mattertal (2005, 2009).

By coincidence, the DEMs from 2010 were measured by the University of Zurich (UZH) and the Federal Office of Topography (swisstopo) on exactly the same day (September 29, 2010). The UZH measured elevation data with an airborne laser scanning system whereas swisstopo used an airborne digital photogrammetry device.

The present master's thesis ties in with the methods of many already carried out glaciological studies (e.g. Baltsavias et al., 2001; Bühler et al., 2012; Rolstad et al., 2009), by comparing the elevation data accuracy of DEMs from ADP and ALS in high-alpine environments. But the data source for this thesis enables a more detailed analysis of the performance of ADP and ALS than normal. In fact, the DEMs from the two simultaneous measurement campaigns, provide the unique opportunity to not only validate the performance of ADP and ALS over stable, unglaciated terrain but also over glaciated terrain (glacier signal to noise). Additionally, areas of shadow and snow are compared between ADP and ALS DEMs and the findings are included as stochastic uncertainties in the glaciological change calculations.

swissALTI^{3D}, the new reference DEM for Switzerland provided by swisstopo, describes the surface of Switzerland without vegetation and development.

In swissALTI^{3D}, the areas below 2000 m.a.s.l. were measured from 2000 to 2008 with airborne laser scanning. Elevation data for the areas above 2000 m.a.s.l. were in contrary recorded from 2008 to 2011 with airborne digital photogrammetry. swissALTI^{3D} is today, the first high-resolution DEM, which is continuously updated (a sixth of the area of Switzerland each year) and available nationwide in homogeneous quality (Swisstopo, 2014b).

The findings concerning potentials and limitations of ADP and ALS are integrated in the glaciological change calculations over the period from 2005 to 2009 in the upper Mattertal and further, help to evaluate the suitability of swissALTI^{3D} for applications in glaciology.

1.3 Objectives and Research questions

The objective of this master's thesis lies in quantifying the glaciological changes in the upper Mattertal, with the main focus on the uncertainty assessment of the compared ADP and ALS DEMs.

In order to derive these glaciological changes from 2005 to 2009, detailed knowledge about the DEMs, their processing steps and acquisition techniques is necessary. In this regard, the objectives are:

- to determine the influence of terrain characteristics and ground cover on elevation data accuracy in DEMs,

- to assess the potentials and limitations of the co-registration method,
- to evaluate the suitability of airborne digital photogrammetry and airborne laser scanning DEMs for applications in glaciology.

The research questions are formulated as follows:

1. How did the glaciers in the upper Mattertal develop over the period from 2005 to 2009?
    - How did the respective area, average thickness and volume change?
    - How do these glaciological changes correspond with the changes for the same period documented in other studies?
2. What are the systematic (ϵ) and stochastic (σ) uncertainties of the glaciological changes?
    - How do the factors *shadow* and *snow* influence the performance of airborne digital photogrammetry?
    - How do the stochastic uncertainties vary for the different calculation methods?
3. Which findings can be drawn from the co-registration of the DEMs?
    - How do the results from co-registered and not co-registered DEMs differ concerning the glaciological changes?
    - What are the identified potentials and limitations of the co-registration method?
4. How suitable prove the DEMs from airborne digital photogrammetry and airborne laser scanning to be for applications in glaciology?
    - Can the advantages and disadvantages of the acquisition techniques be confirmed?
    - How does swissALTI^{3D} perform in high-alpine environments compared with DEMs from airborne laser scanning?

Chapter 2

Theoretical Basics

2.1 Glacier

2.1.1 Definition

A glacier is a perennial mass of surface-ice (and possibly firn and snow) on land, which flows downhill due gravity. It is constrained by internal stress and friction at the base and sides. Glaciers are generally formed and maintained by gaining mass at high altitudes (UNEP, 2007).

In the accumulation area, which is the "part of the glacier where accumulation exceeds ablation in magnitude" (Cogley et al., 2011), glacier mass is accumulated by snow fall, deposition of hoar, freezing rain, solid precipitation in forms other than snow, gain of windborne snow, avalanching and basal accumulation.

In glaciology snow is defined according to Cogley et al. (2011) as "solid precipitation in the form of ice crystals accumulated on the summer surface on a glacier" that transforms to firn at the end of the mass-balance year. Firn is defined as "snow that has survived at least one ablation season but has not been transformed to glacier ice" (Cogley et al., 2011). The compaction and recrystallization of snow are processes that transform snow to firn and ice. The dividing line between snow and firn lies by convention at a density of approximately 400 kg/m^3. Firn has densities of 400 to 830 kg/m^3 and becomes glacier ice near 830 kg/m^3. Glacier ice is after Cogley et al. (2011) defined as "ice that is part of a glacier, having formed by the compaction and recrystallization of snow to a point at which few of the remaining voids are connected, and having survived at least one ablation season". To obtain mass changes over longer time periods, the ice density is approximated and usually assumed as 917 kg/m^3 (Geist et al., 2003).

In the ablation zone, which is "the part of the glacier where ablation exceeds accumulation in magnitude" (Cogley et al., 2011) the main processes are melting and calving or discharge into the sea. The accumulation area is separated from the ablation area by the Equilibrium Line Altitude (ELA), where gain and loss in (ice) mass are balanced (UNEP, 2007).

2.1.2 Classification of glaciers

The formation of glaciers depends on a number of factors. There are atmospheric factors such as temperature and precipitation but as well geomorphological factors such as the terrain, which determines how much solar radiation a glacier surface receives and also where ice and snow are likely to accumulate. The temperature and the amount of precipitation determine the ELA and thus the thermal regime of a glacier (Figure 2.1).

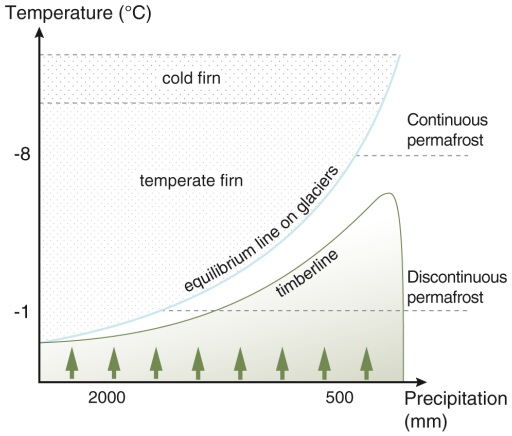

Figure 2.1: Cryosphere diagram (Haeberli et al., 2002).

Temperate glaciers, which are "glaciers consisting of temperate ice over the entire thickness and extent, except for a surface layer of the order of 10 to 15 m thickness, which may experience seasonal cooling" (Cogley et al., 2011), are found in regions that correspond to the temperate firn regime (Figure 2.1). Glaciers in these humid-maritime climates have ELAs at relatively low altitudes. Thick layers of snow melt due to warm temperatures and long melting seasons leading to relatively rapid flow and a high mass turnover.

In dry, continental regimes, depicted by the cold firn zone in Figure 2.1, the ELA is usually at relatively high altitudes with cold temperatures and short melting seasons. These glaciers contain mainly cold firn and ice well below the melting temperatures. In contrast to temperate glaciers, cold glaciers have a low mass turnover and thus a relatively slow flow. Cold glaciers can be surrounded by permafrost (UNEP, 2007).

Polythermal glaciers consist of a mixture of temperate and cold ice. A polythermal glacier has a basal layer of temperate ice, which is superimposed by layers of cold ice (Cogley et al., 2011). The temperate ice develops because of geothermal heating and the high pressure of superimposed ice masses. At the surface, the polythermal glacier has a 10 to 15 m thick layer that seasonally warms to the melting point. The thinner margins of polythermal glaciers can be frozen to the ground (UNEP, 2007).

2.1.3 Glacier observation methods

The **geodetic observation method** determines volume changes by repeated mapping and differencing of glacier surface elevations. This can be done in a number of ways such as ground surveys using theodolites or global navigation satellite systems (GNSS), airborne or spaceborne surveys with photogrammetry, laser scanning or SAR interferometry (Zemp et al., 2013).

Geodetic measurements on a glacier are usually carried out at the end of the hydrological year, when the glacier is free of snow. The hydrological year lasts from the start of the accumulation season (October 1) to the end of the ablation season (September 30). Ideally geodetic surveys are carried out simultaneously with glaciological surveys (Cogley et al., 2011).

The **glaciological observation method** determines the mass balance in situ on the glacier surface by measurements of accumulation and ablation, generally including measurements at stakes and in snow pits (Oestrem and Brugmann, 1991).

2.1.4 Average thickness and volume change

According to Zemp et al. (2013), glacier **volume changes** dV derived from a differencing of DEMs can be expressed by the following equation:

$$dV = r^2 \sum_{k=1}^{K} dh_{\mathrm{k}}, \tag{2.1}$$

where K is the number of raster cells covering the glacier at the maximum extent, dh_k is the elevation difference of the two grids at the raster cell k, and r is the raster cell size. The bedrock elevation is assumed to be constant.

The glacier thickness change dh_k is "the change in thickness of the glacier at a defined horizontal location" whereas the glacier-wide **average thickness change** dh is "the volume change of the entire glacier divided by the mean glacier area during the time span of the measurements" (Cogley et al., 2011). It can be derived from the following equation:

$$dh = \frac{dV}{\overline{S}}, \tag{2.2}$$

where dV is the volume change from Equation 2.1 and $\overline{S}$ is the average glacier area of the two surveys at time *t0* and *t1* assuming a linear change through time as

$$\overline{S} = \frac{S_{\mathrm{t0}} - S_{\mathrm{t1}}}{2} \tag{2.3}$$

(Zemp et al., 2013).

2.2 Study Area

2.2.1 Findelen- and Adlergletscher

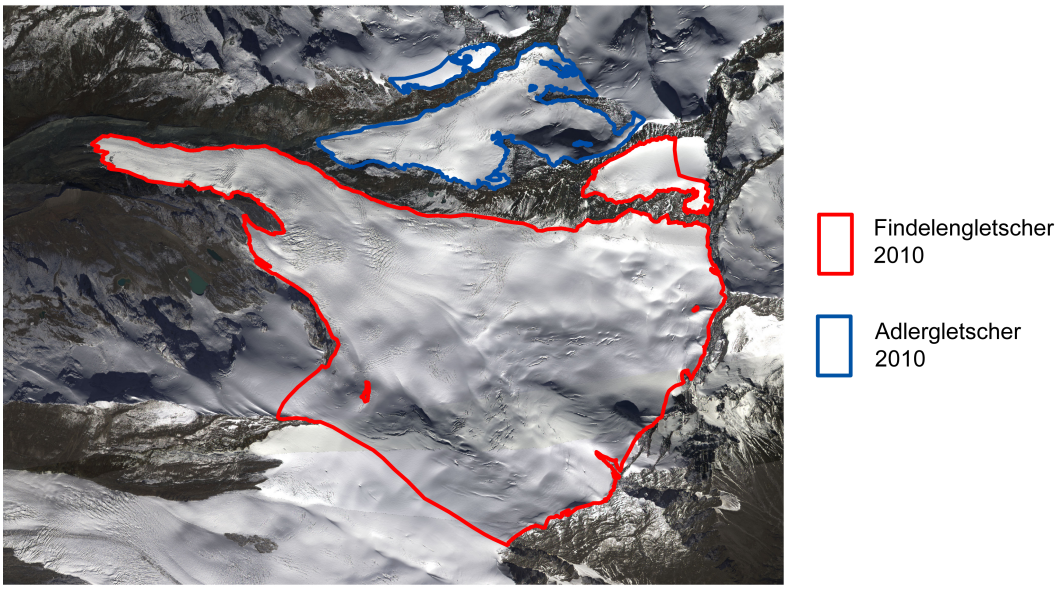

Figure 2.2: Orthophoto of Findelen- and Adlergletscher (September 29, 2010).

The study site of Findelen- and Adlergletscher, also referred to as the perimeter, has a catchment area of 25.72 km^2.

Findelengletscher is a temperate valley glacier located in the area of Zermatt in the southern Valais, Switzerland (46.00° N, 7.87° E). It consists of Findelengletscher and its former tributary Adlergletscher, which separated in the 1990s and are now independent ice bodies (Joerg et al., 2012).

In 1850 (Little Ice Age) Findelengletscher had a surface area of 19.96 km^2 and a length of 10.4 km (Maisch et al., 2000). Since then, the glacier has retreated, leading to an area of 17.36 km^2 in 1973 (Maisch et al., 2000) and 13 km^2 in 2010 (Joerg et al., 2012). The length in 2010 was about 6.7 km (Joerg et al., 2012). Findelengletscher showed some re-advance in the 1890s, 1920s, and 1980s (Maisch et al., 2000). Adlergletscher covers an area of 2.2 km^2 in 2010 (own calculation).

The seasonal mass balances of Findelengletscher from 1908 to 2008 have been reconstructed by Huss et al. (2010). Thereby a cumulative specific mass balance of approximately -26 m water equivalent (w.e.) resulted for the last century. Glaciological mass balance measurements on Findelengletscher started in 2004/2005 to derive punctual mass balance information for the validation of numerical models. The mean annual mass balances from 2004/05 to 2009/10 amount to -0.38 m w.e (Machguth et al., 2006).

Findelengletscher has a west facing aspect (Subfigures 2.3b and 2.3d) and is relatively flat (Subfigures 2.3a and 2.3c) with a distinct tongue and a well-defined outline.

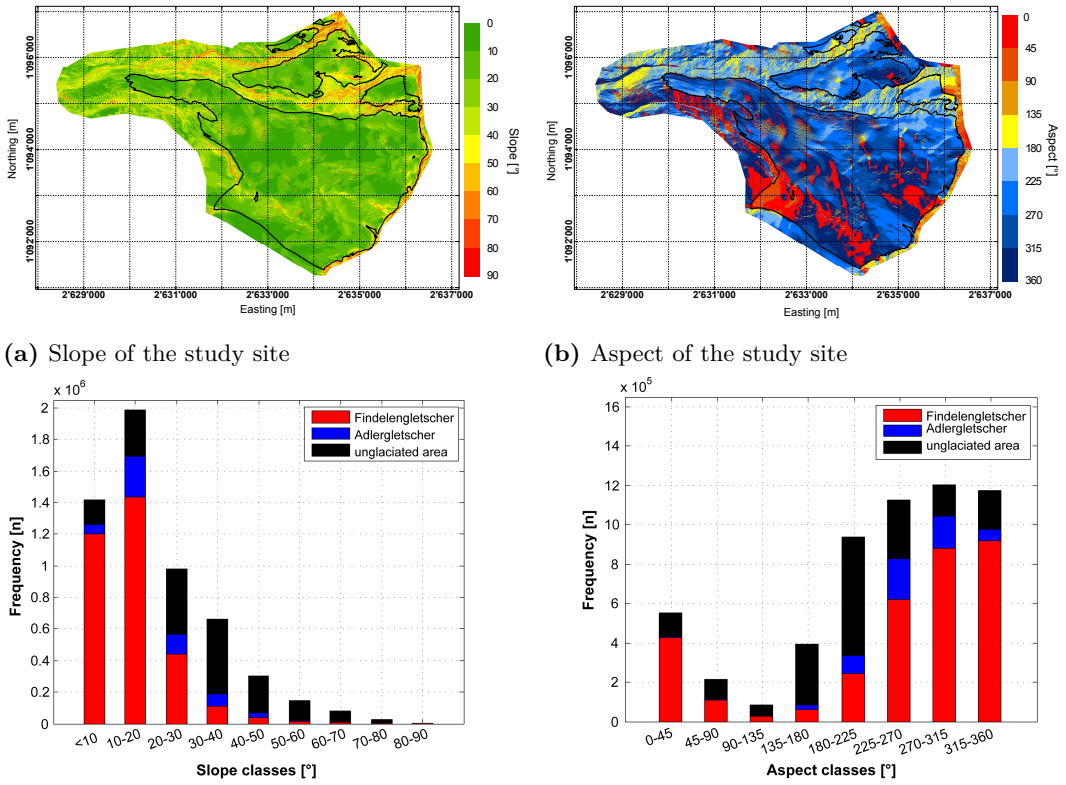

(a) Slope of the study site

(b) Aspect of the study site

(c) Slope distribution

(d) Aspect distribution

Figure 2.3: Slope and aspect of the study site.

The area on and around Findelengletscher is a worthwhile glaciological study site (Joerg et al., 2012) since (a) the glacier's surface is almost free of debris, (b) the glacier has a nearly constant slope, (c) the elevation of the glacier ranges from 2600 to 3900 m.a.s.l., thus the glacier is expected to endure decades of strong melt (Farinotti et al., 2012) and (d) the infrastructure consists of cable cars and a helicopter-base that allow a relatively easy access to the glacier.

2.2.2 Upper Mattertal

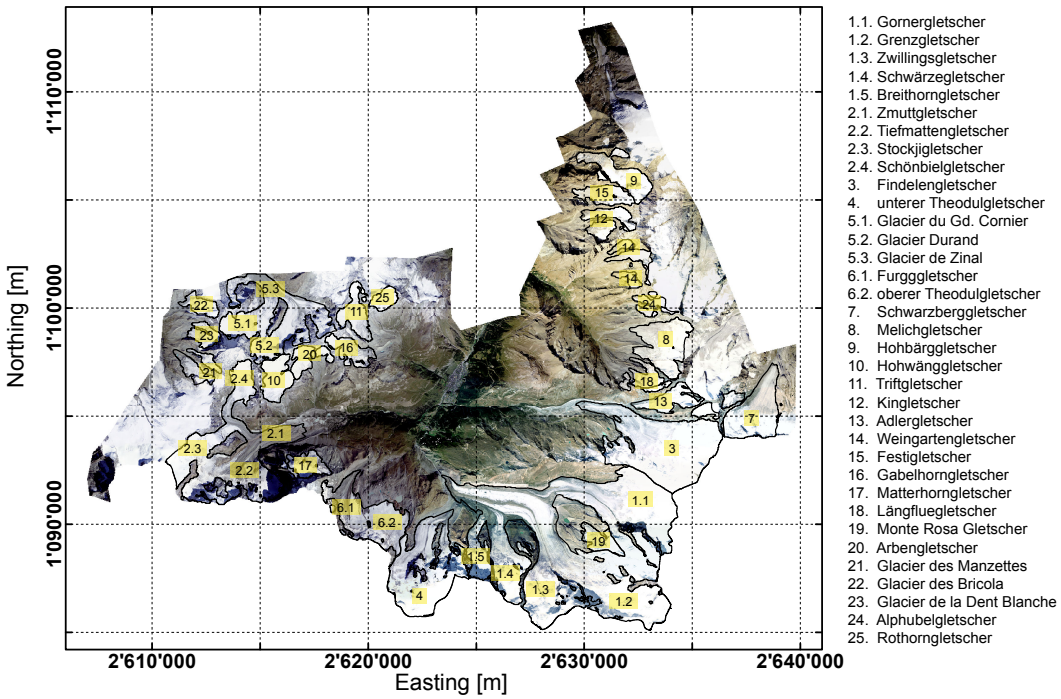

Figure 2.4: Orthophoto of the glaciers in the upper Mattertal perimeter. The numbers are the respective glacier IDs.

The Mattertal lies in the canton of Valais south of the Rhone valley and has a length of about 35 km. The term *upper Mattertal* used in this thesis, describes the southern part of the valley, which covers the large-scale area around Zermatt. The study site is defined by the flight perimeter of the airborne laser scanning campaign in 2005 (Figure 2.4). It has a catchment area of 413.38 km^2.

For the glaciological change calculations only the outlined glaciers are considered. All glaciers in Figure 2.4, which are not outlined, are excluded as their extents were not completely recorded during the ALS measurement campaign. The above described study site of Findelen- and Adlergletscher is also contained in the upper Mattertal perimeter.

2.3 Data acquisition methods and digital elevation models

2.3.1 Reference system, map projection and reference frame

2.3.1.1 Reference system

Because of its complex form, the Earth is usually depicted as an ellipsoid with a geographic coordinate system for reasons of simplification. The coordinate system consists of latitude, longitude and elevation above the ellipsoid.

The size, form and position of the ellipsoid are defined by a reference system which in turn takes the Earth's center, the axis of the Earth and the Greenwich meridian as its basis. Various countries use different national ellipsoids and reference systems due to practical and historical reasons (Swisstopo, 2014a).

2.3.1.2 Map projection

A projection system tries to represent the Earth's surface (or only a fraction of it) onto a flat surface. Because of the curvature of the Earth, this is only possible with restrictions. In practice, even and rectangular coordinates are utilized. A rectangular coordinate grid system results from projections of the ellipsoid on a geometric shape such as a sphere, a cylinder, a cone or a plane.

Since its introduction in 1903, swiss national surveying uses the uniform map projection Swiss Grid, which is an oblique, conformal cylinder projection (Mercator projection). This means that points on the Earth's surface are projected on a cylinder. The point of contact (= fundamental point) between cylinder and the Earth's surface corresponds to the origin of the coordinate system. Swiss Grid is only valid together with the ellipsoid Bessel 1841 and also serves as a standard for the national survey LV95 (Swisstopo, 2014a).

2.3.1.3 Reference frame

According to Swisstopo (2006), the theoretical definition of a reference system and a map projection does not suffice to realize and utilize geodetic reference systems for practical surveying. Additionally, coordinates of geodetic control networks and permanent networks that build the reference frame are required. All georeferenced data are embedded into the reference frame and are thus brought into a geometric relation.

2.3.1.4 Swiss geodetic reference systems

CH1903 LV03 LN02

CH1903 is the swiss geodetic datum, which forms together with the swiss map projection Swiss Grid, the reference system of the old swiss national survey 1903. The corresponding reference frames are divided into the swiss national triangulation network (LV03) and the swiss national leveling network (LN02). **LV03** is based on a geodetic control network from the national survey of 1903. The fundamental point of the coordinate system (oblique, conformal cylinder projection) is the old observatory in Bern (y0 = 600 000.00 m and x0 = 200 000.00 m).

Table 2.1: Swiss geodetic reference systems and reference frames.

Local reference system	**horizontal reference frame**	**vertical reference frame**
CH1903	LV03	LN02
CH1903+	LV95	LHN95

LN02 is the old official height system computed from raw, leveled height differences. The Repère Pierre du Niton in Geneva is taken as a reference with a height of 373.6 m (Swisstopo, 2014a).

CH1903+ LV95 LHN95

The over 100 years old national survey LV03 and the leveling network LN02 will be gradually replaced by the up-to-date national survey LV95 (Swisstopo, 2014a). **CH1903+** uses the same ellipsoid (Bessel 1841) and the same map projection (Swiss Grid) as CH1903. The new horizontal reference frame is LV95 and the vertical reference frame is the national height network LHN95. **LV95** has the coordinate axes notation E (East instead of y) and N (North instead of x) so that the old and the new horizontal reference frames can be easily distinguished. The fundamental point of the coordinate system is the Geostation Zimmerwald (E0 = 2 600 000.000 m and N0 = 1 200 000.000 m). **LHN95** is a potential-theoretic, rigorous height system, which takes kinematic phenomena (uplift of the Alps) into account and is based on orthometric heights. The origin for LHN95 is also the Geostation Zimmerwald. Its orthometric height was defined as H0 = 897.9063 m, so that for the Repère Pierre du Niton the value of 373.6 m is obtained (Swisstopo, 2014a).

2.3.2 Airborne laser scanning

Airborne laser scanning (ALS) is an active, optical remote-sensing technique that uses laser light to densely sample the surface of the Earth from a fixed wing aircraft or a helicopter, producing highly accurate x,y,z measurements (Albertz, 2009).

The basic components of ALS are:

- Light Detection and Ranging (LiDAR) system
- Global navigation satellite system (GNSS) and inertial navigation system (INS)
- Control and data recording unit
- Operator (laptop) and flight management system (Vosselman and Maas, 2010)

2.3.2.1 Principles

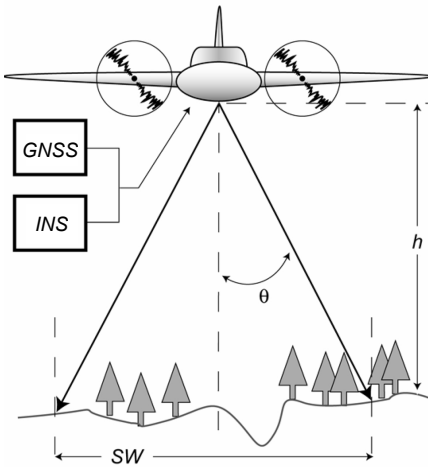

Figure 2.5: ALS geometry: scan angle (θ), platform height (h), and swath width *(SW)* are shown. GNSS and INS systems are on the platform and time-synchronized with the laser scanning system (Deems and Painter, 2006).

The laser scanning system considers two optical beams - the emitted laser beam and the returned signal of the respective beam, which is received by a photo diode in the ALS sensor (Wehr and Lohr, 1999). The distance to the respective objects on the ground can be measured by calculating the elapsed time between the emitted and returned laser signals.

The emitted, pulsed laser beams are deflected from an oscillating mirror in across-track direction (Figure 2.6). Thus, a swiveling mirror directs the laser pulse across the swath, so that through the forward motion of the aircraft a ground strip is recorded as numerous measuring points. Due to the oscillation of the mirror, data points in a terrain strip are recorded in both directions of the scan (= swath), leading to a zigzag scan pattern on the ground (Vosselman and Maas, 2010).

To transform the polar coordinates of the registered objects into the x,y,z coordinates, the position and the orientation of the platform (roll, pitch, yaw) are required.

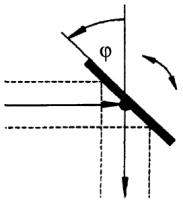

Figure 2.6: Principles of an oscillating mirror (Wehr and Lohr, 1999).

The position of the aircraft is determined by means of GNSS triangulation (and also differential GNSS (DGNSS)) whereas the orientation of the platform is identified via an INS (Deems and Painter, 2006). GNSS and INS together are called a Positioning and Orientation System (POS).

Together with the laser time range, the current angle of the deflection mirror and the measurements from GNSS and INS, the position and directional parameters of the point where the laser beam was emitted, can be derived (Wehr and Lohr, 1999). With forward georeferencing and coordinate transformation, the position of the ground point can be allocated (Joerg et al., 2012) and post-processed into highly accurate georeferenced x,y,z coordinates (e.g. swiss geodetic reference system). These post-processed spatially organized ALS data are called point cloud data (Albertz, 2009).

Data acquisition parameters

The scan pattern and thus the maximum point distance in across and along track directions are determined by the scan angle [°], the scanning frequency [Hz], the flying height above ground [m], the measuring frequency [kHz] and the aircraft ground speed [knot] (Figure 2.5) (Vosselman and Maas, 2010). The average point density [Pt/m^2], is also depending on the above mentioned factors (Baltsavias, 1999). Swaths are overlapped in order to maintain high point densities along the swath margins (Wehr and Lohr, 1999).

Further important data acquisition parameters are the laser wavelength [nm] and the laser beam divergence [mrad].

The wavelength of the emitted laser beam plays an important role. On the one hand the reflectivity of an object depends on the employed wavelength and on the other hand the atmospheric transmissivity has to be taken into account. In addition, attention must be paid to human eye safety. Commercial ALS systems for land applications operate at wavelengths between 800 and 1550 nm (Vosselman and Maas, 2010), preferable laser wavelengths are 1040 bis 1060 nm. Eye-safe wavelengths around 1550 nm are not the optimum choice for glaciological applications, as the reflectivity of snow and ice is low.

The laser beam divergence or beam width leads to the fact that a laser pulse can be reflected by multiple reflection surfaces. The number of returns per laser pulse is determined by the number of reflective surfaces on the ground. Modern ALS systems are able to record first, last or several returned laser pulses (Deems and Painter, 2006). In addition to multiple laser returns, it is possible that some emitted laser pulses are not returning. This is due to total or nearly no reflection.

Total reflection happens on very smooth and reflective surfaces, such as directed reflection on glacier ice. Resulting diffuse laser pulses can later lead to multi path echoes, which have to be detected and extracted because of their long range.

No or weak reflection happens in areas where the absorption is high, leading to the fact that not enough light is reflected to measure the distance. Absorption depends on the incident angle of the laser beam and the ground cover (Kraus, 2004). Absorption of the laser beam could happen because of melt water in the ablation area of a glacier (Geist et al., 2004).

Modern laser scanning systems are able to register the intensity of the received laser beam and can store radiometric information of objects. With a wavelength of 1064 nm the glacier surface facies are well distinguishable and can be classified into snow, firn and ice (Höfle et al., 2007).

The background radiation caused by reflection of the radiation on the Earth's surface and in the atmosphere, has a large influence on the received laser signal. It decreases with increasing wavelengths and has a reduced influence in the near-infrared (NIR) spectrum (Thiel and Wehr, 2004). A further factor to consider is the dark current noise (= a photon flux generated through thermic effects without any incident radiation from the object) in the photo diode (Kraus, 2004).

2.3.2.2 Application of airborne laser scanning in glaciology

According to Schenk (1999) the development of ALS started in the 1970s in North America with the main field of bathymetric applications.

With the emergence of GNSS and INS, the use of ALS has been extended to a wide area of applications including glaciology (Wehr and Lohr, 1999). ALS has been used for glaciological studies since the early 1990s (Baltsavias et al., 2001). Since then, many high-alpine studies to determine glaciological changes were conducted (e.g. Baltsavias et al., 2001; Deems and Painter, 2006; Favey et al., 1999; Geist et al., 2004; Höfle et al., 2007; Joerg et al., 2012; Kennett and Eiken, 1997; Knoll and Kerschner, 2010; Lenhart et al., 2006).

2.3.3 Airborne digital photogrammetry

Airborne digital photogrammetry (ADP) is a passive remote-sensing technique to reconstruct the position and shapes of objects from aerial images (Kraus, 2004). In ADP a distinction is made between opto-mechanic and opto-electronic scanners, which can further be divided in opto-electronic line scanners and opto-electronic frame scanners. The ADP DEMs used in this master's thesis were measured with opto-electronic line scanners also called push-broom or along-track scanners.

The basic components of ADP are:

- Sensor head in a gyro-stabilized sensor mount including INS
- Control unit including GNSS
- Mass memory recorder
- Operator interface (Sandau, 2005)

2.3.3.1 Principles

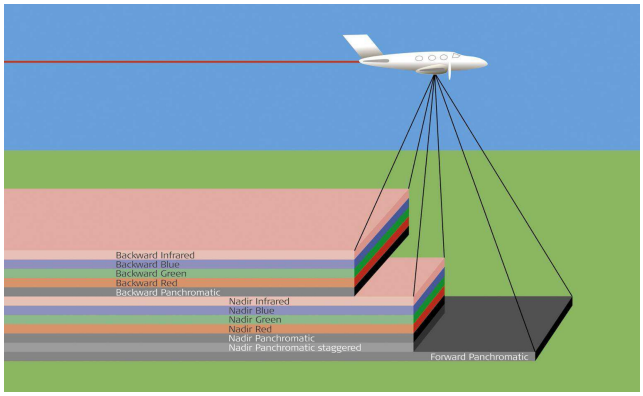

Figure 2.7: The five different spectral bands and three viewing angles of the Leica ADS80 sensor (Bühler et al., 2012).

Opto-electronic line scanners are suitable for aerial image recording of the optical radiation, which contains the visible and near-infrared radiation. Nowadays, only solid state sensors are used for digital image recording. These are composed of a large number of detector arrays, which record the photons of the incident radiation reaching the image plane (Kraus, 2004).

The image recording with opto-electronic line scanners is achieved with linear array charge-coupled devices (CCD). These contain for every image sensor, a photo active region (preferentially made out of silicium) and a shift register, also called transmission region, to read out the measured values. The CCDs consist of a capacitor array in which the photons of the incident radiation build up an electrical charge, which is proportional to the number of photons. In order to read out the electrical charges for each pixel in line, these are transmitted into parallel ordered transfer registers with the same length as the capacitor array.

From there, the charges for all pixels are shifted from each capacitor to its adjacent and read out serially from the last capacitor in line. The photoelectrically derived charges have to be converted into an analyzable voltage. By default, source-follower circuits are used for the conversion, after which the charges produce an image line in form of a video signal (Albertz, 2009; Kraus, 2004).

For the image recording from fixed wing aircrafts, arrays of CCD sensors are aligned in the image plane of the object lens. Thereby it is possible to record all pixels of an across-track oriented image line simultaneously. Through the forward motion of the aircraft and a respective recording frequency a ground strip is recorded line by line (Albertz, 2009).

Equal to the ALS measurements introduced above, a POS is also used for ADP. When post-processing, the coordinates of the pixel at the time of recording can be determined based on the camera parameters, the GNSS and the INS. For the spatial reconstruction of objects it is a precondition that incident radiation from the respective objects is available from at least two directions. With opto-electronic line scanners, an object is recorded under different viewing angles in flight direction (Figure 2.7). The object can then be spatially reconstructed by means of stereo correlation (Sandau, 2005). The further processing of aerial images is described in Section 2.3.5.

When working with CCD cameras there are geometric and radiometric aspects to consider (Kraus, 2004):

Geometric aspects of a CCD camera

Between the aerial images of ADP sensors and the recorded ground surface are geometrical connections. The photogrammetry uses these relations to measure the ground surface. In doing so, it has to be considered that the different acquisition methods have different illustration rules. This leads to the fact that with opto-electronic line scanners - and an assumed ideal and uniform horizontal flying movement - a mixed projection is resulting, namely a parallel projection in flight direction and a central projection in across-track direction. According to this, higher situated objects are in across-track direction, moved to the outside of the aerial image and lower objects to the inner side. Furthermore, the spatial movement of the aircraft plays an important role. As orientation of the platform is measured with GNSS and INS, the resulting distortions can be eliminated (Albertz, 2009; Kraus, 2004).

Radiometric aspects of a CCD camera

In addition to geometric relations between aerial images and objects on the Earth's surface, there also exist physical relations. This is because the image generation is depending on the intensity and spectral composition of the electromagnetic radiation (Albertz, 2009). Radiometric aspects to consider are (Kraus, 2004):

(a) The linearity and sensitivity of the CCD sensors

The electric charges transferred by the capacitors are proportional to the incident number of photons. Close to the saturation values of the CCDs, there are large deviations from linearity. Large amounts of radiation lead to an overflow of charge into neighboring capacitors (= blooming-effect).

(b) Color images

In opto-electronic line scanners, the radiation coming from an object is divided into four light rays by a beamsplitter in the sensor head. Before these light beams reach the CCD array, each beam has to pass an individual color filter. This allows the recording in the spectral bands (R)ed, (G)reen, (B)lue, near-infrared (NIR) and (PAN)chromatic.

(c) Signal to noise ratio

The radiometric sensitivity of CCD sensors over the spectral range can be expressed with the signal to noise ratio. A ratio of 1 means that the signal carrying the relevant information is the same as the noise at the sensor. Reasons for noise are e.g. the dark current noise or noise in the charge transfer between CCDs (= shifts of charges between two neighboring CCDs during the reading process).

If there were no noise, the radiometric resolution would be unlimited large and therefore a distinction of very close point sources possible (Sandau, 2005).

2.3.3.2 Application of airborne digital photogrammetry in glaciology

Airborne analog photogrammetry from gliders and balloons emerged in the middle of the 19th century. Continuous improvements of photogrammetric devices and the electronic computing technology since the 1970s lead to an increasing use of airborne digital photogrammetry (Sandau, 2005), which is nowadays a powerful tool for monitoring mountain areas (Gwinner et al., 2000).

One recent study that used ADP DEMs for glaciological investigations is Haug et al. (2009). Other studies compared ADP with ALS data and used DEMs from one acquisition method as a reference to evaluate elevation data accuracies (e.g. Baltsavias et al., 2001; Bühler et al., 2012; Rolstad et al., 2009; Würländer et al., 2004). These comparisons show promising results of ADP for applications in glaciology.

2.3.4 Comparison of airborne laser scanning and airborne digital photogrammetry

A detailed comparison of ADP and ALS is conducted in Baltsavias (1999). Table 2.2 summarizes the respective advantages and disadvantages of each method for glaciological applications.

Table 2.2: Advantages and disadvantages of ADP and ALS. + stands for advantage and - for disadvantage.

Aspects	**ADP**	**ALS**
Number of flight strips	+	-
Costs	+	-
Density of measurements	-	+
Weather	-	+
Flying date and time	-	+
Areas with low contrast	-	+
Shadow	-	+
External light sources	-	+
Liquid water	+	-
Visible/NIR distinction of snow and ice	+	-
Necessity of GCP	-	+
Orthophoto	+	-

With its smaller swath angles 20° - 40° (ADP up to 108°) and the usually lower flying height of around 1000 - 1500 m above ground (ADP up to 6000 m), ALS needs more overflights resulting in longer flying times and therefore more image strips than ADP (Schenk, 1999; Würländer et al., 2004). Together with the higher equipment and maintenance costs, ALS is overall more expensive than ADP (Bühler et al., 2012; Schenk, 1999). Thus, with ADP the topography of large areas can be registered more time and cost efficiently than with ALS.

The linear CCD sensors of ADP lead to a continuous coverage of the study area. Thereby, the image strip is recorded three times (forward, nadir, backward), which means a three times 100% overlap of the overflown image strip. The ALS point sensors with a polar geometry sample irregular and point wise with gaps, with a recording angle in only one direction (Wehr and Lohr, 1999). Because a CCD sensor has no mechanical parts, it thus is less vulnerable to distortions and blackouts than sensors with mechanical parts, such as the oscillating mirror of ALS (Albertz, 2009).

Since ALS is an active, high-power collimated and monochromatic sensing technique, it is relatively independent of the weather, the flying date and time. ADP as a passive remote sensing technique depends more on weather conditions (e.g. clouds) and can not be used during the night. ALS is thus more flexible in terms of weather, recording date and time.

Furthermore, ADP has a limited accuracy in regions with insufficient contrast (e.g. snow) or changing illumination (e.g. shadow) (Haala et al., 2010). This leads to a decrease in elevation data accuracy due to less corresponding points for image correlation. In contrast, ALS can be used independently of surface texture and

external light sources (Geist et al., 2004). This is an advantage in high-mountain regions, where firn and snow show reduced contrast. With ALS it is also possible to register the reflected radiation intensities, which together with the laser wavelength, give evidence of the glacier surface facies type.

However, because of the absorption of the laser beam in melt water or also from bidirectional reflectance, reduced point densities in the glacier tongue area can occur (Geist et al., 2004).

For ALS the establishment and maintenance of ground control points (GCPs) is not necessary, except for a nearby GNSS reference station. Thus, according to Geist et al. (2004) the study may be expanded to the entire glacier including the remote firn areas. This can be limited for ADP due to a lack of texture or because no suitable GCPs are available.

ADP produces geometrically and radiometrically high quality images with multispectral capabilities (Baltsavias, 1999), including orthophotos, whereas with ALS no imaging or only monochromatic images can be generated. ALS has a high degree of automation with low complexity, whereas ADP has a lower degree of automation requiring also manual updates (Schenk, 1999).

2.3.5 Digital elevation model

2.3.5.1 Definition

A DEM is a quantitative model of a planetary surface in digital form (Burrough and McDonnell, 2005). It consists of a regular array of z-values, referenced to a common datum, representing the elevation of a surface as samples or averages at fixed spacing in two horizontal coordinate directions. DEMs are typically used to represent terrain relief (Cogley et al., 2011).

2.3.5.2 Generation techniques

There is a wide range of DEM generation techniques (e.g. Burrough and McDonnell, 2005; Kääb, 2005; Schenk, 1999). Schenk (1999) provide a detailed explanation for surface reconstruction from ADP and ALS data. In the following Subsection the methods used to generate the DEMs for this master's thesis are explained.

ADP DEM generation from stereophotogrammetry

When preprocessing digital aerial images, usually a calibration and georeferencing are undertaken (Rees, 2005). The calibration is to convert the raw digital numbers measured by the sensor into the physical quantities (e.g. radiances) required. Georeferencing is the "process to establish the relationship between image coordinate system (row and column number of the pixels) and the corresponding object space reference system on the Earth's surface" (Rees, 2005; Schenk, 1999). This is commonly done through GCPs, that are according to Lilesand et al. (2007) "physical points on the ground whose positions are known relative to a coordinate system". When mutually identifiable on the ground and on an aerial image, GCPs can be used to determine the position and orientation of an aerial image relative to the ground at the instant of exposure (Lilesand et al., 2007).

With the image processing technique of stereophotogrammetry, a reconstruction of three dimensional objects from two dimensional aerial images is achieved, by overlapping aerial images to obtain stereo image pairs for the same area.

The image processing can be automated by using image correlation algorithms, which work based on cross-correlation calculations on subsections of the image pairs (Haug et al., 2009).

Thereby, a reference window in one of the overlapping aerial images, that comprises a local neighborhood of pixels around a fixed location (e.g. 5 x 5 pixels), is defined. With a search window in the second aerial image, the central pixel of the reference window is iteratively traced. This is achieved by shifting the subsearch window pixel by pixel about the rows and columns of the search window. The correlation between the values in the reference and subsearch window is gradually computed. The image correlation criteria are fulfilled at the location where the correlation reaches its peak (Lilesand et al., 2007).

Problems to identify similar objects are due to shadow, areas of low contrast or large geometric distortions in the images. Distortions stem from the curvature of the Earth, changes of the position of the platform, atmospheric effects and variation in the elevation of the land surface (Burrough and McDonnell, 2005).

The quality of the derived elevation data products is assessed by visual inspection in a stereoscopic viewing system on the computer screen. If the results of the automatic stereo image correlation are not satisfying (e.g. incorrectly placed elevation values), manual corrections using tie points, breaklines and areas are usually applied. For raster cells, where the elevation values can not be determined, an interpolation from surrounding raster cells is performed (Haug et al., 2009).

One output of stereophotogrammetry are DEMs containing terrain elevations from planetary surfaces (Cukrov and José, 2013). Image correlation softwares are also able to generate digital orthophoto maps. Like maps, orthophotos have a fixed scale and like images, they show the terrain in detail and not by lines or symbols (Lilesand et al., 2007). Orthophotos are increasingly used to provide geometrically correct, highly detailed photographic images (Burrough and McDonnell, 2005).

ALS DEM generation from point cloud data

The three dimensional point cloud data with no topological relationship are hardly a useful end result. Thus a post-processing of the point cloud data is required. Schenk (1999) propose a general post-processing scheme, including a thinning, gridding and segmentation of the laser data.

The thinning is performed to minimize a possible redundancy of points and to reduce the huge sizes of the ALS data set caused by high point densities. The gridding comprises the interpolation of irregularly distributed points to a grid. The resulting range images can then be used for image processing. A next step is the segmentation to extract useful surface properties (e.g. breaklines and abrupt discontinuities), which is necessary for object recognition. In case of several large data set, an additional fusing of them is usually required (Schenk, 1999). The quality of surfaces reconstructed from laser point clouds depends on the calibration of the laser system, which also includes an assessment of systematic errors (Schenk, 1999).

2.3.5.3 Error sources and uncertainty assessment

Since DEMs are representations of the Earth's surface, they will always contain errors and uncertainties.

Sources of errors in DEMs

According to Fisher and Tate (2006), errors in DEMs can result from:

- the data acquisition method
- the data processing
- the characteristics of the Earth's surface

Zemp et al. (2013) divide sources of potential errors into sighting and plotting processes.

Sighting includes errors that are related to the measurement process and thus the data acquisition method. These originate from the platform, the sensor and the interference of the atmosphere. Plotting errors relate to the analogue (e.g. map) or

digital (e.g. DEM) representation of the sighting results, including georeferencing, projection, co-registration, and sampling density (Zemp et al., 2013).

Since a clear distinction and quantification of these errors is not possible, the errors have to be considered as uncertainties.

Classification of errors in DEMs

Errors in DEMs can occur in the horizontal as well as in the vertical direction. Errors that remain after data preparation and processing can be classified into three main groups:

- systematic errors (ϵ)
- random errors ($\pm\sigma$)
- gross errors or blunders (Fisher and Tate, 2006)

Systematic errors (= bias) are defined as the result of a "deterministic system which if known may be represented by some functional relationship" (Fisher and Tate, 2006). These errors result from a deterministic large-scale bias in the data collection or processing, e.g. disagreements between measured and true values (Zemp et al., 2013).

Random or stochastic errors (= noise) in a DEM accrue from a great variety of measurements or operational tasks in producing the DEM. Stochastic errors may be represented conceptually as random variations around the true reference value (Fisher and Tate, 2006) and are present on smaller spatial scales, from the individual pixel level upwards (Rolstad et al., 2009).

Gross errors can be the result of user error or equipment failure. Such errors can occur in commercial DEMs but are infrequent.

The DEMs available for this master's thesis are the results of second-level processing. The procedures from the original data to the final elevation data are difficult to access and thus errors can not be easily physically determined or modeled anymore (Nuth and Kääb, 2011). Therefore, statistical approaches are used to assess the uncertainties.

Chapter 3

Data

3.1 Overview

3.1.1 Digital elevation models

The following DEMs are available for the study site of Findelen- and Adlergletscher or the upper Mattertal.

Table 3.1: DEMs from the UZH and swisstopo for the years 2005, 2009 and 2010. The names in parentheses are referring to the respective DEMs.

	ALS (UZH)	**ADP (swisstopo)**
2005	15.-17.07.2005 (ALS_2005)	-
2005	28.-30.10.2005 (ALS_2005)	-
2005	28.-30.10.2005 (ALS_2005_fin)	-
2009	04.10.2009 (ALS_2009)	07.09.2009 (swissALTI^{3D}_2009)
2010	29.09.2010 (ALS_2010)	29.09.2010 (ADP_2010)

Due to practical reasons, the DEMs are named after the acquisition method *ADP* or *ALS* and the measurement year *2005*, *2009* or *2010*. An exception is made for swissALTI^{3D}_2009, since this is the official name of the data set.

ALS_2005_fin describes the ALS DEM from 2005 for the study site Findelen- and Adlergletscher. ALS_2005 is the DEM for the study site upper Mattertal. It consists of measurements from two ALS campaigns.

The hillshades of the ALS_2005, swissALTI^{3D}_2009, ADP_2010 and ALS_2010 DEMs are depicted in the Appendix 9.1.

3.1.2 Glacier outlines

GLAXPO_outlines
From the ALS research campaign (GLAXPO project) of the UZH, glacier outlines are available for Findelen- and Adlergletscher for the years 2005, 2009 and 2010.

SGI_outlines
Outlines for all glaciers in the upper Mattertal are available on the occasion of the swiss glacier inventory (SGI) for the year 2003 (Paul et al., 2011).

3.2 Digital elevation models from airborne laser scanning

3.2.1 Used laser scanning systems

Figure 3.1: a) Optech ALTM Gemini sensor head with laser and deflection mirror, b) computer-rack, c) operator laptop and d) the pilot screen (©BSF-Swissphoto, Technischer Bericht LiDAR Findelengletscher He10).

The ALS campaign of the University of Zurich was realized by BSF-Swissphoto (Technischer Bericht LiDAR Findelengletscher). The data acquisition parameters and accuracies are documented in Table 3.2.

On July 15 to 17, 2005 and October 28 and 29, 2005 elevation data were measured with the Optech ALTM 3100 laser scanning system for the upper Mattertal (ALS_2005). ALS_2005_fin was extracted from ALS_2005 and contains elevation data for the study site Findelen- and Adlergletscher from =ctober 28 to 30, 2005.

Elevation data for the ALS_2009 DEM were obtained for the area of Findelen- and Adlergletscher on the October 4, 2009, also using the Optech ALTM 3100 laser scanning system.

Table 3.2: Data acquisition parameters and accuracy of the data providers for the respective flying heights of all three ALS flight campaigns (Joerg et al., 2012).

Acquisition parameters	**Unit**	**Oct. 28-29, 2005**	**Oct. 4, 2009**	**Sept. 29, 2010**
Sensor employed	ALTM	3100	3100	Gemini
Measuring frequency	kHz	71-100	71	71
Scanning angle	°	±23	±15	±15
Scanning frequency	Hz	40-50	39	39
Average flying height	m	1500	1000	1000
Across-track overlap	%	55	50	50
Average point density	Pt/m^2	1.1	7.6	14.3
Laser wavelength	nm	1064	1064	1064
Beam divergence	mrad (1/e)	0.30	0.30	0.25
Horizontal accuracy	m	0.75	0.50	0.18
Vertical accuracy	m (1 STDV)	<0.20	<0.15	<0.10

On September 29, 2010 from 8:42 to 12:00 and 15:31 to 17:34 (UTC), elevation data were acquired for the area of Findelen- and Adlergletscher with the Optech ALTM Gemini laser scanning system.

The measuring flights were done with a Pilatus Porter fixed-wing aircraft. For further information about the ALS DEMs see Joerg et al. (2012).

3.3 Digital elevation models from airborne digital photogrammetry

3.3.1 Used digital photogrammetry system

Figure 3.2: The ADS80 sensor employed in a Beechcraft Super King Air (©swisstopo).

For the recording of the two ADP DEMs, swisstopo used the airborne digital sensor 80 with the sensor head 82 (ADS80 SH82), which is an opto-electronic line scanner with the following data acquisition parameters:

The ADS80 SH82 is recording under three different viewing angles (16° backward, nadir, 27° forward) in five different spectral bands (Panchromatic 465 - 680 nm, Red 608 - 662 nm, Green 533 - 587 nm, Blue 428 - 492 nm and near-infrared 833 - 887 nm) (Figure 2.7). The field of view is 64° across track (swath angle) and the f-number is 4 (focal length of 62.7 mm). The focal plates for the SH82 have two 4-band beamsplitters, one in 16° backward and one in nadir direction. There is a total of 12 CCD lines with 12'000 pixels each and a pixel size of 6.5 μm. The 12 CCD lines consist of 2 single PAN lines, 1 pair of PAN lines staggered by a half pixel and 8 spectral lines (2 Red, 2 Green, 2 Blue, 2 NIR).

3.3.2 swissALTI^{3D}_2009

swissALTI^{3D}, the new reference DEM of Switzerland, describes the surface of Switzerland without vegetation and development.

In swissALTI^{3D}, the areas below 2000 m.a.s.l. were measured from 2000 to 2008 with airborne laser scanning. During that time, elevation data for areas in swissALTI^{3D} above 2000 m.a.s.l. originated from the DHM25 (with a resolution of 25 m). A survey with different user groups yielded that there is a demand for a more recent and accurate modeling of high-alpine regions.

Therefore elevation data recordings for the areas above 2000 m.a.s.l., started in 2008 by using airborne digital photogrammetry. The ADP elevation data with raster cell sizes of 2 m, replaced the former DHM25 in regions above 2000 m.a.s.l..

The quality of the stereo correlation was checked systematically for all measured areas. Regions where the quality did not conform to the standards were removed and manually reprocessed by determining new breaklines, areas and stereoscopically collected points (Bovet, 2013).

swissALTI^{3D} is today, the first high-resolution DEM, which is continuously updated (a sixth of the area of Switzerland each year) and available nationwide in homogeneous quality (Swisstopo, 2014b).

Swisstopo documents the accuracy of swissALTI^{3D} as follows:

- laser points (below 2000 m.a.s.l.): $\pm$ 0.5 m 1σ
- stereo correlation (above 2000 m.a.s.l.): 1 - 3 m average error
- manual updates (points, breaklines and areas): 25 cm - 1 m average error

swissALTI^{3D} can serve as:

- an elevation data set in a geographical information system,
- a basis for 3D visualizations, simulations and visibility analyses,
- a basis for mapping small structures and forest paths,
- a planning tool in the fields of spatial planning, telecommunication, natural hazards and forestry,
- a basis for orthorectification of aerial and satellite images

(Swisstopo, 2014b).

3.3.3 ADP_2010

In the framework of a routinely swisstopo data acquisition campaign, digital aerial images with a ground sampling distance of 0.5 m and an across track overlapping of 50% for the area of and around Findelengletscher were recorded on September 29, 2010, the same day as the ALS_2010 DEM.

These aerial images served to generate a DEM based on the method of image correlation. This was done by using the module NGATE (Next Generation Automatic Terrain Extraction) from SocetSet 5.6.0 (BAE Systems). To generate the DEM all spectral bands of the ADS80 image strip were included:

- 3 Panchromatic (16° backward, nadir, 27° forward)
- 2 RGB (16° backward, nadir)
- 2 near-infrared (16° backward, nadir)

The applied settings in SocetSet NGATE are:

- Raster cell size: 2 m
- Maximum Number of Image Pairs per Point: 4
- Correlation strategy: ngate_low_contrast.strategy (for low contrast imagery of snow-covered areas)
- Smoothing: low

The generation of the DEM was automatic and no manual corrections of mismatched points were applied (R. Artuso, personal comment, 06.02.2014).

Figure of Merit (FOM)

As an additional output with the generation of the ADP_2010 DEM, a Figure of Merit data set is produced in SocetSet, which documents the correlation process quality measure with values from 0 (low quality) to 100 (high quality).

FOM is a numerical value assigned by the terrain extraction process. It indicates one of three things for a given post measurement:

- an error flag value indicating that the automatic measurement was questionable,
- a successful or good measurement,
- an edit flag value indicating the type of editing that was used

(BAE Systems, 2013).

Chapter 4

Methods

Different software packages are used for DEM processing. With the Feature Manipulation Engine (FME) Desktop version 2012 (Safe Software, Inc.) the coordinates of the DEMs are reprojected. Tasks related to analyzing and comparing DEMs, are performed in ArcGIS Desktop version 10.0 (ESRI, Inc.). The co-registration is done with the Solver Add-In in Microsoft Excel 2007 (Microsoft, Inc.). Statistics are calculated using PASW Statistics Desktop version 18 (SPSS, Inc) and MATLAB (The MathWorks, Inc). Furthermore, visual and three dimensional analysis are done by using the ArcScene Desktop version 10.0 (ESRI, Inc.).

4.1 Coordinate transformation

The reference systems of the two DEMs have to be homogenized. It was a condition on the part of swisstopo to use the new swiss reference system CH1903+ LV95 LHN95. The ADP DEMs from swisstopo use already the new reference system. Because the ALS DEMs use the old reference system (CH1903 LV03 LN02), they have to be reprojected.

The transformation is done with the "ReframeReprojector" from the swisstopo REFRAME plug-in for FME, which is a planimetry and/or altimetry transformation software for technical surveying or cadastral surveying applications (Swisstopo, 2012). To perform the reference frame change, the planimetric and altimetric input and output frames are chosen as follows. The ALS DEMs are reprojected from the source planimetric reference frame LV03 (CH1903) to the destination planimetric reference frame LV95 (CH1903+). Accordingly, the heights are transformed from the source altimetric reference frame LN02 (leveled heights) to the destination altimetric reference frame LHN95. The raster cell sizes are preserved and the chosen interpolation type is bilinear (providing a reasonable balance of speed and quality).

4.2 Resampling of the digital elevation models

The ALS DEMs have a raster cell size of 1 x 1 m, whereas the ADP DEMs have one of 2 x 2 m. Accordingly, the raster cell sizes of the DEMs have to be unified in a second step.

The level of detail represented by a raster is dependent on the cell size. A raster cell must be small enough to capture the required detail, but large enough, so computer storage and analysis can be performed efficiently (ESRI, 2014c).

The resampling from 2 x 2 m to 1 x 1 m requires an interpolation process to generate 4 cells from 1 cell. On the contrary, a resampling from 1 x 1 m to 2 x 2 m generates 1 raster cell from 4 existing raster cells. Because of the above mentioned reasons and the fact that 2 x 2 m raster cell sizes are still at a very high resolution, a resampling of the ALS DEM to 2 x 2 m raster cell size is performed by using the ArcGIS Resampling tool (ESRI, 2014h).

The resampling parameter chosen is the bilinear option that determines the new value of a cell based on a weighted distance average of the four nearest input cell centers. It is useful for continuous data and will cause some smoothing of the data.

Additionally, the Snap Raster environment, which adjusts the extent of output rasters (so that these match the cell alignment of the specified snap raster) is set as ADP_2010 (ESRI, 2014i).

When ALS DEMs have a raster cell size of 2 x 2 m and the cell alignment matches the one of the ADP DEM, all DEMs are standardized according to their coordinate systems, raster cell sizes and cell axis alignments.

4.3 Co-registration

According to Nuth and Kääb (2011), the most important correction before comparing two DEMs is to co-register the two elevation data products, so that the pixels of each DEM represent the same location and area on the Earth's surface. In this approach Nuth and Kääb (2011) propose a three part process to analyze elevation differences on terrain assumed to be stable for three potential biases:

1. the geo-location of the data (x, y, and z matrices)
2. an elevation dependent bias
3. biases related to the acquisition geometry of the data

In this thesis the main interest lies in the systematic uncertainties resulting from the first point. Figure 4.1 shows the suggested co-registration methodology by Nuth and Kääb (2011).

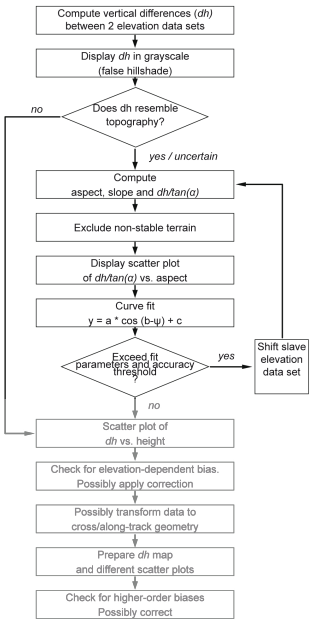

Figure 4.1: A suggested methodology for comparing DEMs for glacier change detection (Nuth and Kääb, 2011).

4.3.1 Horizontal and vertical shifts

Two DEMs of the same terrain surface that are not perfectly aligned, experience a characteristic relationship between elevation differences and the direction of the terrain (aspect), which is precisely related to the x-y-shift vector between them.

Figure 4.2 shows a schematic drawing and a real example, where one DEM is shifted to the second. Resulting elevation differences (dh) are larger on steeper slopes due to the relationship of the magnitude (a) of the shift vector and the elevation errors to the tangent of the slope of the terrain (α):

$$tan(\alpha) = \frac{dh}{a} \tag{4.1}$$

Because the aspect (ψ) is usually defined circular from the North, the direction of the shift can be modeled using the cosine of the difference between ψ and the horizontal directional component of the shift vector. Combining the relation from Equation 4.1, a full analytical solution can be derived by relating the elevation differences to the elevation derivatives, slope and aspect (Kääb, 2005):

$$dh = a \cdot \cos(b - \psi) \cdot tan(\alpha) + \overline{dh} \tag{4.2}$$

where dh is the individual elevation difference, a is the magnitude of the horizontal shift, b is the direction of the shift vector, α is the terrain slope, ψ is the terrain aspect and $\overline{dh}$ is the overall elevation bias between the two elevation data set.

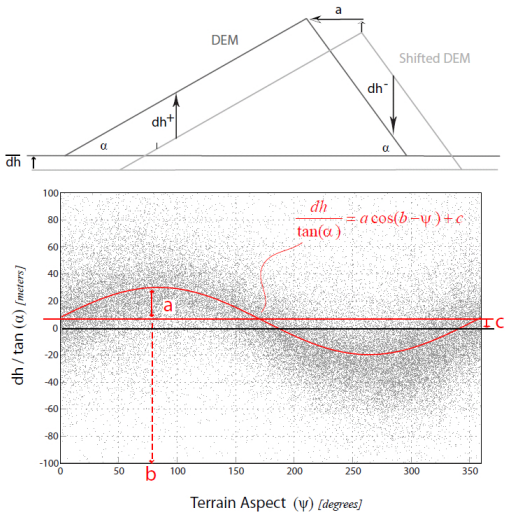

Figure 4.2: Top: 2-D scheme of elevation differences induced by a DEM shift. Bottom: The scatterplot of elevation differences between two DEMs, showing the relationship between the vertical deviations normalized by the slope tangent (y-axis) and terrain aspect (x-axis) (Nuth and Kääb, 2011).

Unaligned DEMs can be detected easily as their elevation differences show a terrain like pattern, similar to the hillshade of the terrain (Figure 4.3).

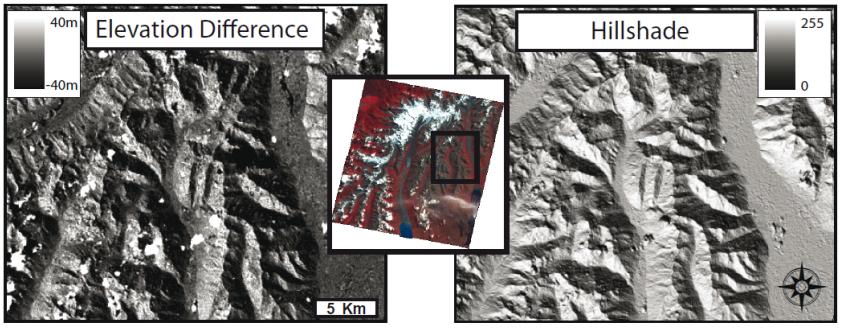

Figure 4.3: The elevation differences (left) between ASTER DEMs before co-registration compared with the hillshade of one DEM (right) (Nuth and Kääb, 2011).

To remove the error dependency on slope due to an x-y-shift, the vertical deviations can be normalized by dividing it by the tangent of slope at the respective pixel. This leads to a sinusoidal relationship between elevation difference and aspect (Figure 4.2, bottom).

$$\frac{dh}{tan(\alpha)} = a \cdot \cos(b - \psi) + c \tag{4.3}$$

where

$$c = \frac{\overline{dh}}{tan(\overline{\alpha})} \tag{4.4}$$

Three cosine parameters (a, b and c) are solved using least squares minimization, where a is directly the magnitude of the shift vector, b is the direction of the shift vector, and c is the overall elevation bias $\overline{dh}$ between the DEMs divided by $tan(\overline{\alpha})$, the mean slope tangent of the terrain. Because the terrain is not an analytical surface, the first solution is not the final solution and iterations of the process are required. Nuth and Kääb (2011) choose to stop the iteration if the improvement of the standard deviation is less than 2% or if the magnitude of the solved shift vector is less than 0.5 m.

The mean elevation bias is determined by solving Equation 4.4 for $\overline{dh}$ using an estimate of the mean slope of the unglaciated terrain. The parameters a and b are transfered into x and y coordinates using basic trigonometric relations.

4.3.2 Co-registration applied

The co-registration is performed in ArcGIS Desktop version 10.0 (calculation and extraction of variables) and in Microsoft Excel 2007 (curve fit, calculation of shift parameters) with a co-registration file prepared and documented by J. Lindenmann and P. Rastner (Lindenmann, 2012).

Areas used for co-registration should be on unglaciated, stable terrain and should comprise an equal distribution of the aspect in order to detect horizontal shifts in every direction. Further, the slope in the co-registration areas should be steeper than 10° (Kääb, 2005). Areas with forest should be masked out, since the ADP DEMs reflect the vegetation height instead of the bedrock height (Rolstad et al., 2009).

The following variables have to be extracted from the DEMs:

- elevation difference (slave minus master)
- aspect (ψ) of the master DEM
- slope (α) $> 10°$ of the master DEM

dh/tan(α) is calculated and then plotted against the aspect (ψ) (Figure 4.2, bottom).

A best fit to the curve

$$\frac{dh}{tan(\alpha)} = a \cdot \cos(b - \psi) + c \tag{4.5}$$

is aspired using the Solver Add-Inn (Microsoft, 2014) running in Microsoft Excel. The curve fit is done based on the dependency of the normalized elevation differences ($\frac{dh}{tan(\alpha)}$) from the aspect (ψ). This dependency is governed by the shift of the DEMs.

The co-registration areas for ADP_2010 and ALS_2010 are depicted in Subfigure 4.4a and for the upper Mattertal between swissALTI^{3D}_2009 and ALS_2005 in Subfigure 4.4b.

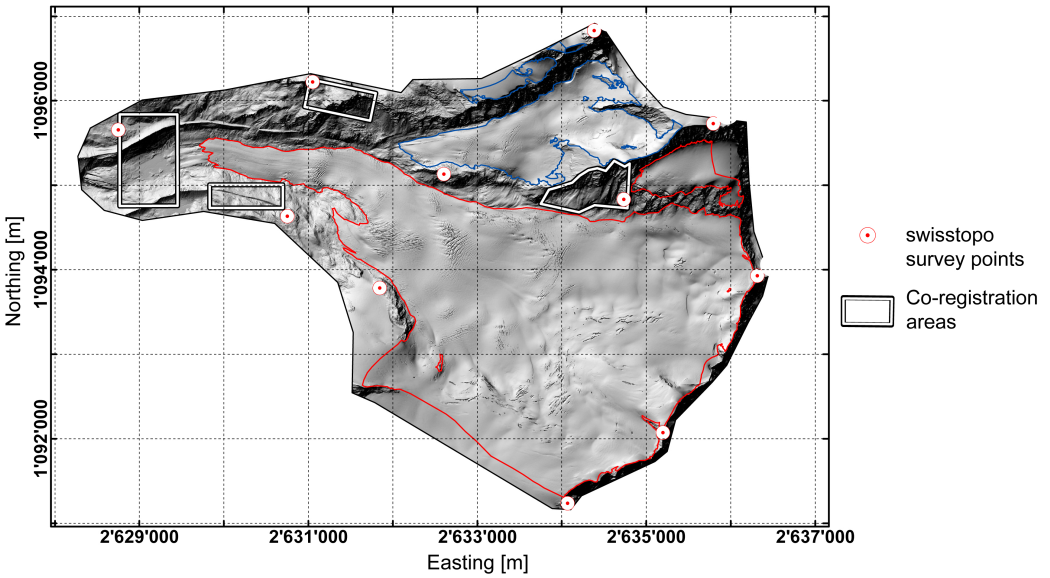

(a) Swisstopo survey points and co-registration areas for Findelen- and Adlergletscher.

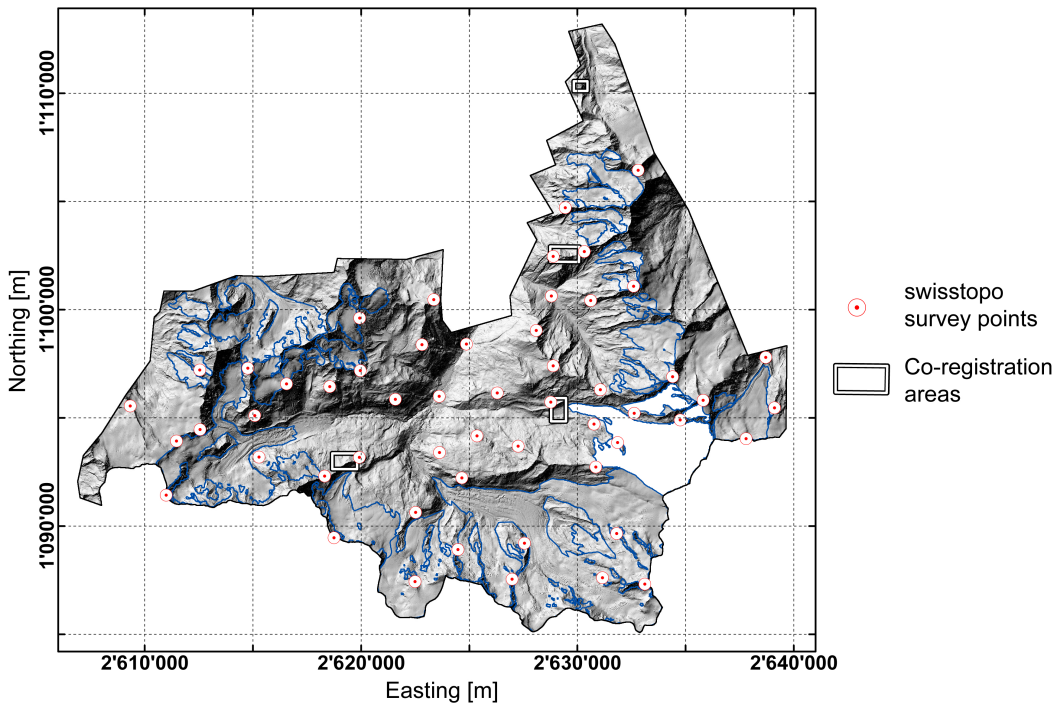

(b) Swisstopo survey points and co-registration areas for the upper Mattertal. The three (south-) eastern survey points in the accumulation area of Findelengletscher (Figure 4.4a) are extracted, since they are too close to the national border and are therefore not contained in swissALTI^{3D}. As a reference, Findelen- and Adlergletscher are marked.

Figure 4.4: Swisstopo survey points and co-registration areas for (a) Findelen- and Adlergletscher and (b) the upper Mattertal.

4.4 Digital elevation model differencing

In the previous Section it is made sure that the DEMs are uniform according to their reference frames, raster cell sizes and horizontal alignment.

As the extent of the ADP_2010 DEM is larger than the flight perimeter of the ALS_2010 DEM, it is necessary to exclude overlapping raster cells by using the Extract by Mask tool in ArcGIS (ESRI, 2014d). This tool extracts the cells of a raster data set (ADP_2010) that correspond with the areas defined by a mask (flight perimeter ALS_2010).

After this step, the elevation differences can be calculated by using the Raster Calculator in ArcGIS (ESRI, 2014g). Due to the wide range of resulting elevation differences from minimum to maximum, outliers have to be removed. A standard method for the removal is to exclude values that lie outside of the threshold: $\text{mean}_{\text{dh}} \pm 3 * \text{STDV}_{\text{dh}}$ (Bühler et al., 2012).

4.5 Digital elevation model uncertainty assessment

4.5.1 Comparison with ground control points

The calculation of (a) the mean, (b) the root mean square error (RMSE), (c) the standard deviation (STDV) and (d) the standard error (SE) are common methods to compare the elevation of a set of independent reference points with the elevation at the corresponding coordinates in a DEM (Koblet et al., 2010).

As shown in Subfigure 4.4a, there is a total of 11 former geodetic survey points by swisstopo present on exposed summits within the study area of Findelen- and Adlergletscher. For the upper Mattertal there are 54 of these survey points chosen (Subfigure 4.4b).

Although these coordinates are outdated, the accuracy is still expected to be an order of magnitude higher than a single laser point. Therefore, valid reference data in regions where no other data are available, is provided with a favorably distribution around the ALS perimeter (Joerg et al., 2012).

For the comparison of raster data with point data, the following approach is applied. Each swisstopo survey point is compared with the average elevation of the five nearest raster cells of the respective DEM. For this, the raster cell on which the swisstopo survey point is located, as well as the four closest raster cells (top, left, bottom, right), are determined. The raster cell values are converted to point data using the Raster to Point tool in ArcGIS (ESRI, 2014f).

After extracting the statistical measures for each swisstopo survey point, the average over all points is calculated and a separate analysis performed for each DEM (Table 4.1).

Because of the exposed position of the swisstopo survey points, a small shift in the horizontal direction leads to large differences in the vertical direction. Thus, the same outlier treatment of $\text{mean}_{\text{dh}} \pm 3 * \text{STDV}_{\text{dh}}$ is applied.

The applied method shows lower mean values for all four DEMs compared with the respective swisstopo survey points. This is because of the fact that the average

Table 4.1: Comparison of DEMs with swisstopo survey points.

		Frequency [n]	**mean** [m]	**RMSE** [m]	**STDV** [m]	**SE** [m]
Findelen- and Adlergletscher	ALS_2010	10	-1.37	1.38	0.51	0.09
	ADP_2010	10	-1.31	1.26	0.62	0.15
Upper Mattertal	ALS_2005	54	-1.39	1.84	1.22	0.57
	swissALTI^{3D}_2009	54	-1.82	2.37	1.53	0.39

of the five nearest cell values is compared with one single point value. So actually, the average elevation of 20 m^2 raster cells is compared with a single point located in exposed terrain. However, this is not problematic as the method is done in the same way for all DEMs.

The mean differences between the DEMs and the survey points, are relatively high with values from -1.31 to -1.82 m. The differences in the mean values indicate that there could be some systematic elevation shifts between the DEMs. The SE, which can also be used to described stochastic uncertainties, is relatively low for the area around Findelen- and Adlergletscher and considerably higher for the upper Mattertal DEMs. From the comparison of the DEMs with the GCPs it can also be checked, whether the DEMs are tilted in some direction. This could easily be identified if the differences between the DEMs and survey points are systematically increasing or decreasing in one direction. However, there is no tilt visible and large differences occur mainly due to the exposed locations of the survey points.

4.5.2 Glacier signal to noise

By performing a Student's T test, it can be determined, whether the elevation differences on the glacier (glacier signal) differ significantly from the elevation differences on the unglaciated, stable terrain (noise) (Koblet et al., 2010).

For the Student's T test the following hypotheses are formulated:

$$H0 : dh_{\text{ADP-ALS}}unglaciated = dh_{\text{ADP-ALS}}glaciated \tag{4.6}$$

$$H1 : dh_{\text{ADP-ALS}}unglaciated \neq dh_{\text{ADP-ALS}}glaciated \tag{4.7}$$

The elevation differences on unglaciated terrain, Findelen- and Adlergletscher are taken as samples for the Student's T test between the ADP_2010 and ALS_2010 DEMs. For the Student's T test between ALS_2005 and swissALTI^{3D}_2009 DEMs only a subset of the elevation differences over glaciated and unglaciated terrain is taken (because of the large sample size of approximately 30 mio raster cells). The selection is performed by creating a point grid with raster cell sizes of 20 meters, which is further put over the DEMs for the upper Mattertal. Every raster cell that is overlayed by a grid point is included in the subsample. This leads to a homogeneously distributed subsample of elevation differences for the Student's T

test. The subsamples consist of 524964 sample points over unglaciated terrain and 336406 sample points over glaciated terrain. Due to uncertainties arising from forest, only unglaciated terrain with elevations above 2600 m.a.s.l. is chonsidered.

All evaluations between unglaciated and glaciated terrain yielded p-values of 0.000 and can therefore be considered as significant. This means, the Nullhypothesis H0 is rejected. Hence, the elevation differences over glaciated terrain (glacier signal) differ significantly from the error in unglaciated terrain (noise).

4.6 Uncertainties from ground cover and terrain characteristics

Since the zonal, stochastic uncertainties in the ALS DEMs are very small (Joerg et al., 2012), it is assumed that the stochastic uncertainties in the glaciological change calculations for the upper Mattertal from 2005 to 2009 stem to a large degree from the limitations of ADP. Therefore, the uncertainty analysis complies with the influence of shadow and snow on elevation data accuracy.

4.6.1 Uncertainties from shadow and potential solar radiation

The blocking of direct solar radiation causes areas of cast shadow in high-alpine terrain. In aerial images from ADP, these areas of cast shadow show reduced values of reflectance compared to non-shady areas with similar ground cover characteristics (Giles, 2001).

Therefore, analysis of elevation differences in areas of cast shadow are performed. Shadow models are calculated by P.C. Joerg in ArcGIS using the Area Solar Radiation tool (ESRI, 2014a). As input raster, the ALS DEM for the study site Findelen- and Adlergletscher is chosen. Furthermore, the following settings are applied:

- Latitude: 46 ° (automatic)
- Sky size: 1024 x 1024 cells
- Time configuration: within a day
- Day number: 272 (September 29, 2010)
- Hour interval: 0.1 (adds the radiation for 6 minutes)
- Diffuse model type: uniform sky
- Diffuse proportion: 0.2
- Transmissivity: 0.8

The resulting shadow models show the potential solar radiation for 6 minutes (0.1 hour interval) and have the unit watt hours per square meter [Wh/m^2].

The ADP_2010 DEM for the perimeter of and around Findelen- and Adlergletscher was recorded on September 29, 2010 at 11.14 UTC. Therefore, the shadow model from 11.12 to 11.18 is taken (6 minute interval). This model is visually and qualitatively compared with the ADP_2010 orthophoto (September 29, 2010) (Figure 2.2) by creating three dimensional surfaces in ArcScene.

In a discrete approach, not taking any diffuse potential solar radiation or continuous transitions from shadow to no shadow into account, potential solar radiation (PSR) classes based on intensity value thresholds from the shadow model are determined. These divide the perimeter into three PSR classes; (a) cast shadow (0 - 15 Wh/m^2), (b) transition from shadow to no shadow (15 - 85 Wh/m^2) and (c) directly illuminated with no shadow (85 - 122 Wh/m^2).

A quantitative analysis of the influence of PSR on resulting elevation differences is performed in detail on Findelen- and Adlergletscher and also for different ground cover types. The potential solar radiation values are additionally plotted against the elevation differences to show interdependencies between the incoming potential solar radiation and elevation differences of the DEMs.

4.6.2 Uncertainties from snow

Because of the low contrast in areas of snow, DEMs from ADP can show a decrease in elevation data accuracy. A comparison of the elevation differences over snow and ice is therefore advisable.

Towards the end of the hydrological year, a glacier surface can theoretically be divided into two zones, which are separated by the snowline. According to Cogley et al. (2011), the snowline is "the line separating snow surfaces from ice or firn surfaces" on the glacier. It is normally easy to recognize, as the snow above the snowline is brighter than the firn or ice below it and may be mapped by analysis of suitable imagery (Cogley et al., 2011).

Unfortunately, in 2010 there was a snowfall event just before the measurements were carried out (Joerg et al., 2012). This fact makes it impossible to recognize the snowline on Findelen- and Adlergletscher in the ADP_2010 orthophoto and thus prevents a direct comparison of the elevation differences in areas of snow or ice.

However, a Student's T test between the elevation differences of the DEMs in the tongue area (61181 sample points) and in the accumulation area (94520 sample points) of Findelengletscher is performed to test whether there is a statistically significant difference between elevation data from ADP and ALS over snow. The hypotheses for the Student's T test are:

$$H0 : dh_{\text{ADP-ALS}}tongue = dh_{\text{ADP-ALS}}accumarea \tag{4.8}$$

$$H1 : dh_{\text{ADP-ALS}}tongue \neq dh_{\text{ADP-ALS}}accumarea \tag{4.9}$$

The evaluation yielded p-values of 0.000 and can therefore be considered as significant. This means that the formulated Nullhypothesis H0 will be rejected.

Hence, the snow pack properties of the tongue area differ from the ones in the accumulation area. This could be attributed to melting processes, leading to a thinner snow cover and therefore higher contrast (due to underlying ice) in the tongue area compared with the thicker and thus lower contrast snow cover in the accumulation area.

4.7 Determination of the glacier area changes

4.7.1 Findelen- and Adlergletscher

Area changes for Findelen- and Adlergletscher are calculated from the GLAXPO_outlines with the Calculate Area tool in ArcGIS (ESRI, 2014b).

4.7.2 Upper Mattertal

Glacier areas in 2005

The outlines for the glaciers in the upper Mattertal are available as ESRI Shapefiles from the SGI in 2003 (SGI_2003) (Paul et al., 2011). In order to calculate the average thickness change, the mean glacier area has to be derived from the two surveys in 2005 and 2009 (Equation 2.3).

The elevation differences (swissALTI^{3D}_2009 minus ALS_2005) for the upper Mattertal are overlaid by the SGI_2003 outlines. Areas within these SGI_2003 outlines that show no glacial retreat are assumed to be unglaciated and thus stable.

By taking the independently derived GLAXPO_2005 outlines for Findelengletscher, this approach is proven to be correct. The left image in Figure 4.5 shows the available outlines for Findelengletscher (SGI_2003 and GLAXPO_2005). It can be verified that the stable, unglaciated terrain is where no elevation differences within the SGI_2003 outlines can be found. On the right image, the blue outline is the one adjusted from the SGI_2003 to the glacier extents in 2005. This is done for all glaciers in the upper Mattertal.

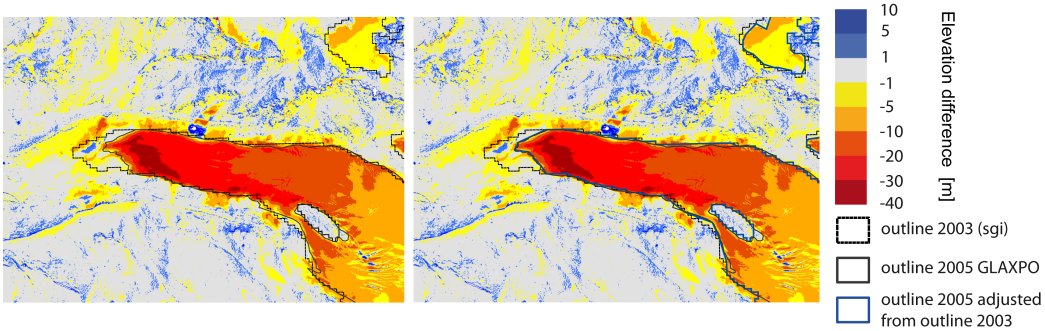

Figure 4.5: Adjusted glacier outlines for the year 2005 based on the SGI_2003 outlines.

Glacier areas in 2009

A swissimage orthophoto with a resolution of 2 m for the years 2009 and 2010 is available for the perimeter of the upper Mattertal. The eastern part of the Mattertal is included in the orthophoto from 2009, whereas the western side is unfortunately part of the orthophoto from 2010. Outlines for the 2009 glacier extents in the upper Mattertal are derived by using orthophoto from 2009 and the hillshades of swissALTI^{3D}. Employing these two sources, the glacier outlines for 2009 are derived from re-adjusting the SGI_2005 outlines.

4.8 Calculation of the average thickness and volume changes

Average thickness and volume changes are calculated from Equations 2.1 and 2.2 from Subsection 2.1.4.

4.9 Estimation of the systematic and stochastic uncertainties

4.9.1 Systematic uncertainties from the co-registration

The overall elevation bias ($\overline{dh}$; from the co-registration) between two elevation data set can be considered as the systematic uncertainty for the average thickness and volume changes.

$$\epsilon_{\text{DEM.unglaciated.sys}} = \overline{dh} \tag{4.10}$$

Note: $\overline{dh}$ from the co-registration is calculated by the subtraction of slave minus master DEM. Resulting in positive values if the overall elevation bias of the slave is higher and vice versa. If $\overline{dh}$ is taken as the systematic uncertainty for the average thickness and volume changes, the algebraic sign is changing for the ADP_2010 DEM, because the ADP_2010 is no longer the minuend (slave minus master) but the subtrahend (ALS_2005_fin minus ADP_2010).

4.9.2 Stochastic uncertainties from different ground cover and terrain characteristics

The standard error provides a measure for the respective stochastic uncertainty (Koblet et al., 2010):

$$\sigma_{\text{DEM.unglaciated.stoc}} = \pm\frac{STDV}{\sqrt{n}} \tag{4.11}$$

where $STDV$ is the standard deviation of the elevation differences and n is the number of raster cells. It has to be taken into account that the elevation differences need to be independent to calculate the SE. Because of the autocorrelation resulting from stereophotogrammetry this is not the case. Koblet et al. (2010) used older aerial images, thus it is assumed that the autocorrelation of raster cells with distances over 100 m is insignificant. For the high-resolution DEMs in this study a less conservative distance of 10 m is taken. The number of n is derived by laying a 10 x 10 m grid (5 x 5 pixels) over the sample area.

(a) **Stochastic uncertainties from unglaciated terrain** ($\pm\sigma_{\textbf{unglaciated}}$)

Usually, the stochastic uncertainties for glaciological change calculations are derived from the SE of the elevation differences over unglaciated terrain (Koblet et al., 2010).

In this thesis, the SE is calculated based on the elevation differences in the co-registration areas over stable, unglaciated terrain. This method yields uniform stochastic uncertainties independent of the glacier size.

According to Rolstad et al. (2009), uncertainties in elevation data derived from photogrammetry may be different over rock, snow and ice for three main reasons:

- There are different image contrasts over rock, blue ice and snow and variations in sun and shadow. Leading up to a lack of contrast, especially in snow areas.
- Due to the steep terrain in unglaciated regions, horizontal positional errors can lead to large vertical errors. Resulting elevation differences can thus be larger for hillsides than for glaciers.
- The terrain roughness varies between unglaciated and glaciated terrain, with generally smoother glacier surfaces than rock surfaces. With the same raster cell sizes the uncertainties in elevation differences over rocks may be larger than for glaciers (Rolstad et al., 2009).

Thus, it makes sense to consider not only unglaciated but also glaciated terrain for stochastic uncertainty estimations.

(b) **Stochastic uncertainties from glaciated terrain** ($\pm\sigma_{\mathbf{glaciated}}$)
Because of the above mentioned reasons, SEs from different terrains (unglaciated, steep blue ice, flat blue ice and snow) can vary considerably. According to Rolstad et al. (2009), estimated stochastic uncertainties are largest for unglaciated terrain, due to rougher surface characteristics and steeper slopes than on glaciated terrain.
By estimating the stochastic uncertainties from glaciated terrain, the glacier surface properties (snow, firn and ice) can be included into the analysis. Resulting SEs are based on the glacier's surface characteristics and take the glacier area into account.

(c) **Stochastic error from glaciated terrain under consideration of potential solar radiation classes** ($\pm\sigma_{\mathbf{glaciated\ with\ shadow}}$)
The existing data source enables a third method, which pursues the approaches by Rolstad et al. (2009) but integrates uncertainties caused by shadow. Again the STDV of the elevation differences over glaciated terrain is considered, but the glacier is partitioned into the three above introduced potential solar radiation classes (a) cast shadow, (b) transition from shadow to no shadow and (c) directly illuminated areas. Assuming that the uncertainties in elevation differences are mainly caused by shadow in the ADP DEMs, the influence of shadow on the performance of ADP and thus on the results of glaciological changes can be determined.
In this method each glacier is divided into the three potential solar radiation classes at the time of recording (e.g PSR classes for Grenz-Gornergletscher: 10.24% cast shadow, 41.20% transition from shadow to no shadow, 48.56% directly illuminated areas). Then the SE of the elevation differences is calculated for the PSR classes on each glacier (e.g stochastic uncertainty for each PSR class over Grenz-Gornergletscher: $\pm$0.024 m cast shadow, $\pm$0.017 m transition from shadow to no

shadow, ±0.019 m directly illuminated areas) and weighted according to the PSR distribution (e.g for Grenz-Gornergletscher: 0.10 * ±0.024 m + 0.41 * ±0.017 m + 0.49 * ±0.019 m = 0.018 m).

This gives the opportunity to determine the stochastic uncertainties in elevation data from the influence of shadow over glaciated terrain.

Above, three individual methods to derive stochastic uncertainties are presented. These methods have to be treated individually. So for every glacier there will be three different stochastic uncertainties. These have a varying degree of complexity, that increases from unglaciated to glaciated and glaciated with shadow. The objective of this analysis is to give a recommendation for the use of one of the three methods for future glaciological studies.

Chapter 5

Results

5.1 Qualitative evaluation of the digital elevation models

For the qualitative comparison, shaded reliefs, also called hillshades, are created for each DEM (Appendix 9.1) by using the ArcGIS Hillshade tool ESRI (2014e).

5.1.1 ADP_2010 and ALS_2010

When looking at the hillshades in full-screen view (Figures 9.1 and 9.2), the glaciated and unglaciated surfaces appear different for the the ADP_2010 than the ALS_2010 hillshade. Thereby, the ADP hillshade seems to be coarse, even blurred for some local areas and pervaded by irregularities. The ALS hillshade shows smoother surfaces with a higher contrast.

When zooming in, different phenomena can be noticed. Over glaciated terrain, the differences in crevasses are remarkable. In the hillshade from ALS, the crevasses are more pronounced than in the hillshade from ADP, which seems to smoothen the crevasse areas. That in turn leads to a reduction in the number of depicted crevasses.

In shady areas, no clear visual decrease in elevation data quality over Findelengletscher is visible in the ADP hillshade, whereas a decreased quality for the shady areas of Adlergletscher can be noticed (southern part of Adlergletscher). The surface characteristics of Adlergletscher appear granular compared to the ALS hillshade. The influence of shadow on elevation data quality can also be demonstrated on the western side of Findelengletscher where it borders on a rock. This rock, that is partly covered by cast shadow, appears less sharp in the ADP than in the ALS hillshade.

The differences between ADP and ALS that occur due to the snow cover, seem to become perceivable by the rugged surface in the ADP hillshade on the accumulation area of Findelengletscher. If this effect is really stemming from the snow cover, can not be fully confirmed, since areas with e.g. glacier ice for comparison are not existing in the perimeter. However, these effects do not appear in the ALS hillshade.

Over unglaciated terrain, raw edges are depicted sharper in the ALS hillshade, whereas some edges in the ADP hillshade tend to appear blurred (e.g. rocks in the glacier fore field).

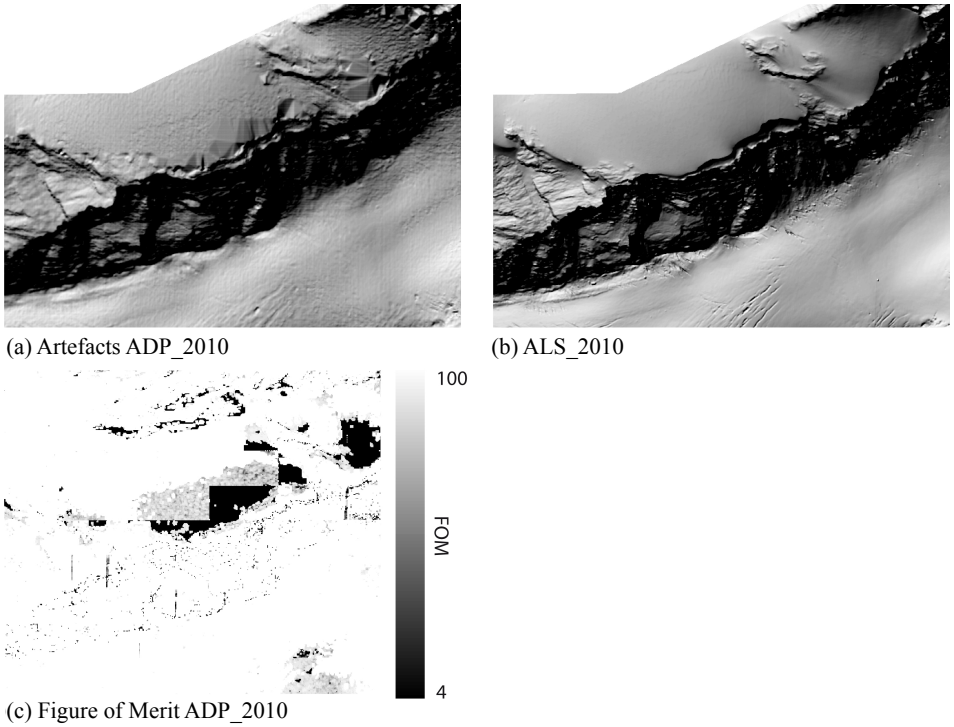

(a) Artefacts ADP_2010

(b) ALS_2010

(c) Figure of Merit ADP_2010

Figure 5.1: Local artefacts in the ADP_2010 DEM. FOM is the Figure of Merit documenting the correlation process quality measure.

With increased zoom levels, local artefacts become visible in the ADP hillshade, which are not present in the ALS hillshade. These have a triangular, irregular network structure (TIN) and could originate from the DHM25 that is used to fill data voids of the measurement process (Figure 5.1). These lead to a decreased resolution and thus to clearly recognizable elevation differences between the DEMs (Figure 5.4). Such local artefacts can be found in the North of the Adlergletscher close to Länfluegletscher and also on the northern side of the separate ice body that belongs to Findelengletscher.

The FOM shows the correlation process quality which is low for such areas (Figure 9.5). The FOM can generally be used for qualitative elevation data analysis. Low FOM values are shown in shady areas over Adlergletscher. On Findelengletscher low FOM values appear only in the accumulation area. This could be due to the poorer performance of ADP over firn or fresh snow. Interesting are also the low FOM strips over the unglaciated terrain between Findelen- and Adlergletscher. These could appear because of the steep, snow covered areas.

5.1.2 ALS_2005 and swissALTI^{3D}_2009

From the comparison of the swissALTI^{3D} and the ALS_2005 hillshades for the upper Mattertal (Figures 9.3 and 9.4), similar differences as between the ADP_2010 and ALS_2010 hillshades can be identified.

An important issue is thereby that swissALTI^{3D} was manually updated to a high degree, thus showing nearly no local artefacts.

Again the overall impression is that ALS leads to smoother surfaces compared with the still coarser ADP surfaces. The areas below 2000 m.a.s.l., that were for both DEMs measured with ALS, show good agreement. Concerning glaciated areas, it can be observed that crevasses are also smoothed in swissALTI^{3D}, leading also to a decreased contrast and number of shown crevasses. Large-scale glacier surface features e.g. on Grenz-Gornergletscher are clearly visible in both DEMs. The influence of shadow on resulting elevation data accuracies is not visible to the naked eye.

5.2 Co-registration

5.2.1 ADP_2010 and ALS_2010

The ALS_2010 is the master DEM and ADP_2010 the slave DEM to be adjusted.

Table 5.1 shows the outcomes of the co-registration between ADP_2010 and ALS_2010. The horizontal shifts of 0.24 m (Δx) and -0.29 m (Δy) are clear in the sub pixel range. Therefore, no further iteration is performed (Iteration 0).

The systematic elevation shift ($\overline{dh}$) amounts to 0.57 m indicating that the ADP_2010 DEM seems to overestimate the elevation values.

Table 5.1: Co-registration outcome between ADP_2010 and ALS_2010. ($STDV$) is the standard deviation, (a) is the magnitude of the shift vector, (b) is the direction (azimuth) of the shift vector, ($\overline{dh}$) is the overall elevation bias of the DEMs, (Δx) is the shift in x-direction (east-west), (Δy) is the shift in y-direction (north-south).

DEMs	**STDV** [m]	**a**	**b** [°]	$\overline{dh}$ [m]	**Δx** [m]	**Δy** [m]
Iteration 0						
ADP_2010 (slave) ALS_2010 (master)	1.37	0.38	-50.80	0.57	0.24	-0.29

Figure 5.2 shows the outcome of the curve fit based on the observed dependency of the normalized elevation differences and the aspect, which results from the horizontal shift of the DEMs. The distribution of the scatterplot follows the red line (the theoretical optimum value), which also indicates qualitatively that there is no further iteration necessary.

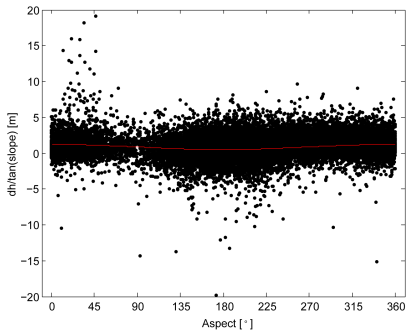

Figure 5.2: Scatterplot of the elevation differences (ADP_2010 minus ALS_2010) normalized by the slope tangent (y-axis) and terrain aspect (x-axis). The red line shows the theoretical sinusoidal curve fit from Equation 4.5 (Nuth and Kääb, 2011).

5.2.2 ALS_2005 and swissALTI^{3D}_2009

swissALTI^{3D}_2009, as the reference DEM for Switzerland, is the master DEM and ALS_2005 the slave DEM to be adjusted.

The outcomes of iteration 0 and 1 of the co-registration between swissALTI^{3D}_2009 and ALS_2005 are shown in Table 5.2. The results of iteration 1 show finally a reduction of the horizontal shifts, which lie clearly in the sub pixel range and amount to -0.53 m (Δx) and -0.07 m (Δy). The overall elevation bias ($\overline{dh}$) does not change much between iteration 0 and 1 and is still 0.55 m. This implies that elevation values are overestimated by the ALS_2005 DEM.

Table 5.2: Co-registration outcome between swissALTI^{3D}_2009 and ALS_2005. ($STDV$) is the standard deviation, (a) is the magnitude of the shift vector, (b) is the direction (azimuth) of the shift vector, ($\overline{dh}$) is the overall elevation bias of the DEMs, (Δx) is the shift in x-direction (east-west), (Δy) is the shift in y-direction (north-south).

DEMs	**STDV** [m]	**a**	**b** [°]	$\overline{dh}$ [m]	**Δx** [m]	**Δy** [m]
Iteration 0						
ALS_2005 (slave) swissALTI^{3D}_2009 (master)	2.42	1.31	93.68	0.54	1.32	0.08
Iteration 1						
ALS_2005 (slave) swissALTI^{3D}_2009 (master)	2.13	-0.74	84.44	0.55	-0.53	-0.07

From Subfigure 5.3a deviations between the scatterplot and the red line are visible, which indicate the need for a further iteration. Subfigure 5.3b, shows the resulting approximation of the scatterplot to the course of the red line after iteration 1.

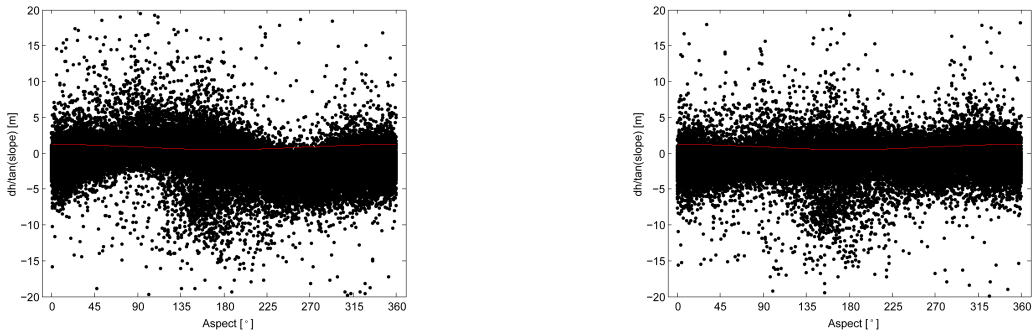

(a) Iteration 0 **(b)** Iteration 1

Figure 5.3: Scatterplot of the elevation differences (swissALTI^{3D}_2009 minus ALS_2005) normalized by the slope tangent (y-axis) and terrain aspect (x-axis). The red line shows the theoretical sinusoidal curve fit from Equation 4.5 (Nuth and Kääb, 2011). (a) shows the state before applying corrections (Iteration 0) and (b) is the state with applied corrections (Iteration 1).

5.3 Elevation differences of the digital elevation models

5.3.1 ADP_2010 minus ALS_2010

Table 5.3 shows the elevation differences from ADP_2010 minus ALS_2010. While the mean elevation differences for Findelen- and Adlergletscher are 0.81 m and 0.69 m respectively, the mean elevation difference over unglaciated terrain is 0.43 m. The findings from the Student's T test indicate that these differences are statistically significant (Subsection 4.5.2).

After the removal of outliers, the STDVs amount to values around 1 m with the only exception of Findelengletscher (0.66 m). The large STDV in unglaciated areas could be due to steep terrain. The minimum value after the removal of outliers is set to -10 m and the maximum value to 10 m.

Table 5.3: Summary of the elevation differences (ADP_2010 minus ALS_2010) for Findelen-, Adlergletscher and unglaciated terrain. Perimeter comprises the whole study site and (r.o.) stands for elevation differences after the removal of outliers [outl]. Positive mean values indicate that ADP overestimates the elevation values compared to ALS.

	Frequency [n]	**mean** [m]	**STDV** [m]	**min** [m]	**max** [m]	**outl** [n]	**outl** [%]
Perimeter	6418449	0.70	3.31	-207.11	147.06		
Perimeter (r.o.)	6375510	0.69	0.97	-10	10	38604	0.6
Findelen	3259223	0.82	0.83	-39.88	55.15		
Findelen (r.o.)	3256222	0.81	0.66	-10	10	2590	0.07
Adler	558767	0.70	1.61	-49.28	55.93		
Adler (r.o.)	555913	0.69	1.07	-10	10	2657	0.4
Unglaciated	1804502	0.33	2.30	-114.92	49.23		
Unglaciated (r.o.)	1790637	0.43	1.09	-10	10	11330	0.6

Figure 5.4 shows that the elevation differences over Findelengletscher are positive over large areas. In the accumulation area, the elevation differences are higher positive than in the ablation area. Negative elevation differences over Findelengletscher occur in areas of crevasses. These areas are very heterogenuous, with some parts over- and other parts underestimated. As a consequence, these areas are clearly visible in Figure 5.4. Moderate elevation differences can be found in the ablation area.

Elevation differences over Adlergletscher are mainly positive in the shady areas of the accumulation zone in the North of the Adlerhorn. In the surroundings of the Adlerpass, positive elevation differences occur next to negative ones. The crevasse areas show a similar pattern as on Findelengletscher. Between Adlergletscher and Längfluegletscher the area is dominated by negative elevation differences from ADP artefacts (Figure 5.1).

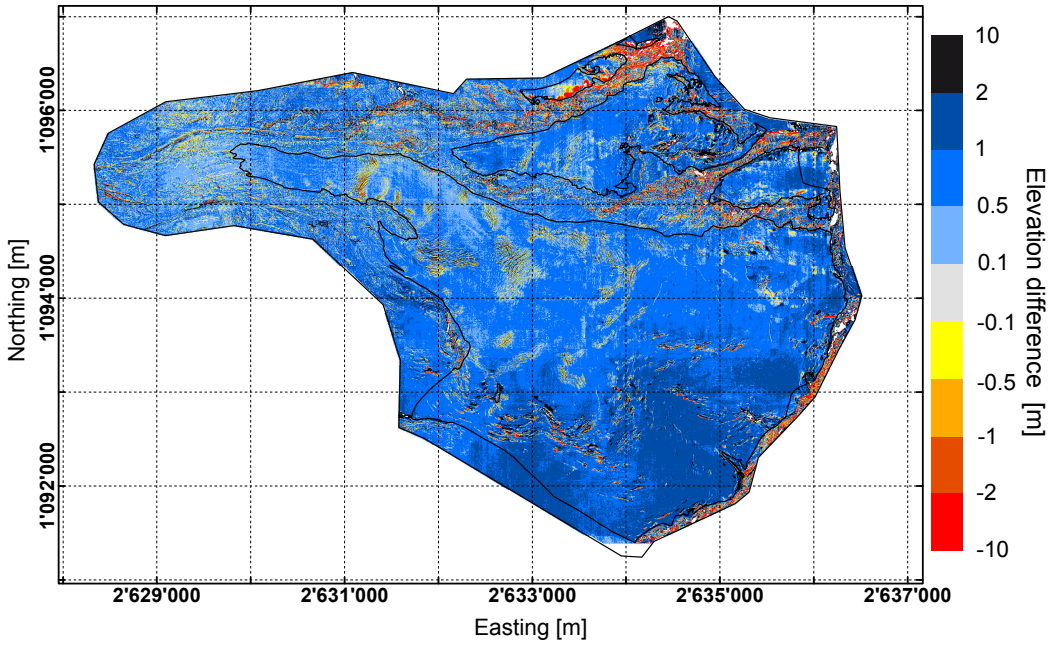

Figure 5.4: Elevation differences from ADP_2010 minus ALS_2010.

Over unglaciated terrain, positive elevation differences are found in areas of cast shadow (e.g. on the moraine south of the glacier tongue), whereas negative elevation differences occur mainly in areas with aspects towards south - southeast and also in steep areas. Moderate differences are located in flat terrain (e.g. in the flood plain close to the glacier tongue).

5.3.2 swissALTI^{3D}_2009 minus ALS_2005

Table 5.4 shows elevation differences for the upper Mattertal for the period 2005 to 2009. The unglaciated area is divided in two classes, according to the data acquisition technique. Below 2000 m.a.s.l. both DEMs were measured using ALS. The resulting mean elevation differences of -0.02 m are smaller than for the unglaciated terrain above 2000 m.a.s.l., where the elevation differences are -0.79 m. The relatively large STDV for the the unglaciated areas above 2000 m.a.s.l. could be due to the steep terrain. After the removal of outliers the minimum values are -50 m and the maximum values 10 m.

Table 5.4: Summary of the elevation differences (swissALTI^{3D}_2009 minus ALS_2005) for the upper Mattertal. Perimeter comprises the whole study site and (r.o.) stands for elevation differences after the removal of outliers [outl]. $>$ 2000 m is unglaciated terrain above 2000 m.a.s.l. and $<$ 2000 m is unglaciated terrain below 2000 m.a.s.l. (measured with ALS).

	Frequency [n]	**mean** [m]	**STDV** [m]	**min** [m]	**max** [m]	**outl** [n]	**outl** [%]
Perimeter	103325476	-2.25	6.88	-196	3202		
Perimeter (r.o.)	102638309	-2.40	4.73	-50	10	687167	0.7
Glaciers	49012098	-4.09	6.22	-196	379		
Glaciers (r.o.)	48664971	-4.24	5.88	-50	10	347127	0.7
Unglaciated							
$>$ 2000 m	51583758	-0.63	7.20	-126	3202		
$>$ 2000 m (r.o.)	51245361	-0.79	2.42	-50	10	338397	0.7
$<$ 2000 m	2731604	-0.02	0.97	-72	57		
$<$ 2000 m (r.o.)	2729948	-0.02	0.80	-50	10	1656	0.06

Figure 5.5 depicts the resulting elevation differences for the co-registered (a) and the not co-registered (b) DEMs. Generally positive differences appear in the accumulation areas of the glaciers on the eastern side of the Mattertal, whereas negative differences occur in the ablation areas all over the perimeter. Moderate elevation differences are located over unglaciated terrain and especially below 2000 m.a.s.l..

When comparing the differences between co-registered and not co-registered DEMs, a shift in east-west direction becomes visible. For the not co-registered DEMs (Subfigure 5.5b) the elevation differences are more negative on the eastern side of the Mattertal and more positive on the western side. This becomes clear over unglaciated terrain. The east-west shift results in differing glaciological changes. Therefore, changes in the ablation and accumulation areas are either over- or underestimated. The glaciological change calculations are shown in Table 5.10.

In Subsection 6.2.2 the effects of the co-registration are discussed.

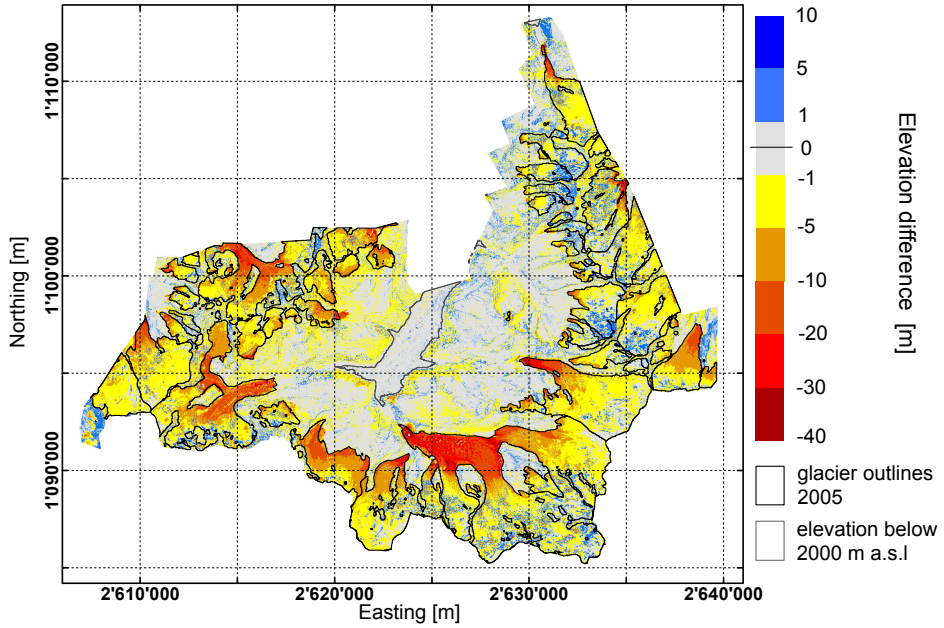

(a) co-registration applied

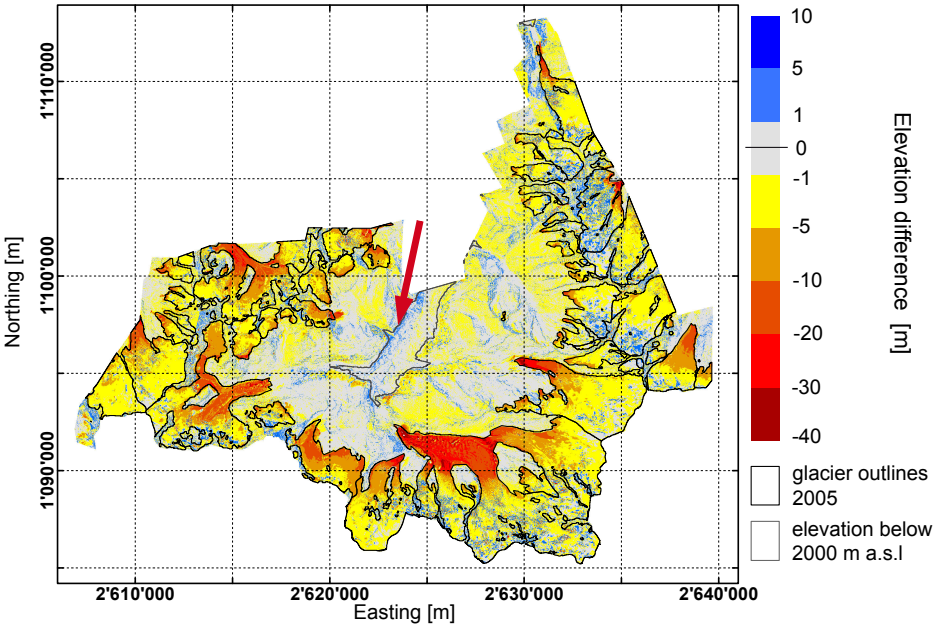

(b) no co-registration applied

Figure 5.5: Elevation differences from swissALTI^{3D}_2009 minus ALS_2005. The elevation values below 2000 m.a.s.l. in swissALTI^{3D}_2009 were measured by using ALS.

5.4 Uncertainties from ground cover and terrain characteristics

5.4.1 Uncertainties from shadow and potential solar radiation

Figure 5.6 shows the potential solar radiation on September 29, 2010 at 11.12 UTC.

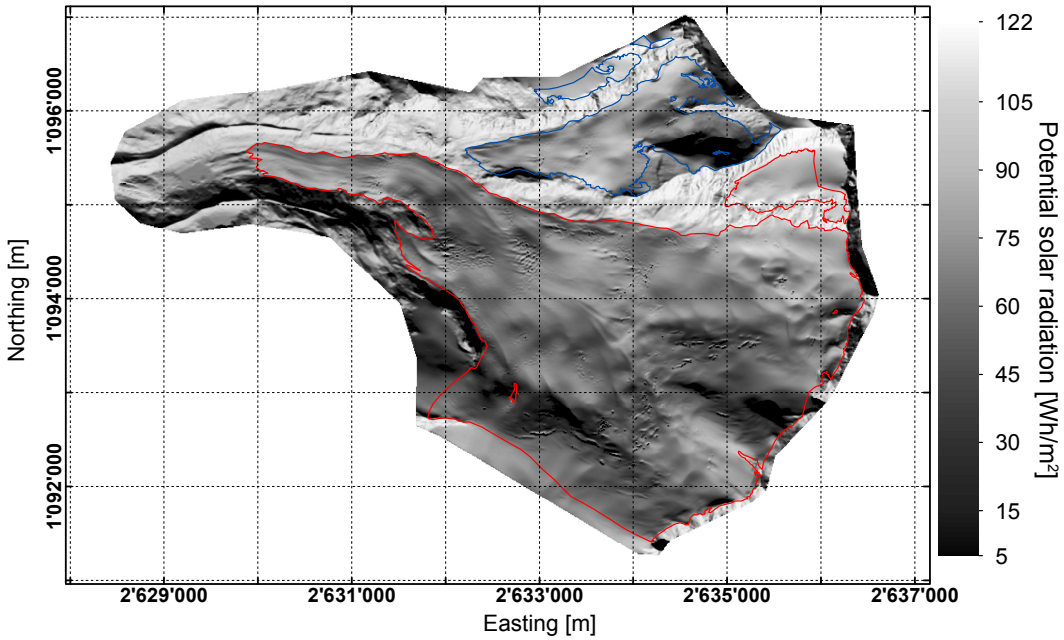

Figure 5.6: Potential solar radiation for the study site on September 29, 2010 at 11.12 UTC (0 - 15 Wh/m^2 = cast shadow, 15 - 85 Wh/m^2 = transition, 85 - 122 Wh/m^2 = direct illumination).

The analysis of the effects of shadow on resulting elevation differences (ADP_2010 minus ALS_2010) over Findelen- and Adlergletscher are listed in Table 5.5.

Areas under cast shadow on Findelengletscher show mean elevation differences of 1.98 m. This amounts approximately to the double of the elevation differences in transition areas (0.92 m) and the ternary of the elevation differences in fully illuminated areas (0.62 m).

The same trend can be seen for Adlergletscher. With mean elevation differences of 1.13 m for areas under cast shadow, 0.84 m in transition areas and 0.52 m in directly illuminated areas. The influence of weak illumination appears in rising STDVs and an increase in outlier occurrence shown by the Q95 values.

The negative effect of cast shadow on elevation data accuracy appears also over rock and snow covered rock as shown in Table 5.6. The mean values differ slightly

Table 5.5: Summary of elevation differences (ADP_2010 minus ALS_2010) for Findelen- and Adlergletscher under different illumnation conditions (0 - 15 Wh/m^2 = cast shadow, 15 - 85 Wh/m^2 = transition, 85 - 122 Wh/m^2 = direct illumination).

	Frequency [n]	**mean** [m]	**STDV** [m]	**RMSE** [m]	**Q95** [m]
Findelen cast shadow	20643	1.98	1.93	2.76	5.91
Findelen transition	2513060	0.92	0.64	1.15	1.56
Findelen direct illumination	722519	0.62	0.68	0.92	1.41
Adler cast shadow	32682	1.13	1.93	2.24	4.38
Adler transition	251873	0.84	0.90	1.23	1.97
Adler direct illumination	271553	0.52	0.76	1.16	1.36

for rock (0.98 m and 1.37 m) and very clearly for snow covered rock (0.71 m and 1.46 m). The STDVs and the Q95 increase also for areas under shadow. It can be seen that snow covered rock seems to be mapped more inaccurate than bare rock under cast shadow, whereas in contrary bare rock is more inaccurate in non-shady areas.

Table 5.6: Summary of elevation differences for the ADP_2010 and ALS_2010 DEMs for varying ground covers with and without shadow (0 - 15 Wh/m^2 = shadow, 15 - 122 Wh/m^2 = no shadow).

	Frequency [n]	**mean** [m]	**STDV** [m]	**RMSE** [m]	**Q95** [m]
Rock	3038	0.98	0.46	1.08	1.73
Rock shadow	2852	1.37	0.90	1.64	3.03
Snow covered rock	10639	0.71	0.48	0.85	1.37
Snow covered rock shadow	11149	1.46	1.38	2.01	3.87

Figure 5.7 shows the scatterplot of incoming potential solar radiation for each raster cell and the corresponding elevation difference. From Subfigure 5.7a, a spread of elevation differences in cast shadow (0 - 15 Wh/m^2) but no clear trend of elevation difference decrease towards the transition and directly illuminated area is visible.

Subfigure 5.7b shows a clear spread of elevation differences under cast shadow followed by smaller spreads in the transition area from 15 to 60 Wh/m^2). The trend is interrupted by outlier occurrences between 60 and 122 Wh/m^2. There are no signs of larger elevation spreads in the directly illuminated areas due to saturation effects from snow.

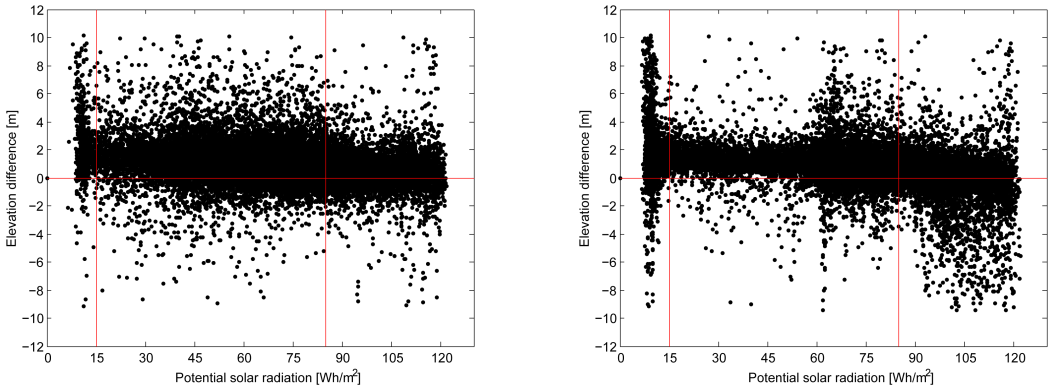

(a) Findelengletscher **(b)** Adlergletscher

Figure 5.7: Scatterplot of the elevation differences (ADP_2010 minus ALS_2010) and the potential solar radiation (0 - 15 Wh/m^2 = cast shadow, 15 - 85 Wh/m^2 = transition, 85 - 122 Wh/m^2 = direct illumination).

5.5 Glacier area changes

5.5.1 Findelen- and Adlergletscher (2005 - 2010)

In Table 5.7, the changes in glacier area for Findelen- and Adlergletscher are listed.

Table 5.7: Glacier area change from 2005 to 2010 for Findelen- and Adlergletscher. The glacier change in m^2 and % is relative to the glacier extent in 2005. Used glacier outlines are from the GLAXPO project.

Year	**Findelen**			**Adler**		
	Area [m^2]	change [m^2]	change [%]	Area [m^2]	change [m^2]	change [%]
2005	13'311'054			2263226		
2009	13'079'643	-231'411	-1.74	2'242'344	-20'882	-0.92
2010	13'036'838	-274'216	-2.06	2'234'955	-28'271	-1.24

The calculations show an area reduction of 2.06% for Findelengletscher and 1.24% for Adlergletscher during the period from 2005 to 2010. The decrease in glacier area is considerably higher for Findelen- than for Adlergletscher.

5.5.2 Upper Mattertal (2005 - 2009)

Table 5.8 shows the changes in glacier area for the glaciers in the upper Mattertal from 2005 to 2009.

Table 5.8: Glacier area change from 2005 to 2009 for each glacier in the upper Mattertal. The total shows the sum for all glaciers, except for (ø), which stands for the average value. Used glacier outlines are from the SGI_2003.

Glacier	**Area 2005** [m^2]	**Change** [m^2]	**Change** [%]
1. Grenz-Gorner	45'529'584	-1'091'302	-2.40
2. Zmutt	15'267'344	-170'742	-1.12
3. Findelen	14'650'330	-199'362	-1.36
4. Theodul	10'235'935	-245'371	-2.40
5. Zinal	10'024'398	-131'934	-1.32
6. Furgg	6'637'231	-173'517	-2.61
7. Schwarzberg	5'833'495	-165'342	-2.83
8. Melich	4'741'845	-65'186	-1.37
9. Hobärg	3'342'356	-77'097	-2.31
10. Hohwäng	2'335'440	-76'839	-3.29
11. Trift	2'178'392	-86'097	-3.95
12. Kin	2'157'379	-249'520	-11.57
13. Adler	2'090'840	-26'531	-1.27
14. Weingarten	1'905'358	-394'643	-20.71
15. Festi	1'835'196	-34'788	-1.90
16. Gabelhorn	1'800'674	-246'834	-13.71
17. Matterhorn	1'742'052	-248'461	-14.26
18. Längflue	1'734'767	-44'570	-2.57
19. Monte Rosa	1'489'231	-127'417	- 8.56
20. Arben	1'435'774	-5'352	-0.37
21. Manzettes	1'687'465	-199'271	-11.80
22. Bricola	1'122'557	-134'623	-11.99
23. Dent Blanche	1'102'459	-57'733	-5.24
24. Alphubel	1'074'442	-50'190	-4.67
25. Rothorn	943'110	-52'979	-5.62
Total	142'897'655	-4'355'504	-5.56 (ø)

The overall glacier area change amounts to -4'355'504 m^2 with a mean area change of -5.56% (2005 to 2009) and an annual area change of -1.4%.

5.6 Average thickness and volume changes

5.6.1 Findelen- and Adlergletscher (2005 - 2010)

Table 5.9 documents the average thickness and volume changes for Findelen- and Adlergletscher derived with ADP and ALS measurements.

Table 5.9: Average thickness and volume changes from 2005 to 2009/2010 for Findelen- and Adlergletscher. The systematic and stochastic uncertainties are considered in Table 5.13. Used glacier outlines are from the GLAXPO project.

	Period		**dh** [m]	**dV** [mio m^3]
Findelen-gletscher	ALS_2005_fin	ALS_2010	-3.66	-48.2
	ALS_2005_fin	ADP_2010	-2.84	-37.3
	ALS_2005_fin	ALS_2009	-2.88	-38.1
	ALS_2005_fin	swissALTI^{3D}_2009	-2.76	-36.4
Adler-gletscher	ALS_2005_fin	ALS_2010	-2.08	-4.6
	ALS_2005_fin	ADP_2010	-1.37	-3.1
	ALS_2005_fin	ALS_2009	-1.50	-3.4
	ALS_2005_fin	swissALTI^{3D}_2009	-1.27	-2.9

As can be seen from Table 5.9, the calculated glaciological changes vary between the different measurement methods. For both observation periods the changes derived from ALS measurements are larger than from ADP measurements. Similar differences in average thickness and volume changes can also be observed for Adlergletscher. Again, the changes derived from ALS measurements are larger than from ADP . The results under consideration of systematic and stochastic errors are discussed in Section 6.1.

In Figure 5.8, the elevation differences between the ADP and ALS DEMs for the years 2005, 2009 and 2010 are depicted. Differences between ADP and ALS DEMs show similar characteristics as the elevation differences from ADP_2010 minus ALS_2010 (Figure 5.4). Remarkable are the variations of elevation differences in the accumulation area of Findelengletscher, which are generally more negative for ALS than ADP.

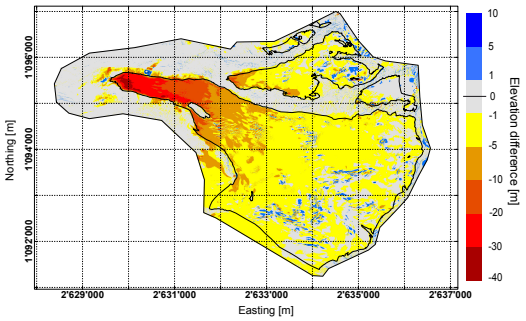

(a) ALS_2010 minus ALS_2005_fin

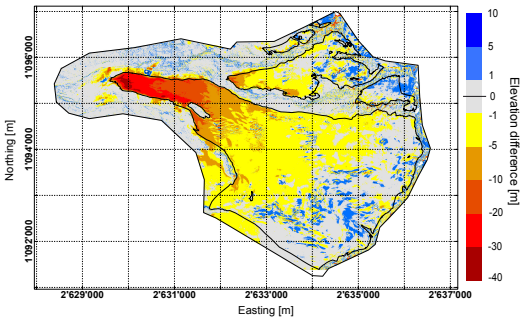

(b) ADP_2010 minus ALS_2005_fin

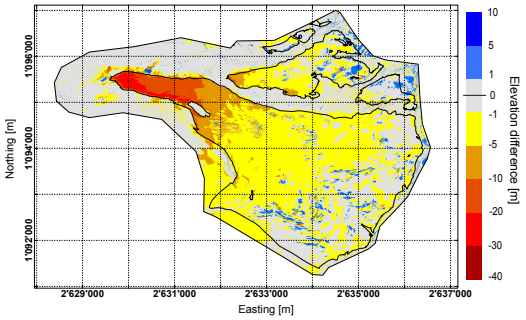

(c) ALS_2009 minus ALS_2005_fin

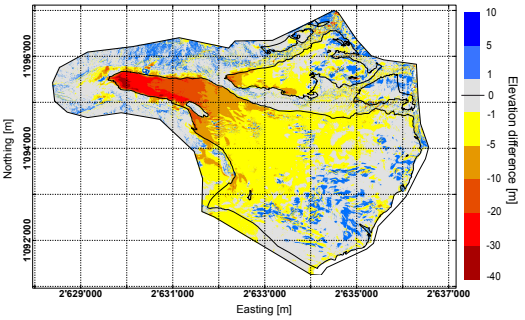

(d) ADP_2009 minus ALS_2005_fin

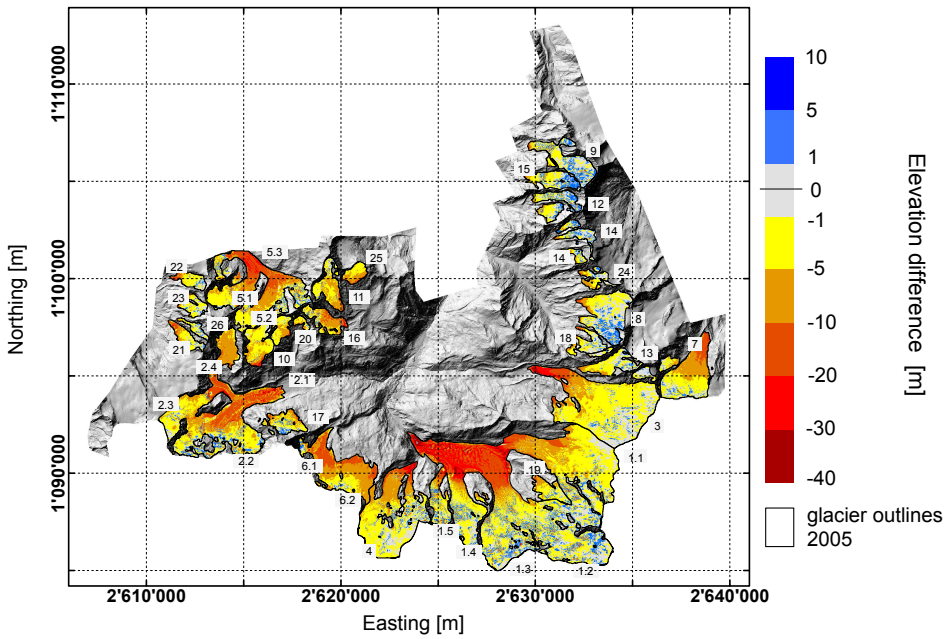

(e) swissALTI^{3D}_2009 minus ALS_2005. The numbers are the glacier IDs from Figure 2.4.

Figure 5.8: Elevation differences from ADP and ALS DEMs for the years 2005 to 2009 (c, d, e) and 2010 (a, b) for the glaciers in the study sites. The systematic and stochastic uncertainties are not applied.

5.6.2 Upper Mattertal (2005 - 2009)

In Figure 5.8e the elevation changes from 2005 to 2009 for the glaciers in the upper Mattertal are listed. Table 5.10 shows the respective average thickness and volume changes.

Table 5.10: Average thickness and volume changes from 2005 to 2009 for each glacier in the upper Mattertal. The systematic and stochastic uncertainties are considered in Table 5.14 and 5.15. Diff. co-reg. describes the differences between co-registered and not co-registered DEMs. Positive differences indicate that the average thickness and volume changes are smaller for the co-registered DEMs than for the not co-registered DEMs. Used glacier outlines are from the SGI_2003.

Glacier	**dh** [m]	diff. co-reg. [m]	**dV** [mio m^3]	diff. co-reg. [mio m^3]
1. Grenz-Gorner	-5.51	0.19	-248.02	8.33
2. Zmutt	-6.17	-0.18	-93.74	-2.69
3. Findelen	-3.65	0.21	-53.17	3.01
4. Theodul	-3.91	0.12	-39.53	1.26
5. Zinal	-6.43	-0.05	-64.03	-0.45
6. Furgg	-7.30	-0.19	-47.84	-1.24
7. Schwarzberg	-5.18	-0.25	-29.78	-1.47
8. Melich	-0.98	0.53	-4.60	2.48
9. Hobärg	-0.76	0.47	-2.51	1.55
10. Hohwäng	-4.68	-0.09	-10.74	-0.22
11. Trift	-4.62	-0.38	-9.86	-0.81
12. Kin	-0.83	0.71	-1.69	1.44
13. Adler	-2.07	0.59	-4.30	1.22
14. Weingarten	-1.33	0.88	-2.26	1.51
15. Festi	-0.94	0.77	-1.70	1.41
16. Gabelhorn	-6.45	-0.73	-10.82	-1.22
17. Matterhorn	-3.68	-0.24	-5.96	-0.38
18. Längflue	-2.09	0.55	-3.57	0.95
19. Monte Rosa	-3.15	0.60	-4.50	0.86
20. Arben	-4.34	-0.30	-6.22	-0.43
21. Manzettes	-3.62	0.71	-2.30	0.75
22. Bricola	-4.31	0.71	-4.55	0.78
23. Dent Blanche	-2.73	0.79	-2.93	0.84
24. Alphubel	-2.54	0.64	-2.66	0.67
25. Rothorn	-5.84	-0.23	-5.35	-0.20
Mean	-3.72	0.26		
Total			-665.22	18.40

All glaciers together underwent an average thickness change of -3.72 m. Without co-registration the average thickness change would be 0.26 m larger (= -3.98 m). The overall volume decrease amounts to -665.22 mio m^3. With no applied co-registration the volume decrease would be 18.40 mio m^3 higher (= -683.62 mio m^3).

5.7 Systematic and stochastic uncertainties

5.7.1 Systematic uncertainties

The systematic uncertainty ($\overline{dh}$ from the co-registration) between ADP_2010 and ALS_2010 is 0.57 m and between swissALTI^{3D}_2009 and ALS_2005 0.55 m.

5.7.2 Stochastic uncertainties

Table 5.11 shows that the stochastic uncertainties between the simultaneous DEMs are largest over unglaciated terrain and smallest over glaciated terrain (*Note*: DEMs from the same day, therefore very small stochastic uncertainties). With the conservative method of 100 m raster cell distances to avoid autocorrelation effects, the stochastic uncertainty increases by the factor of 10.

Table 5.11: Stochastic uncertainties derived with different approaches for ADP_2010 and ALS_2010 on and around Findelengletscher. See Subsection 4.9.2 for explanations about the stochastic uncertainty calculations.

Glacier	$\pm\sigma_{\textbf{unglaciated}}$ [m]	$\pm\sigma_{\textbf{glaciated}}$ [m]	$\pm\sigma_{\textbf{glaciated}}$ with shadow [m]
Findelen (10 m)	0.005	0.002	0.003
Findelen (100 m)	0.05	0.02	0.03

Table 5.12:

Stochastic uncertainties derived with different mthods for swissALTI^{3D}_2009 and ALS_2005 for each glacier in the upper Mattertal. See Subsection 4.9.2 for explanations about the stochastic uncertainty calculations.

Glacier	$\pm\sigma_{\textbf{unglaciated}}$ [m]	$\pm\sigma_{\textbf{glaciated}}$ [m]	$\pm\sigma_{\textbf{glaciated}}$ with shadow [m]
1. Grenz-Gorner	0.015	0.012	0.018
2. Zmutt	0.015	0.015	0.023
3. Findelen	0.015	0.014	0.019
4. Theodul	0.015	0.016	0.025
5. Zinal	0.015	0.019	0.028
6. Furgg	0.015	0.016	0.024
7. Schwarzberg	0.015	0.019	0.026
8. Melich	0.015	0.014	0.020
9. Hobärg	0.015	0.018	0.030
10. Hohwäng	0.015	0.029	0.034
11. Trift	0.015	0.023	0.036
12. Kin	0.015	0.023	0.038
13. Adler	0.015	0.020	0.031
14. Weingarten	0.015	0.026	0.041
15. Festi	0.015	0.025	0.038
16. Gabelhorn	0.015	0.038	0.061
17. Matterhorn	0.015	0.031	0.043
18. Längflue	0.015	0.025	0.036
19. Monte Rosa	0.015	0.028	0.043
20. Arben	0.015	0.033	0.045
21. Manzettes	0.015	0.040	0.050
22. Bricola	0.015	0.045	0.059
23. Dent Blanche	0.015	0.030	0.040
24. Alphubel	0.015	0.029	0.035
25. Rothorn	0.015	0.036	0.043
Mean	0.015	0.025	0.037

For the stochastic uncertainty estimations of the glaciological changes in the upper Mattertal (Table 5.12), 10 m raster cell distances to avoid autocorrelation effects, are chosen. The mean values are now smallest for the stochastic uncertainty derived from unglaciated terrain and highest for the method considering the influence of shadow.

The stochastic uncertainties are smallest for the method considering unglaciated terrain and largest for glaciated with shadow. This is due to the complexity of the applied methods.

5.8 Average thickness and volume changes with applied systematic and stochastic uncertainties

Table 5.13: Average thickness and volume changes from 2005 to 2009/2010 for Findelen- and Adlergletscher with applied systematic uncertainties.

	Period		**dh** + ϵ [m]	**dV** + ϵ [mio m^3]
Findelen-gletscher	ALS_2005_fin	ALS_2010	-3.34	-44.03
	ALS_2005_fin	ADP_2010	-3.41	-44.86
	ALS_2005_fin	ALS_2009	-2.37	-31.45
	ALS_2005_fin	swissALTI^{3D}_2009	-2.21	-29.08
Adler-gletscher	ALS_2005_fin	ALS_2010	-1.76	-3.88
	ALS_2005_fin	ADP_2010	-1.94	-4.29
	ALS_2005_fin	ALS_2009	-0.99	-2.26
	ALS_2005_fin	swissALTI^{3D}_2009	-0.72	-1.66

The comparison of Tables 5.9 and 5.13 shows that with the application of systematic uncertainties, the deviations of the glaciological changes between ADP and ALS can be considerably reduced.

Tables 5.14 and 5.15 show the average thickness and volume changes for all glaciers in the upper Mattertal with applied systematic and stochastic uncertainties.

Table 5.14: Average thickness changes from 2005 to 2009 with applied systematic and stochastic uncertainties for the glaciers in the upper Mattertal. See Section 4.9 for explanations about the systematic and stochastic uncertainty calculations.

Glacier	dh [m]	ϵ [m]	dh + ϵ [m]	dh + ϵ $\pm\sigma_{\text{unglaciated}}$ [m]	dh + ϵ $\pm\sigma_{\text{glaciated}}$ [m]	dh + ϵ $\pm\sigma_{\text{glaciated with shadow}}$ [m]
1. Grenz-Gorner	-5.51	0.55	-4.96	-4.96 ±0.015	-4.96 ±0.012	-4.96 ±0.018
2. Zmutt	-6.17	0.55	-5.62	-5.62 ±0.015	-5.62 ±0.015	-5.62 ±0.023
3. Findelen	-3.65	0.55	-3.10	-3.10 ±0.015	-3.10 ±0.014	-3.10 ±0.019
4. Theodul	-3.91	0.55	-3.36	-3.36 ±0.015	-3.36 ±0.016	-3.36 ±0.025
5. Zinal	-6.43	0.55	-5.88	-5.88 ±0.015	-5.88 ±0.019	-5.88 ±0.028
6. Furgg	-7.30	0.55	-6.75	-6.75 ±0.015	-6.75 ±0.016	-6.75 ±0.024
7. Schwarzberg	-5.18	0.55	-4.63	-4.63 ±0.015	-4.63 ±0.019	-4.63 ±0.026
8. Melich	-0.98	0.55	-0.43	-0.43 ±0.015	-0.43 ±0.014	-0.43 ±0.020
9. Hobärg	-0.76	0.55	-0.21	-0.21 ±0.015	-0.21 ±0.018	-0.21 ±0.030
10. Hohwäng	-4.68	0.55	-4.13	-4.13 ±0.015	-4.13 ±0.029	-4.13 ±0.034
11. Trift	-4.62	0.55	-4.07	-4.07 ±0.015	-4.07 ±0.023	-4.07 ±0.036
12. Kin	-0.83	0.55	-0.28	-0.28 ±0.015	-0.28 ±0.023	-0.28 ±0.038
13. Adler	-2.07	0.55	-1.52	-1.52 ±0.015	-1.52 ±0.020	-1.52 ±0.031
14. Weingarten	-1.33	0.55	-0.78	-0.78 ±0.015	-0.78 ±0.026	-0.78 ±0.041
15. Festi	-0.94	0.55	-0.39	-0.39 ±0.015	-0.39 ±0.025	-0.39 ±0.038
16. Gabelhorn	-6.45	0.55	-5.90	-5.90 ±0.015	-5.90 ±0.038	-5.90 ±0.061
17. Matterhorn	-3.68	0.55	-3.13	-3.13 ±0.015	-3.13 ±0.031	-3.13 ±0.043
18. Längflue	-2.09	0.55	-1.54	-1.54 ±0.015	-1.54 ±0.025	-1.54 ±0.036
19. Monte Rosa	-3.15	0.55	-2.60	-2.60 ±0.015	-2.60 ±0.028	-2.60 ±0.043
20. Arben	-4.34	0.55	-3.79	-3.79 ±0.015	-3.79 ±0.033	-3.79 ±0.045
21. Manzettes	-3.62	0.55	-3.07	-3.07 ±0.015	-3.07 ±0.040	-3.07 ±0.050
22. Bricola	-4.31	0.55	-3.76	-3.76 ±0.015	-3.76 ±0.045	-3.76 ±0.059
23. Dent Blanche	-2.73	0.55	-2.18	-2.18 ±0.015	-2.18 ±0.030	-2.18 ±0.040
24. Alphubel	-2.54	0.55	-1.99	-1.99 ±0.015	-1.99 ±0.029	-1.99 ±0.035
25. Rothorn	-5.84	0.55	-5.29	-5.29 ±0.015	-5.29 ±0.036	-5.29 ±0.043
Mean	-3.72	0.55	**-3.17**	-3.17 ±0.015	-3.17 ±0.025	**-3.17 ±0.037**

Table 5.15: Volume changes from 2005 to 2009 with applied systematic and stochastic uncertainties for the glaciers in the upper Mattertal. See Section 4.9 for explanations about the systematic and stochastic uncertainty calculations.

Glacier	dh [mio m^3]	ϵ [mio m^3]	dh + ϵ [mio m^3]	dh + ϵ $\pm\sigma_{\text{unglaciated}}$ [mio m^3]	dh + ϵ $\pm\sigma_{\text{glaciated}}$ [mio m^3]	dh + ϵ $\pm\sigma_{\text{glaciated with shadow}}$ [mio m^3]
1. Grenz-Gorner	-248.02	100.16	-147.86	-147.86 ±0.683	-147.86 ±0.546	-147.86 ±0.820
2. Zmutt	-93.74	33.58	-60.16	-60.16 ±0.229	-60.16 ±0.229	-60.16 ±0.351
3. Findelen	-53.17	32.23	-20.94	-20.94 ±0.220	-20.94 ±0.205	-20.94 ±0.278
4. Theodul	-39.53	22.52	-17.01	-17.01 ±0.154	-17.01 ±0.164	-17.01 ±0.256
5. Zinal	-64.03	22.05	-41.98	-41.98 ±0.150	-41.98 ±0.190	-41.98 ±0.281
6. Furgg	-47.84	14.60	-33.24	-33.24 ±0.100	-33.24 ±0.106	-33.24 ±0.159
7. Schwarzberg	-29.78	12.83	-16.95	-16.95 ±0.088	-16.95±0.111	-16.95 ±0.152
8. Melich	-4.60	10.43	5.83	5.83 ±0.071	5.83 ±0.066	5.83 ±0.095
9. Hobärg	-2.51	7.35	4.84	4.84 ±0.050	4.84 ±0.060	4.84 ±0.100
10. Hohwäng	-10.74	5.14	-5.60	-5.60 ±0.035	-5.60 ±0.068	-5.60 ±0.079
11. Trift	-9.86	4.80	-5.06	-5.06±0.033	-5.06 ±0.050	-5.06 ±0.078
12. Kin	-1.69	4.74	3.05	3.05 ±0.032	3.05 ±0.050	3.05 ±0.082
13. Adler	-4.30	4.60	0.30	0.30 ±0.031	0.30 ±0.042	0.30 ±0.065
14. Weingarten	-2.26	4.20	1.94	1.94 ±0.029	1.94 ±0.050	1.94 ±0.078
15. Festi	-1.70	4.04	2.34	2.34 ±0.028	2.34 ±0.046	2.34 ±0.070
16. Gabelhorn	-10.82	3.96	-6.86	-6.86 ±0.027	-6.86 ±0.068	-6.86 ±0.110
17. Matterhorn	-5.96	3.83	-2.13	-2.13 ±0.026	-2.13 ±0.054	-2.13 ±0.075
18. Längflue	-3.57	3.82	0.25	0.25 ±0.026	0.25 ±0.043	0.25 ±0.062
19. Monte Rosa	-4.50	3.27	-1.23	-1.23 ±0.022	-1.23 ±0.042	-1.23 ±0.064
20. Arben	-6.22	3.16	-3.06	-3.06 ±0.022	-3.06 ±0.047	-3.06 ±0.065
21. Manzettes	-4.89	3.49	-1.40	-1.40 ±0.025	-1.40 ±0.067	-1.40 ±0.084
22. Bricola	-4.55	2.47	-2.08	-2.08 ±0.017	-2.08 ±0.051	-2.08 ±0.066
23. Dent Blanche	-2.93	2.43	-0.50	-0.50 ±0.017	-0.50 ±0.033	-0.50 ±0.044
24. Alphubel	-2.66	2.36	-0.30	-0.30 ±0.016	-0.30 ±0.031	-0.30 ±0.038
25. Rothorn	-5.35	2.07	-3.28	-3.28 ±0.014	-3.28 ±0.034	-3.28 ±0.041
Total sum	-665.22	314.13	**-351.09**	-351.09 ±0.086	-351.09 ±0.098	**-351.09 ±0.144**

Chapter 6

Discussion

6.1 Glaciological changes in the upper Mattertal from 2005 to 2009 with applied systematic and stochastic uncertainties

One objective of the present master's thesis is to quantify the glaciological changes from 2005 to 2009 in the upper Mattertal. From the differencing of the DEMs, a clear trend towards glacier retreat is visible.

For the upper Mattertal the total glacier area change is -4'355'504 m^2, which means an average area loss of -5.56% per glacier. The mean average thickness change of all glaciers amounts to -3.17 $\pm$0.037 m and the total volume change to -351.09 $\pm$0.144 mio m^3 (Tables 5.14 and 5.15).

The stochastic uncertainties stem from the calculation method that considers potential solar radiation classes over glaciated terrain. The justification follows in Subsection 6.2.3.

6.1.1 Average thickness changes

The interdependency between the average thickness changes and the glacier area is depicted in Figure 6.1. It can be seen, that small- and large-area glaciers do not show strictly the same trend. Large-area glaciers tend to have average thickness changes of around -4 m to -7 m, whereas for small-area glaciers the average thickness changes amount from -1 m to -7 m.

Applying the systematic uncertainty, leads for every glacier to an average thickness change reduction of 0.55 m, resulting in final average thickness changes of close to 0 m for some glaciers (Table 5.14). This is the case for Hobärg-, Kin-, Festi- and Melichgletscher. Due to a lack of reference data, it can not be shown, how representative these average thickness change of close to 0 are.

It becomes clear that for glaciers with smaller average thickness changes, the magnitude of the systematic shift has a large influence on the final glaciological change.

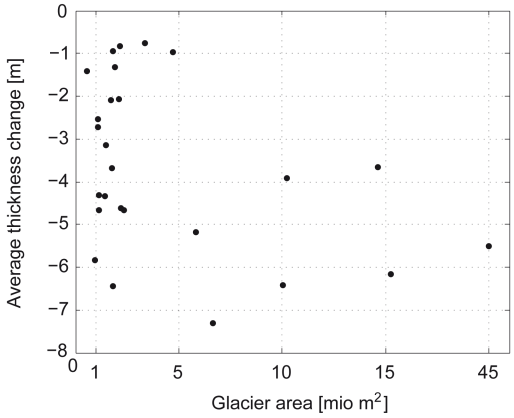

Figure 6.1: Scatterplot of average thickness changes (2005 - 2009) and the area.

6.1.2 Volume changes

Similar to the average thickness changes, no clear trend of volume changes for small- and large-area glaciers becomes visible (Table 5.15). Generally, glaciers with larger areas have higher volume losses, with the exception of some glaciers that show a much larger volume loss than glaciers with similar areas. These are for example Howäng-, Trift- and Gabelhorngletscher.

When applying the systematic uncertainties to the volume changes, a different trend than for the average thickness changes results. For certain glaciers the volume change turns from negative to positive, indicating volume gain instead of volume loss. Affected glaciers are Melich, Hobärg, Kin, Adler, Weingarten, Festi and Längflue. The representativity of these positive volume changes can not be evaluated against independent data for all concerned glaciers. For Adlergletscher there are reference values from ALS_2005_fin - ALS_2009/ADP_2009 available (Table 5.13). These values show a clear volume decrease after the application of systematic uncertainties. Therefore, the results from Table 5.15 that show volume gain, have to be interpreted with caution.

Looking at the total sum of the glacier volume changes in the upper Mattertal, it becomes clear how important it is to consider uncertainties. Especially the systematic uncertainties have a large effect on the final volume changes. The total glacier volume loss in the upper Mattertal from 2005 to 2009 decreased by 47.23% after applying the systematic uncertainties.

6.2 Uncertainty assessment

6.2.1 Systematic uncertainties from the co-registration

The overall elevation bias ($\overline{dh}$) from the co-registration is employed as the systematic uncertainty between two DEMs. The importance of the co-registration for glaciological change detection is emphasized e.g. in Cook et al. (2012), Karimi et al. (2012) and Zemp et al. (2013). Karimi et al. (2012) state that for a reliable glaciological change detection, it is essential that the DEMs are accurately adjusted. If not, one is misleaded to wrong estimates of glacier volume changes. Furthermore Cook et al. (2012) emphasize that without a horizontal co-registration of the DEMs, one can not be sure whether the greater vertical bias with increasing slope is due to data error or due to greater elevation differences caused by mis-alignment.

The $\overline{dh}$ between ADP_2010 and ALS_2010 amounts to 0.57 m which is, considering the fact that the DEMs were recorded on the same day, a surprisingly high overall elevation bias. It has to be assumed that some uncertainties are introduced, which will be discussed in Section 6.4.

The $\overline{dh}$ between ALS_2005 and swissALTI^{3D}_2009 is 0.55 m. This can partly be explained with a snowfall event leading to a snow cover of 0.47 m in this area (Joerg et al., 2012). Other possible reasons for systematic elevation shifts are also discussed in Section 6.4.

On the example of Table 5.9 and 5.13, it is shown that by applying the systematic uncertainties, the deviations between the final glaciological changes derived with the two acquisition methods can be reduced. Before applying the systematic uncertainties, the average thickness changes calculated from ALS_2005_fin minus ALS_2010 and ADP_2010 are -3.66 m and -2.84 m respectively. After applying the systematic uncertainties, the average thickness changes are -3.34 m and -3.41 m. This demonstrates impressively the importance of the systematic uncertainty assessment.

6.2.2 Potentials and limitations of the co-registration

Potentials

The co-registration file by Lindenmann (2012) is validated by artificially shifting the ALS_2010 DEM 4 m in x- and 4 m in y-direction. Thereby, the curve fit equation from the co-registration file detected the shift with an accuracy of $\pm$0.2 m.

The effect of the co-registration can be demonstrated with Figure 5.5. The very accurate areas below 2000 m.a.s.l., which were measured with ALS for both DEMs, show only minor deviations in elevation differences for the co-registered DEMs (light gray, -1 to 1 m; Subfigure 5.5a). For the not co-registered DEMs there are positive elevation differences visible on the western side of the upper Mattertal (blue, 1 - 5 m; Subfigure 5.5b).

The quantitative deviations of average thickness and volume changes between co-registered and not co-registered DEMs are shown in Table 5.10 (column diff. co-reg.). Thereby, a clear interdependency between the differences from co-registered minus not co-registered DEMs and the glacier's aspect becomes visible.

For glaciers on the eastern side of the upper Mattertal, the deviations of the

glaciological changes from co-registered and not co-registered DEMs are generally positive. The only exception on the eastern side, which shows a negative difference is Schwarzberggletscher. This can also be seen from the artefacts in Subfigure 5.5a. The same trend becomes visible on the western side of the upper Mattertal. Glaciers with aspects towards east show negative differences for glaciological changes from co-registered minus not co-registered DEMs, whereas glaciers with western aspects have positive differences (Glacier des Bricola, Glacier des Manzettes, Glacier de la Dent Blanche; column diff. co-reg. in Table 5.10).

In case of a relative horizontal shift between two DEMs, the aspect of the glacier contributes to varying glaciological changes for co-registered and not co-registered DEMs. Expressed in numbers this means that not co-registered DEMs have on average a 7.00 % higher average thickness change and a overall 2.77 % larger volume change. These deviations indicate, that the effect size of the co-registration is large and considerable.

Limitations

Results from the co-registration are an analytical solution of a 3D-shift vector between two DEMs. Bolch et al. (2011) found that the corrections of the systematic shifts, determined with the co-registration, can in some cases even worsen the accuracy of the elevation data in DEMs. This is especially the case when there are complex and non-linear distortions or tilts present in the DEMs. One DEM can then not completely be adjusted relative to the other.

The outcome of the co-registration is strongly based on the choice of the unglaciated terrain. For varying unglaciated co-registration areas, different solutions will result. Therefore, a differentiated consideration of suitable unglaciated areas for the co-registration is advisable.

Co-registration areas should be large enough to be representative and should contain a regular distribution of the terrain aspect. Furthermore slopes flatter than 10° should be removed as the relation $\frac{dh}{tan(\alpha)}$ becomes infinite for $\alpha = 0$ and noise in dh is too much exaggerated for small slopes (Kääb, 2005). Additionally, the raster cell size of DEMs to be co-registered needs to be appropriate to detect horizontal shifts. If the raster cell size is too large, small-scale patterns that indicate horizontal shifts (e.g crevasses, moraines and ridges) could disappear within a large raster cell.

Some of the above mentioned conditions are in direct contradiction to the actual purpose of the co-registration. Namely, if the DEMs are thought for glaciological applications, the unglaciated terrain should also be representative for the glaciated terrain. This would imply unglaciated terrain characteristics, which resemble the ones of glaciers, in other words, a tendency towards flatter slopes and not rough but rather smooth morphological features. The representativity of the bedrock surrounding the glacier for statistical uncertainty analysis is also considered in Zemp et al. (2013). If the systematic elevation bias is corrected for glaciated terrain, which does not resemble the stable, unglaciated terrain, a falsification of the elevation values in the DEMs would result. Thus, the co-registration could contribute to plotting errors cf. Zemp et al. (2013).

When conducting a co-registration, the above mentioned factors should carefully be taken into account in order to avoid misleading outcomes from the co-registration.

6.2.3 Stochastic uncertainties

Effect of shadow on elevation data accuracy

In many glaciological publications performed with ADP shadow is mentioned as a weak point, leading to a decrease in elevation data accuracy. The shadow analysis performed in this thesis considers the influence of shadow on elevation data accuracy by comparing areas under shadow with directly illuminated areas (Subsecion 4.6.1).

The findings of the effect of shadow on elevation data accuracy, agree well with the results from another study documenting the effect of shadow on elevation data accuracy. Bühler et al. (2012) also compared elevation data from ALS with ADP data measured with the ADS80 sensor. They observed higher elevation differences in areas under shadow, emphasizing the shortcomings of ADP. The differences of RMSE for debris and shady debris amounts to 0.40 m, and for slight snow and shady slight snow to 0.29 m (Bühler et al., 2012).

Results from the present thesis show RMSE differences of 0.56 m for rock and shady rock and 1.16 m for shady and non-shady snow covered rock. The distinction between debris in Bühler et al. (2012) and rock in this study is not clear, however the trend points towards an increase in RMSE differences for areas under shadow compared to non-shady areas.

Remarkable is the fact that the RMSE differences are larger for snow covered rock than for rock. Considering the weaknesses of ADP, one could assume that areas with more contrast such as snow covered rock (consisting of darker and brighter pixels) perform better under shadow than areas with lower contrast such as rock (consisting only of darker pixels).

For directly illuminated areas, this assumption is confirmed, since snow covered rock has lower mean elevation differences than rock, whereas in areas of shadow, snow covered rock shows larger mean elevation differences than rock and also higher STDVs. The better contrast of partly snow covered rock seems to disappear in shady areas.

Stochastic uncertainties from different ground cover and terrain characteristics

Three different methods to calculate stochastic uncertainties are introduced in Subsection 4.9.2 and the respective stochastic uncertainties for each glacier in the upper Mattertal are shown in Tables 5.11 and 5.12.

For the simultaneous DEMs over Findelengletscher, the stochastic uncertainties derived from unglaciated terrain are 0.005 m and from glaciated terrain 0.002 m. This agrees well with the findings documented in Rolstad et al. (2009), who stated that estimated stochastic uncertainties are largest for unglaciated bedrock, which is because of the rougher surface characteristics and the steeper slopes than on glaciated terrain.

The mean stochastic uncertainty derived from unglaciated terrain (0.015 m) for the period 2005 to 2009 in the upper Mattertal is in contrast smaller than the mean of all individual stochastic uncertainties derived from glaciated terrain (0.025 m). This has to a large extent to do with the sample size, which is smaller for the unglaciated areas (= co-registration areas) than for each individual glacier. The two above discussed methods are widely used for stochastic uncertainty estimations in glaciology.

The third method to estimate stochastic uncertainties applied in this thesis does consider potential solar radiation classes over glaciated terrain. This is motivated by the fact that shadow has a large influence on resulting elevation data accuracy. For every raster cell of the glacier, the potential solar radiation during the time of elevation data measurement is determined and classified. The glaciological changes are then set into relation with the potential solar radiation. Thereby, the decreased accuracy of elevation differences in areas of cast shadow can be considered, which is not possible with the two above discussed methods. This last method is the most sophisticated, of the stochastic uncertainty estimations applied in this thesis, and can therefore be recommended for further glaciological studies.

6.3 Comparison with glaciological changes from other studies

In order to find out whether the derived glaciological changes from the present thesis are valid and representative, they are compared with glaciological changes from other studies.

Glacier area changes

The glacier area change (Section 5.5) is exclusively depending on the used glacier outlines. The mean glacier area change of 5.56% for the glaciers in the upper Mattertal (SGI_outlines) is relatively high. This is because of some glaciers that show large changes and thus influence the average glacier area change.

The area changes for Findelen- and Adlergletscher do approximately correspond between the SGI_outlines and the GLAXPO_outlines. The differences appear probably due to the varying outline resolutions (SGI_outlines are derived from 30 x 30 m raster data) and unequal glacier extents (Findelengletscher contains the area around Stockhorn and Stockhornpass in SGI_outlines, but not in the GLAXPO_outlines).

Average thickness and volume changes

Joerg et al. (2012) used the ALS_2005_fin DEM as a basis and calculated changes with the ALS_2009 and ALS_2010 for the respective periods. To evaluate the representativity of the glaciological changes from the ADP DEMs, the ALS_2009 and ALS_2010 are in that case replaced by the swissALTI^{3D}_2009 and the ADP_2010 DEMs. Thus for the period 2005 to 2009/2010 there are calculated glaciological changes from two independent DEMs available (Table 5.13).

For the period 2005 to 2010 the average thickness change with applied systematic uncertainties from ALS and ADP differ by 0.07 m for Findelengletscher and 0.18 m for Adlergletscher. The volume changes deviate by 0.83 mio m^3 and 0.41 mio m^3 respectively (Table 5.13).

From 2005 to 2009 the deviations are larger between ALS and ADP. The differences of the average thickness changes are 0.16 m for Findelengletscher and 0.27 m for Adlergletscher with repsective differences in volume changes of -2.37 mio m^3 and 0.60 mio m^3. swissALTI^{3D} was recorded on September 7, 2009, thus three weeks earlier than the end of the hydrological year, which leads to reduced glaciological changes compared to the ALS_2009 DEM (recorded on October 4, 2009).

The comparison from Table 5.13 yields that the ADP DEMs show good agreement with the ALS DEMs, which have already proven to be very accurate. Based on these findings, the glaciological changes for the upper Mattertal derived from ALS_2005 and swissALTI^{3D}_2009 can be assumed as valid and representative.

Looking at the distribution of the elevation differences in Figure 5.8, the same trend as for the elevation differences of ADP_2010 minus ALS_2010 becomes visible. Elevation differences for 2005 to 2009 and 2010 from ADP (Subfigures 5.8b and 5.8d) are by trend more positive in the accumulation area than for ALS. This leads to a smaller elevation differences compared with ALS. ADP shows large-scale elevation differences of around -1 to 1 m (light gray) and even above 1 m (blue).

Thickness changes from ALS indicate a decrease for the accumulation area of below -1 m (yellow). The rather unrealistic positive elevation differences from 2005 to 2009/2010 in the accumulation area indicate that ADP tends to have difficulties with image correlation in areas with lower contrast, such as the accumulation area on Findelengletscher.

Unfortunately, the glaciological changes for the upper Mattertal from 2005 to 2009 can not be compared with other studies for the same periods.

Farinotti et al. (2009) investigated area and volume changes of large swiss glaciers for different periods. They calculated a volume change of 50 mio m^3 for Findelengletscher from 1995 to 1999 (1.89 $\pm$0.47 km^3 - 1.84 $\pm$0.48 km^3). A change of 50 mio m^3 over four years is a lot more than the calculated changes in this thesis. The volume losses of -31.45 mio m^3 (ALS) and -29.08 mio m^3 (ADP) derived from the GLAXPO_outlines as well as -32.23 mio m^3 from the SGI_outlines, are much smaller than the volume losses calculated by Farinotti et al. (2009). In the 1990s, Findelen- and Adlergletscher separated, thus it could be that the volume changes from Adlergletscher are also contained in the volume changes of Findelengletscher calculated by Farinotti et al. (2009).

A more meaningful comparison would be to look at the average thickness changes per year (dh/a).

Table 6.1: Average thickness change per year for Findelengletscher.
[1)] *dh* from 1995 to 1999 is calculated by dV/S from Farinotti et al. (2009).

Period	**dh** [m]	**dh/a** [m]	**Remarks**
1995 - 1999	-2.64[1)]	-0.66	Farinotti et al. (2009)
ALS_2005_fin - ALS_2009	-2.37	-0.59	GLAXPO_outlines
ALS_2005_fin - ADP_2009	-2.29	-0.55	GLAXPO_outlines
ALS_2005 - swissALTI^{3D}_2009	-3.10	-0.77	SGI_outlines

Table 6.1 shows, that the average thickness changes per year are all approximately in the same range except for the upper Mattertal calculations from swissALTI^{3D}_2009 minus ALS_2005. This difference can partly be attributed to the larger area of Findelengletscher in the SGI_outlines and the fact that ALS_2005 consists of data from two measurement campaigns (15.-17.07.2005 and 28.-30.10.2005). Overall the glaciological changes show good agreement between the different DEMs.

The observation periods from 1995 to 1999 and 2005 to 2009 would fit well into the investigated periods in "Changes in area and volume of all Swiss glaciers over the last 25 years" based on the DHM25 (1985) and swissALTI^{3D}_2009 by Fischer, Huss and Hölzle that is announced but not yet published. With that study the glaciological changes from this thesis could be evaluated.

6.4 Methodological limitations

6.4.1 Data processing

According to Zemp et al. (2013) sources of potential errors in elevation data can be divided into sighting and plotting processes. Errors in the ALS DEMs that are related to the measurement process are documented in Joerg et al. (2012). These can originate from the platform, the sensor and the interference with the atmosphere. Plotting errors stem from the digital representation of elevation data and include errors from georeferencing, projection, co-registration and sampling density.

In this study, possible plotting errors can result from a number of different processing steps.

The coordinate transformation with the "ReframeReprojector" could lead to systematic uncertainties. The ADP DEM was already available in CH1903+ LV95 LHN95, whereas planimetric and altimetric reference frames of all ALS DEMs are reprojected from LV03 LN02 to LV95 LHN95. For swissALTI^{3D}_2009, the coordinate transformation comprised only the reprojection of the altimetric reference frame. It is not clear whether the direct coordinate transformation during DEM generation, the combined planimetric and altimetric coordinate transformation or only the altimetric coordinate transformation lead to differing elevation values.

The coordinate transformation could therefore be a possible reason for the relatively high systematic elevation shifts resulting from the co-registration for all DEMs.

The Resampling tool in ArcGIS with the additional snap environment is based on an interpolation process. What exactly happens to the elevation data, especially when snapping remains unknown. This processes resembles a black box and unknown uncertainties are possibly introduced.

6.4.2 Uncertainty assessment

The potential solar radiation for the upper Mattertal is modeled with the Area Solar Radiation tool. Due to performance reasons the raster cell size is chosen as 10 x 10 m. Since there is no orthophoto available for September 7, 2009, the same potential solar radiation classes as for the analysis over Findelengletscher on the September 29, 2010 are chosen. These PSR classes are obviously based on the potential solar radiation from another day and thus derived from different azimuth and zenith angles.

Further uncertainties result from the diffuse, non-direct sources of radiation. The Area Solar Radiation tool considers diffuse radiation but especially in high-mountain environments the diffuse radiation is very complex and influences the radiation that is received at the sensor (Giles, 2001).

For the calculation of the stochastic uncertainties, the distance of independence of the raster cells is assumed as 10 m (Koblet et al., 2010). This could be done without assumption but based on an autocorrelation analysis as suggested in Rolstad et al. (2009). With their approach, the stochastic errors would prove more realistic and would not be based on assumed values.

6.4.3 Glaciological change calculations

There are a number of reasons for differing glaciological changes between DEMs from the same year.

One could be the differences between the used glacier outlines. For the detailed analysis of Findelen- and Adlergletscher the outlines are from the GLAXPO project whereas the outlines used for the upper Mattertal are from the SGI_2003. Glacier masks and areas should be kept consistent within geodetic analyses (Zemp et al., 2013).

A second reason could stem from the fact that the derivation of the SGI_2009 outlines from the original SGI_2003 outlines based on orthophotos, is complicated. This is the case as some glaciers are under shadow in the orthophoto and thus a visual distinction of the glacier from unglaciated terrain is difficult. This fact hinders the glacier change assessment for Kin-, Weingarten-, Gabelhorn- and Matterhorngletscher from the orthophoto.

A third reason for differing glaciological changes could be because some glaciers, such as the Glacier des Manzettes and the Glacier des Bricola are only available in the orthophoto from 2010 (but 2009 required). Thus the adjusted glacier outlines are not exactly the ones from 2009.

6.5 Suitability of airborne digital photogrammetry and airborne laser scanning digital elevation models for applications in glaciology

6.5.1 Advantages and disadvantages of each method

Aspects from Table 2.2, which are identified as either advantages or disadvantages of one method are discussed in the following Subsection.

Number of flight strips, costs and density of measurements

The ADP_2010 DEM was generated from one image strip whereas the ALS_2010 DEM consists of approximately 30 flight strips that were recorded over 4 hours. After Joerg and Zemp (2014), the price of an ALS dataset depends on the point density and the survey area to be covered. With the same area but a larger point density for ALS (ALS: point density of 14.3 Pt/m^2; ADP: ground sampling distance of 0.5 m) the costs are likely to be much higher for the ALS campaign.

The point density in turn has a large influence in rough areas, such as steep, unglaciated terrain or crevasses. Crevasses in photogrammetrical DEMs are flattened out, whereas the laser beams from ALS may penetrate deeper into the crevasses resulting in more accurate elevation values (Rolstad et al., 2009). This fact is well observable in the ADP and ALS hillshades (Section 9.1).

Areas with low contrast and shadow

Regions with large elevation differences are found in snow covered areas with poor contrast, such as the accumulation zone of Findelengletscher. Similar findings concerning the performance of ADP over areas with low contrast were already reported (e.g. Baltsavias et al., 2001; Haala et al., 2010; Koblet et al., 2010; Rolstad et al., 2009; Würländer et al., 2004).

The influence of shadow on elevation data accuracy is extensively discussed in Subsection 6.2.3. Elevation data accuracy in areas of cast shadow still seems to be a weak point of ADP.

Orthophoto

The orthophoto generated from ADP proved to be very useful for the updating of the glacier outlines in the upper Mattertal and the definition of the potential solar radiation classes for the uncertainty assessment.

The findings from this thesis agree well with the argumentation of Schenk (1999), who generally stated that for some applications the two methods compete, whereas other applications are clear-cut cases for one of the two methods.

6.5.2 Recommendations for the use of swissALTI^{3D} in glaciological research

From the comparison of the elevation differences between the simultaneously derived ADP_2010 and ALS_2010 DEMs, the suitability of ADP for applications in glaciology is evaluated. The general conclusions about the performance of ADP, or namely of the ADS80 SH82 sensor in high-alpine environments, are transferred to swissALTI^{3D} for areas above 2000 m.a.s.l..

Assigning these findings from ADP_2010 to swissALTI^{3D} should be done with caution, because the ADP_2010 DEM was not manually updated after the generation, whereas the available version of swissALTI^{3D} was manually updated. For a detailed description of the performed corrections and updates in swissALTI^{3D} see Swisstopo (2013).

Overall, the qualitative and especially quantitative analyses have shown that swissALTI^{3D} proves to be a suitable DEM for applications in glaciology.

The experiences gained in this thesis from working with swissALTI^{3D} are subsequently listed in form of recommendations. For glaciological studies with similar objectives, the consideration of these recommendations is advisable.

- swissALTI^{3D} has the standard geodetic reference system CH1903+ LV95 LN02. A coordinate transformation of another DEM to work with uniform geodetic reference frames might be required.
- swissALTI^{3D} has a raster cell size of 2 m. A resampling to get uniform raster cell sizes for DEM differencing is highly recommended.
- Possible uncertainties introduced from homogenizing DEMs should be quantified in an uncertainty assessment.
- Although areas with insufficient elevation data quality are manually updated, regions with areas of snow and shadow still tend to have lower elevation data accuracies in swissALTI^{3D}. A thorough uncertainty assessment is advisable for these regions.
- swissALTI^{3D} is totally updated in a cycle of 6 years. Certain regions can therefore consist of data from two or more measurement years.
- swissALTI^{3D}_2009 was not recorded at the end of the hydrological year but on September 7, 2009 for the upper Mattertal. This has to be taken into account for glaciological change interpretations.

6.5.3 Recommendations for swisstopo

As shown in this thesis, swissALTI^{3D} is very well suited for applications in glaciology. Nevertheless, some shortcomings of swissALTI^{3D} and the offered services by swisstopo are recognized. The clarification of these deficiencies would allow a more comprehensive interpretation of the glaciological changes calculated in this thesis.

Recording of the elevation data

It is not totally clear, which ALS and ADP devices were used to measure the elevation data for swissALTI^{3D} and if these remained the same for all years (ALS: 2001 to 2008) and ADP (2008 to 2011). This would imply, that adjacent regions could have varying elevation data accuracies because of different used devices.

The documentation of swissALTI^{3D} informs about the year of measurement but does not provide any information about the recording date, which is of great importance for glaciological change interpretation.

Processing of the elevation data and DEMs

The importance of a standardized reference system becomes obvious from the performed coordinate transformations in this thesis. The "ReframeReprojector" from the swisstopo REFRAME plug-in for FME uses non-linear transformations to change the planimetric and altimetric reference frames. In this thesis, combined planimetric and altimetric (ALS DEMs) and only altimetric (swissALTI^{3D}) reference frame changes are applied. Thereby, the operations in the "ReframeReprojector" resemble a black box. It is not clear what effects the reference frame changes have on elevation data accuracy. A thorough documentation of the effects could help to better understand the processes when transforming reference frames.

The accuracies of the manual updates are documented in Swisstopo (2014b). Nevertheless, the question arises whether there are still considerable suspect areas with relatively low degrees of confidence in swissALTI^{3D}.

Documentation of the accuracies

Currently, the accuracies of swissALTI^{3D} are documented according to the acquisition methods (a) laser points, (b) stereo correlation and (c) manual updates (Subsection 3.3.2).

Thereby, the accuracies of the stereo correlation show a relatively large range, which probably results from varying performances over different ground covers. If possible, it would make sense to document the accuracies of each acquisition technique in dependency on the ground cover classes. This could be achieved by using reference elevation data from e.g ALS. According to Schenk (1999), a combination of ADP and ALS would lead to more accurate elevation data products with no increase of data acquisition time. A user could then benefit from more detailed accuracy specifications. For glaciological applications, respective ground cover classes would be the ones investigated in this thesis (e.g. snow, ice and steep, unglaciated terrain).

Chapter 7

Conclusions

The glaciological changes calculated with the geodetic observation method indicate that the glaciers in the upper Mattetal retreated over the period from 2005 to 2009. The total glacier area decreased by about -4'355'504 m^2, which means an average area loss of -5.56% per glacier. The average thickness change of all glaciers is -3.17 $\pm$0.037 m and the total volume change is -351.09 $\pm$0.144 mio m^3.

In contrast with a study, that documents the glaciological changes for Findelen- and Adlergletscher from airborne laser scanning (ALS) (Joerg et al., 2012), the glaciological changes from the photogrammetrically derived swissALTI^{3D} show good agreement. This is however only the case when vertical, systematic uncertainties are considered. For the comparison with a second study, that calculated the volume change of Findelengletscher from 1995 to 1999 (Farinotti et al., 2009), the average thickness changes per year are derived. The results of Farinotti et al. (2009) conform well to the ones from swissALTI^{3D} and ALS. Deviations are mainly caused by varying glacier outlines.

By means of the co-registration, horizontal shifts between two DEMs can be detected and iteratively reduced. The remaining overall elevation bias after the co-registration is taken as the systematic uncertainty for glaciological change calculations. In this thesis it is shown, that the glaciological changes from horizontally shifted DEMs are considerably larger than the glaciological changes from co-registered DEMs. This means a difference of 7% for the average thickness changes and 2% for the volume changes. For the glaciological change calculations in the upper Mattertal from 2005 to 2009, the systematic uncertainty has to be considered. Not accounting for systematic uncertainties would lead to an overestimation of the glaciological changes.

The co-registration is identified as a useful method to quantify horizontal and vertical shifts between DEMs. Nevertheless, the co-registration is only an analytical solution that approximates optimum values by repeated iterations. It has limitations, which can affect the efficiency of the horizontal and vertical shift detection.

The performance of airborne digital photogrammetry (ADP) in regions of shadow and snow is validated by using reference data from simultaneous ALS measurements over Findelengletscher. Based on the glacier signal to noise analysis, it is shown that over glaciated terrain the elevation differences between ADP and ALS are larger than over unglaciated terrain. The same trend is observed for areas under shadow, which show larger deviations between ADP and ALS for different ground covers than non-

shady areas. These findings agree well with other studies about this topic.

For the assessment of the stochastic uncertainties resulting from the limitations of ADP (shadow and snow), two widely used methods are applied. These estimate the standard error from unglaciated and glaciated terrain. Motivated by the findings, a third method to estimate stochastic uncertainties is presented in this thesis. That sophisticated method considers the influence of shadow on elevation data accuracy over glaciated terrain and shows therefore the largest stochastic uncertainties.

The assessment shows that systematic uncertainties have considerable influence on resulting glaciological changes and are an order of magnitude larger than the stochastic uncertainties.

The known advantages and disadvantages of ADP and ALS are confirmed in this thesis. Although the limitations of ADP lead to a decrease in elevation data accuracy, the glaciological change calculations from swissALTI^{3D} show promising results and good accordance with the ones from ALS.

Therefore it can be concluded that swissALTI^{3D} with its high resolution and continuous updates is very well suited for applications in glaciology.

Lessons learned

- Glaciers in the upper Mattertal retreated from 2005 to 2009.
- The co-registration is a useful method to detect horizontal shifts between DEMs and to quantify systematic uncertainties.
- Airborne digital photogrammetry still shows limitations concerning the performance in areas of shadow and snow.
- swissALTI^{3D} with its high resolution and the update cycle of six years is very well suitable for applications in glaciology.

Chapter 8

Outlook

Two crucial open questions can be identified from the findings of the present master's thesis. Their clarification in the near future could lead to more accurate elevation data products.

On the one hand, it is open how the acquisition techniques are going to evolve. The possibility to combine airborne digital photogrammetry and airborne laser scanning on the same platform yields a large potential and remains an object of research. Theoretically, data from ADP could be used for the generation of orthophotos and optical tasks such as interpretation or visualization, whereas ALS would provide elevation data with a high resolution and accuracy. Thereby, the optimum acquisition method could be used for every specific task. Additionally, reference data from simultaneous measurements would be available for every DEM. This proved to be very useful in this thesis.

On the other hand, efficient methods for the uncertainty assessment need to be developed. Although the benefit from the uncertainty assessment is considerable, it is not applied in all glaciological studies since it is time-consuming. Therefore, the question arises, whether the effort could be reduced by automating the uncertainty assessment in a geographical information system. At the same time, there are questions regarding the reliability of the outcomes from automated versus man-made uncertainty assessment.

These identified issues are important and need to be investigated in further studies.

Chapter 9

Appendix

9.1 Hillshades of the digital elevation models

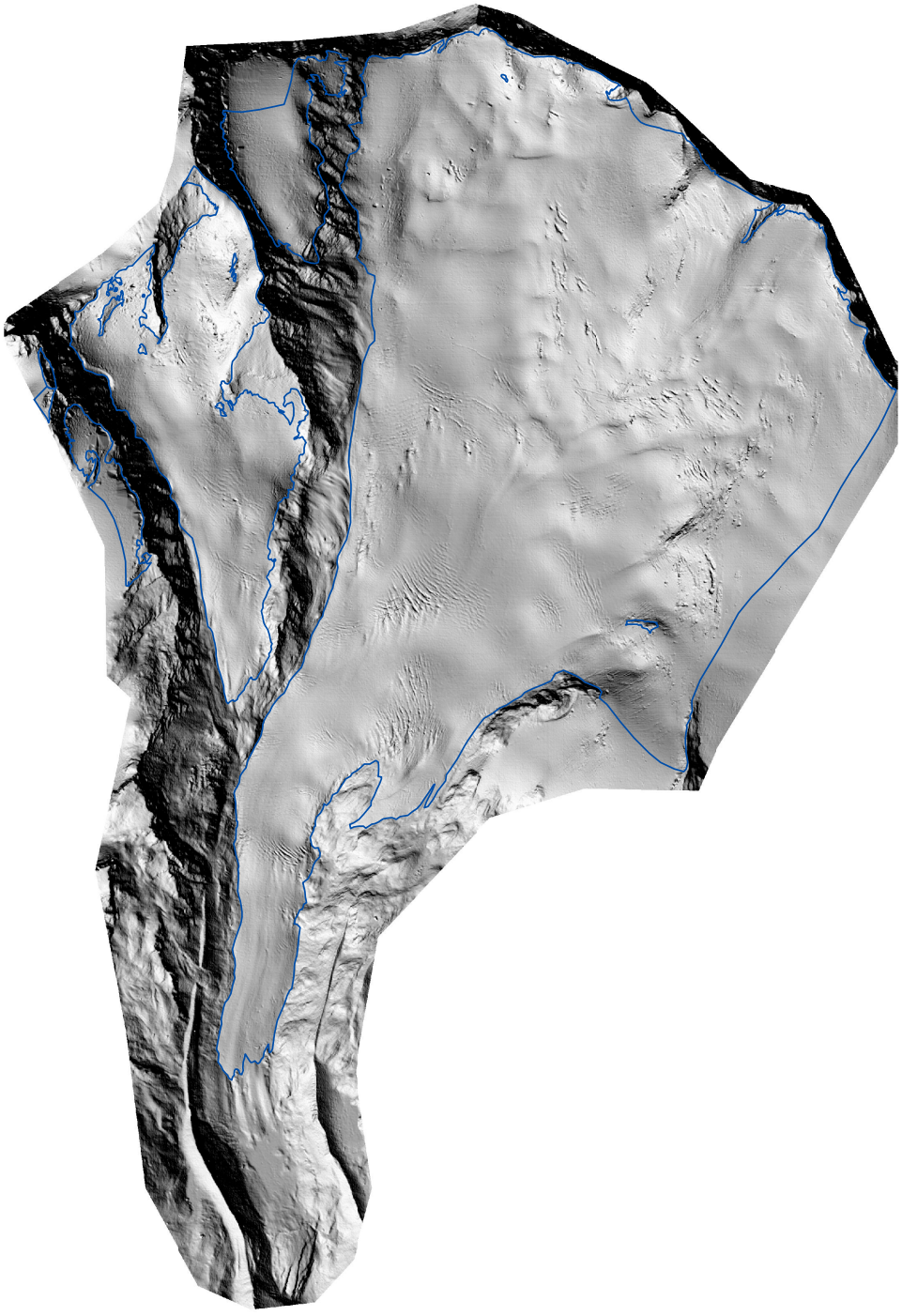

Figure 9.1: Hillshade of the ADP_2010 DEM.

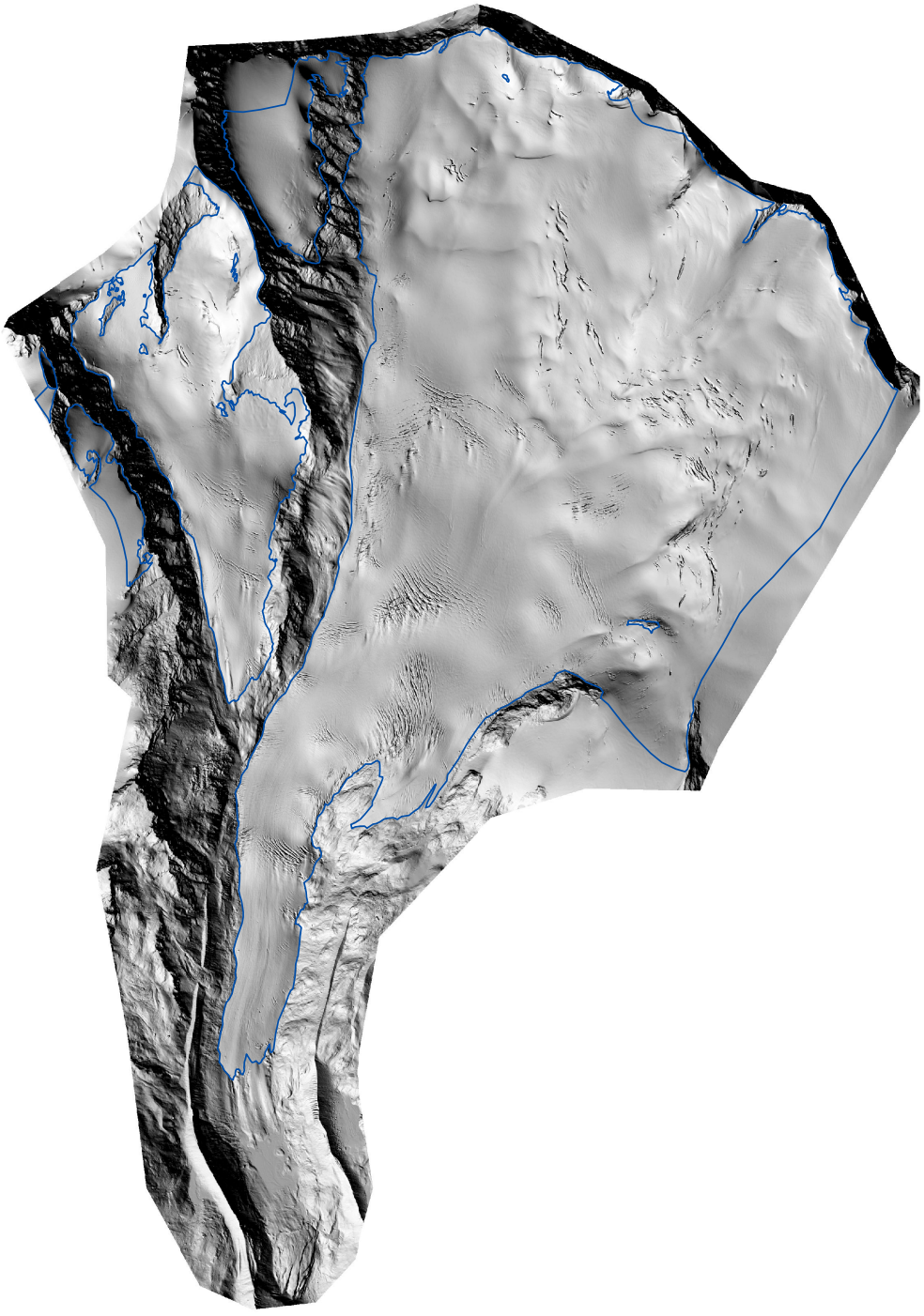

Figure 9.2: Hillshade of the ALS_2010 DEM.

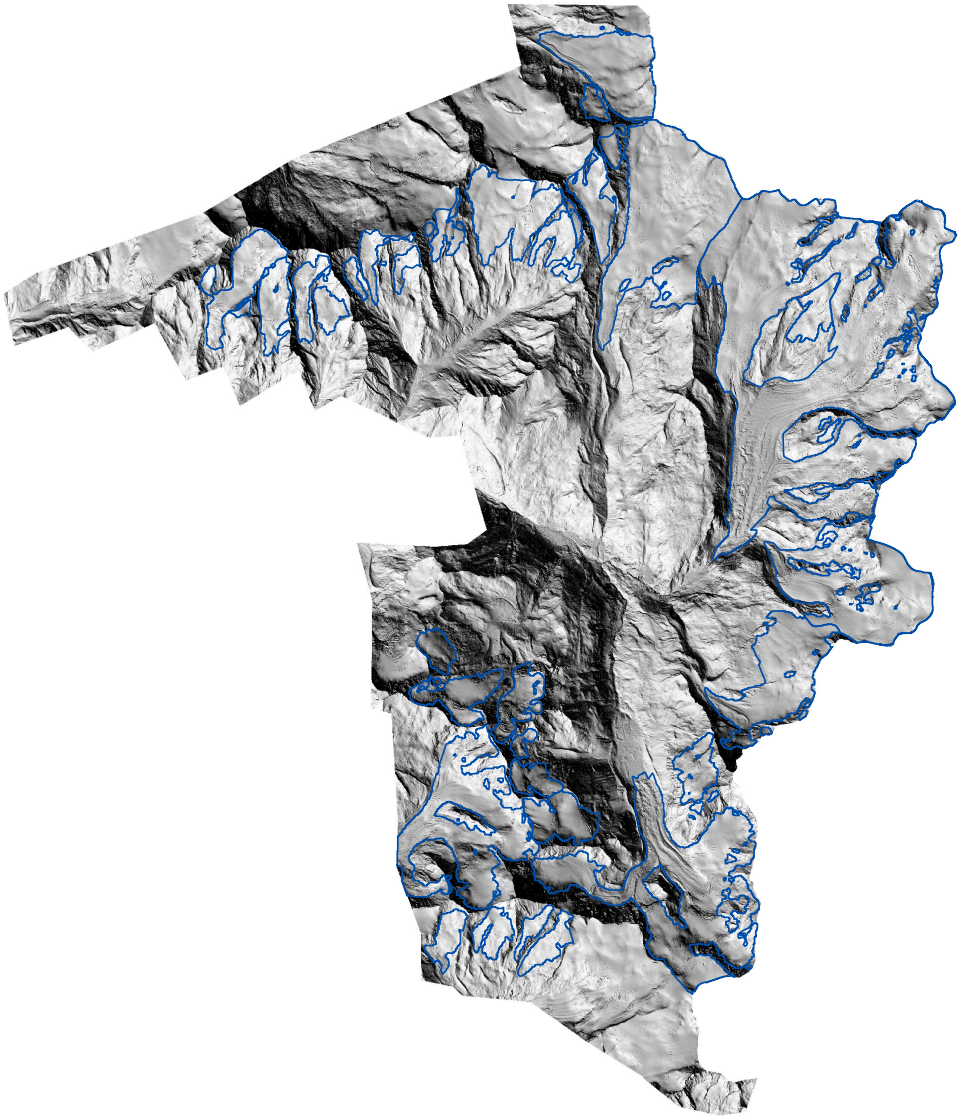

Figure 9.3: Hillshade of the swissALTI^{3D}_2009 DEM.

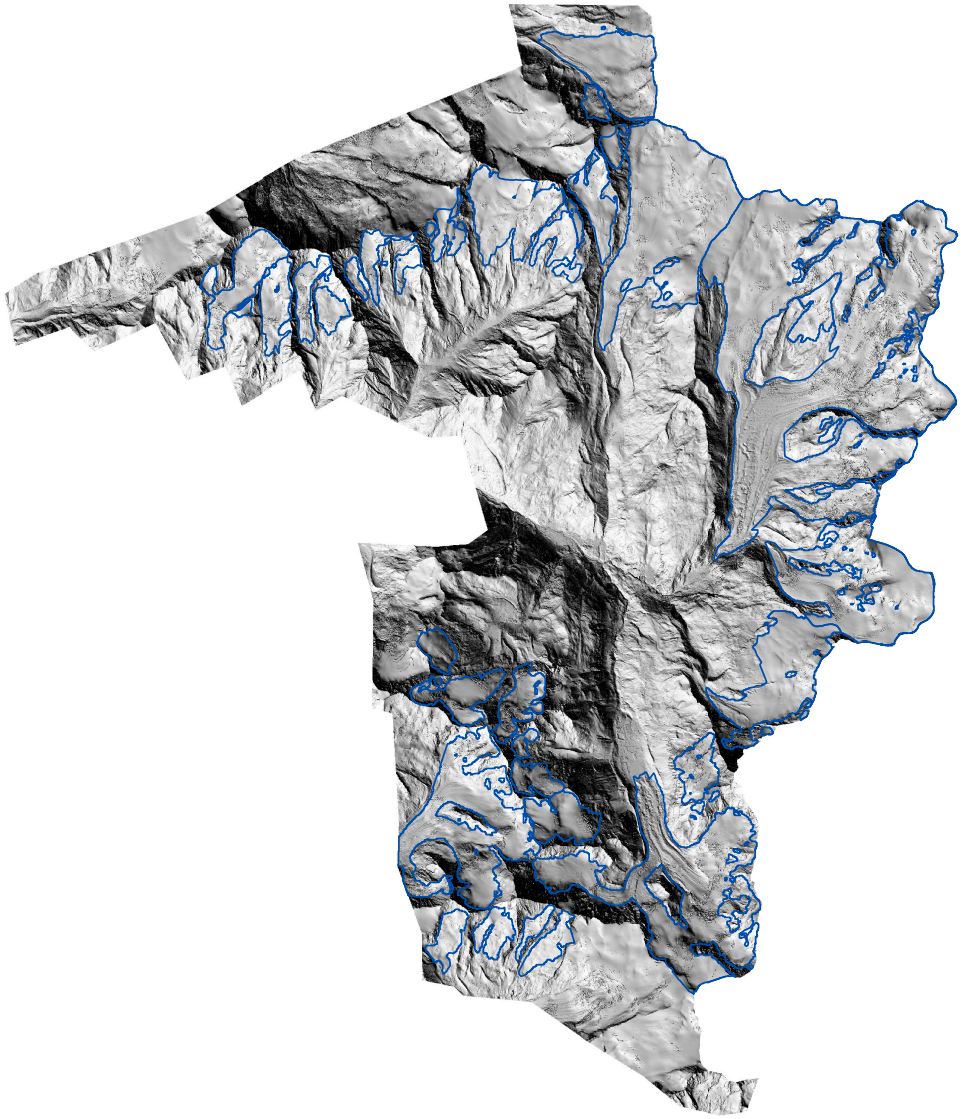

Figure 9.4: Hillshade of the ALS_2005 DEM.

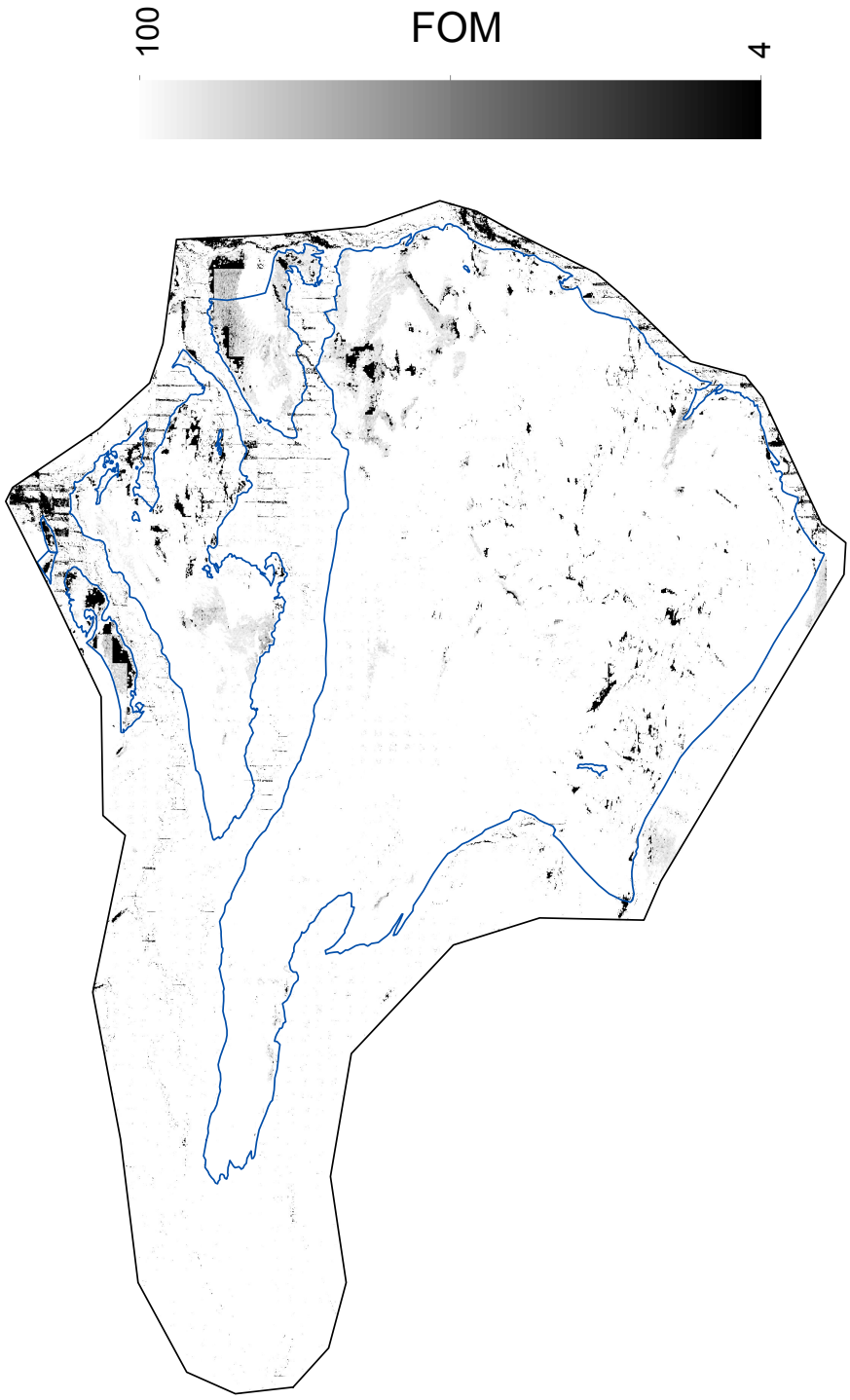

Figure 9.5: Figure of Merit map for the ADP_2010 DEM.

9.2 Uncertainties from slope classes

The elevation differences (ADP_2010 minus ALS_2010) are analyzed according to different slope classes in the terrain. For each slope class, elevation differences are extracted for Findelen- and Adlergletscher, unglaciated terrain and the whole study site (perimeter) and shown in a boxplot (Bühler et al., 2012). Additionally to their approach, the number of raster cells for each slope class is plotted below the boxplot. This is to normalize the effect of a decreasing number of raster cells with increasing slope.

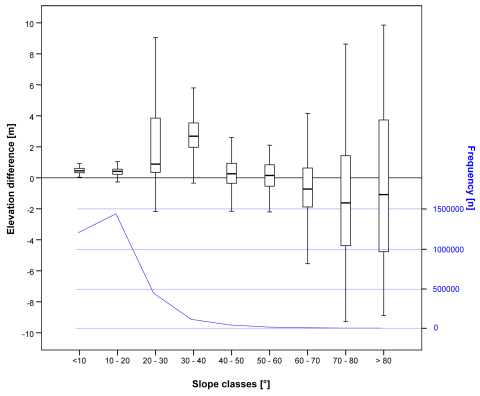

(a) Slope Findelen

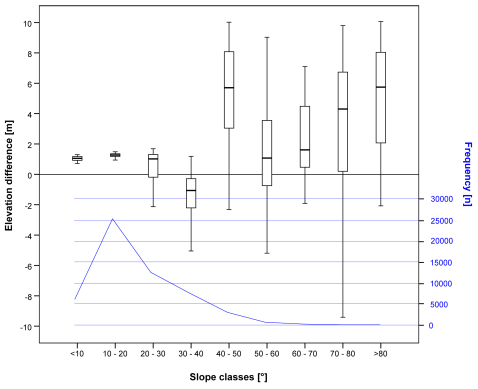

(b) Slope Adler

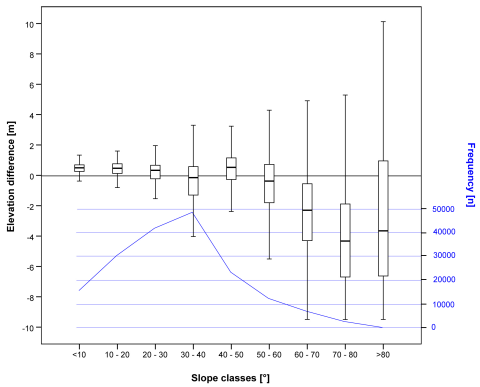

(c) Slope Unglaciated

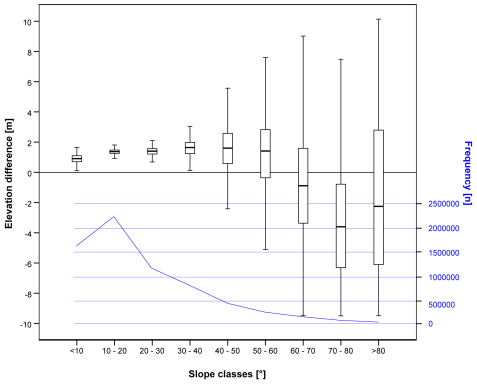

(d) Slope Perimeter

Figure 9.6: Boxplot of the elevation differences from ADP_2010 minus ALS_2010 for different slope classes.

Bibliography

Albertz, J., 2009. Einführung in die Fernerkundung: Grundlagen der Interpretation von Luft-und Satellitenbildern. Wissenschaftliche Buchgesellschaft Darmstadt, Darmstadt.

BAE Systems, 2013. SOCET SET Users Manual - Figures Of Merit. Tech. rep.

Baltsavias, E., 1999. A comparison between photogrammetry and laser scanning. ISPRS Journal of Photogrammetry and Remote Sensing 54 (2), 83–94.

Baltsavias, E. P., Favey, E., Bauder, A., Bosch, H., Pateraki, M., 2001. Digital surface modelling by airborne laser scanning and digital photogrammetry for glacier monitoring. The Photogrammetric Record 17 (98), 243–273.

Bolch, T., Pieczonka, T., Benn, D. I., Apr. 2011. Multi-decadal mass loss of glaciers in the Everest area (Nepal Himalaya) derived from stereo imagery. The Cryosphere 5 (2), 349–358.

Bovet, S., 2013. SwissALTI3D. Geomatik 9.

Bühler, Y., Marty, M., Ginzler, C., Oct. 2012. High Resolution DEM Generation in High-Alpine Terrain Using Airborne Remote Sensing Techniques. Transactions in GIS 16 (5), 635–647.

Burrough, P. A., McDonnell, R., 2005. Principles of Geographical Information Systems. Oxford University Press, Oxford.

Cogley, J., Hock, R., Rasmussen, L., Arendt, A., Bauder, A., Braithwaite, R., Jansson, P., Kaser, G., Möller, M., Nicholson, L., Zemp, M., 2011. Glossary of glacier mass balance and related terms. IHP-VII technical documents in Hydrology 86.

Cook, A. J., Murray, T., Luckman, A., Vaughan, D. E., Barrand, N. E., 2012. A new 100-m Digital Elevation Model of the Antarctic Peninsula derived from ASTER Global DEM: methods and accuracy assessment. Earth System Science Data 4 (1), 129–142.

Cukrov, G., José, S., 2013. Using Stereo Photogrammetry to Create Digital Elevation Models of Planetary Surfaces. 2013 NCUR.

Deems, J. S., Painter, T. H., 2006. Lidar measurement of snow depth: accuracy and error sources. In proceedings of the international snow science workshop, 1–6.

ESRI, 2014a. Area Solar Radiation. (Retrieved March 24, 2014).
URL http://resources.arcgis.com/de/help/main/10.1/index.html#//009z000000t5000000

ESRI, 2014b. Calculate Areas. (Retrieved March 24, 2014).
URL http://resources.arcgis.com/en/help/main/10.1/index.html#//005p0000003q000000

ESRI, 2014c. Cell size of raster data. (Retrieved March 24, 2014).
URL http://help.arcgis.com/en/arcgisdesktop/10.0/help/index.html#//009t00000004000000

ESRI, 2014d. Extract by Mask. (Retrieved March 24, 2014).
URL http://help.arcgis.com/en/arcgisdesktop/10.0/help../index.html#//009z0000002n000000.htm

ESRI, 2014e. Hillshade. (Retrieved March 24, 2014).
URL http://resources.arcgis.com/en/help/main/10.1/index.html#//00q900000036000000

ESRI, 2014f. Point to Raster. (Retrieved March 24, 2014).
URL http://resources.arcgis.com/en/help/main/10.1/index.html#//00120000002z000000

ESRI, 2014g. Raster Calculator. (Retrieved March 24, 2014).
URL http://resources.arcgis.com/en/help/main/10.1/index.html#//009z000000z7000000

ESRI, 2014h. Resample. (Retrieved March 24, 2014).
URL http://help.arcgis.com/en/arcgisdesktop/10.0/help/index.html#//00170000009t000000

ESRI, 2014i. Snap Raster. (Retrieved March 24, 2014).
URL http://help.arcgis.com/en/arcgisdesktop/10.0/help/index.html#//001w0000000m000000

Farinotti, D., Huss, M., Bauder, A., Funk, M., 2009. An estimate of the glacier ice volume in the Swiss Alps. Global and Planetary Change 68 (3), 225–231.

Farinotti, D., Usselmann, S., Huss, M., Bauder, A., Funk, M., Jun. 2012. Runoff evolution in the Swiss Alps: projections for selected high-alpine catchments based on ENSEMBLES scenarios. Hydrological Processes 26 (13), 1909–1924.

Favey, E., Geiger, A., Gudmundsson, G. H., Wehr, A., 1999. Evaluating the Potential of an Airborne Laserscanning System for Measuring Volume Changes of Glaciers. Geografiska Annaler: Series A, Physical Geography 81 (4), 555–561.

Fisher, P. F., Tate, N. J., Aug. 2006. Causes and consequences of error in digital elevation models. Progress in Physical Geography 30 (4), 467–489.

Geist, T., Heller, A., Stötter, J., 2004. Digitale Geländemodelle aus Airborne Laserscanningdaten - eine qualitative hochwertige Grundlage für glaziologische Fragestellungen. Angewandte Geoinformatik, 163–171.

Geist, T., Lutz, E., Stötter, J., 2003. Airborne laser scanning technology and its potential for applications in glaciology. International Archives of Photogrammetry, Remote Sensing and Spatial Information Science 34 (3), 101–106.

Giles, P., 2001. Remote sensing and cast shadows in mountainous terrain. Photogrammetric engineering and remote sensing 67 (7), 833–840.

Gwinner, K., Hauber, E., Jaumann, R., Neukum, G., 2000. High-resolution, digital photogrammetric mapping: A tool for Earth science. Eos, Transactions American Geophysical Union 81 (44), 513–520.

Haala, N., Hastedt, H., Wolf, K., Ressl, C., Baltrusch, S., 2010. Digital photogrammetric camera evaluation generation of digital elevation models. Photogrammetrie-Fernerkundung-Geoinformation (2), 99–115.

Haeberli, W., Burn, C. R., Sidle, R. C., 2002. Natural hazards in forests: glacier and permafrost effects as related to climate change. Environmental changes and geomorphic hazards in forests, 167–202.

Haug, T., Rolstad, C., Elvehoy, H., Jackson, M., Maalen-Johansen, I., Mar. 2009. Geodetic mass balance of the western Svartisen ice cap, Norway, in the periods 1968-1985 and 1985-2002. Annals of Glaciology 50 (50), 119–125.

Höfle, B., Geist, T., Rutzinger, M., Pfeifer, N., 2007. Glacier surface segmentation using airborne laser scanning point cloud and intensity data. International Archives of Photogrammetry, Remote Sensing and Spatial Information Sciences 36(Part 3), W52.

Huss, M., Hock, R., Bauder, A., Funk, M., May 2010. 100-year mass changes in the Swiss Alps linked to the Atlantic Multidecadal Oscillation. Geophysical Research Letters 37 (10).

IPCC, 2007. Climate Change 2007: impacts, adaptation and vulnerability: contribution of Working Group II to the fourth assessment report of the Intergovernmental Panel on Climate Change, 4th Edition. Cambridge University Press, Cambridge.

Joerg, P. C., Morsdorf, F., Zemp, M., 2012. Uncertainty assessment of multitemporal airborne laser scanning data: A case study on an Alpine glacier. Remote Sensing of Environment 127, 118–129.

Joerg, P. C., Zemp, M., Feb. 2014. Evaluating Volumetric Glacier Change Methods Using Airborne Laser Scanning Data. Geografiska Annaler: Series A, Physical Geography.

Kääb, A., 2005. Remote sensing of mountain glaciers and permafrost creep. Ph.D. thesis, Universität Zürich.

Karimi, N., Farokhnia, A., Shishangosht, S., Elmi, M., Eftekhari, M., Ghalkhani, H., 2012. Elevation changes of Alamkouh glacier in Iran since 1955, based on remote sensing data. International Journal of Applied Earth Observation and Geoinformation 19, 45–58.

Kennett, M., Eiken, T., 1997. Airborne measurement of glacier surface elevation by scanning laser altimeter. Annals of Glaciology 24, 293–296.

Knoll, C., Kerschner, H., Feb. 2010. A glacier inventory for South Tyrol, Italy, based on airborne laser-scanner data. Annals of Glaciology 50 (53), 46–52.

Koblet, T., Gärtner-Roer, I., Zemp, M., Jansson, P., Thee, P., Haeberli, W., Holmlund, P., Sep. 2010. Reanalysis of multi-temporal aerial images of Storglaciären, Sweden (1959 - 1999) - Part 1: Determination of length, area, and volume changes. The Cryosphere 4 (3), 333–343.

Kraus, K., 2004. Photogrammetrie. Band 1. Geometrische Informationen aus Photographien und Laserscanneraufnahmen, 7th Edition. Walter de Gruyter, Berlin, New York.

Lenhart, D., Kager, H., Eder, K., Hinz, S., Stilla, U., 2006. Hochgenaue Generierung des DGM vom vergletscherten Hochgebirge - Potential von Airborne Laserscanning, 36th Edition.

Lilesand, T. M., Kiefer, R. W., Chipman, J. W., 2007. Remote Sensing and Image Interpretation, 6th Edition. John Wiley & Sons Ltd.

Lindenmann, J., 2012. Untersuchung dekadischer Gletschervolumenänderungen im Langtang Himalaya, Nepal, basierend auf DHM-Analysen verschiedener Datensätze inklusive statistischer Unsicherheitsanalyse. MSc. thesis, Universität Zürich.

Machguth, H., Paul, F., Hoelzle, M., Haeberli, W., 2006. Distributed glacier mass-balance modelling as an important component of modern multi-level glacier monitoring. Annals of Glaciology 43, 335–343.

Maisch, M., Wipf, A., Denneler, B., Battaglia, J., Benz, C., 2000. Die Gletscher der Schweizer Alpen: Gletscherhochstand 1850 - Aktuelle Vergletscherung - Gletscherschwund-Szenarien 21. Jahrhundert, 2nd Edition. vdf Hochschulverlag AG an der ETH Zürich.

Microsoft, 2014. Define and solve a problem by using Solver. (Retrieved March 24, 2014).
URL `http://office.microsoft.com/en-us/excel-help/define-and-solve-a-problem-by-using-solver-HP010072691.aspx`

Nuth, C., Kääb, A., 2011. Co-registration and bias corrections of satellite elevation data sets for quantifying glacier thickness change. The Cryosphere 5 (1), 271–290.

Oestrem, G., Brugmann, M., 1991. Glacier mass-balance measurements: A manual for field and office work. Oslo: NVE.

Paul, F., Frey, H., Le Bris, R., 2011. A new glacier inventory for the European Alps from Landsat TM scenes of 2003: challenges and results. Annals of Glaciology 52 (59), 144–152.

Rees, W. G., 2005. Remote sensing of snow and ice. CRC Press.

Rolstad, C., Haug, T., Denby, B., 2009. Spatially integrated geodetic glacier mass balance and its uncertainty based on geostatistical analysis: application to the western Svartisen ice cap, Norway. Journal of Glaciology 55 (192), 666–680.

Sandau, R., 2005. Digitale Luftbildkamera, Einführung und Grundlagen. Wichmann Verlag, Heidelberg.

Schenk, T., 1999. Photogrammetry and laser altimetry. International archives of photogrammetry and remote sensing 32(Part 3), W14.

Swisstopo, 2006. Neue Koordinaten für die Schweiz. Bern: Federal Office of Topography swisstopo.

Swisstopo, 2012. REFRAME plug-in for FME. Bern: Federal Office of Topography swisstopo.

Swisstopo, 2013. swissALTI3D & die Gebiete über 2000 m.ü.M. Bern: Federal Office of Topography swisstopo.

Swisstopo, 2014a. Geodesy. (Retrieved March 24, 2014).
URL `http://www.swisstopo.admin.ch/internet/swisstopo/en/home/topics/survey/sys/refsys/switzerland.html`

Swisstopo, 2014b. SwissALTI3D. (Retrieved March 24, 2014).
URL `http://www.swisstopo.admin.ch/internet/swisstopo/en/home/products/height/swissALTI3D.html`

Thiel, K. H., Wehr, A., 2004. Performance capabilities of laser scanners - an overview and measurement principle analysis. Proceedings of the ISPRS working group VIII/2, Laser-Scanners for Forest and Landscape Assessment XXXVI Part8 (W2), 14–18.

UNEP, 2007. Glaciers and ice caps. Part I: Global overview and outlook. Part II: Glacier changes around the world. Global outlook for ice and snow. United Nations Environment Programme, Nairobi.

Vosselman, G., Maas, H.-G., 2010. Airborne and Terrestrial Laser Scanning. Whittles Publishing, Caithes, Great Britain.

Wehr, A., Lohr, U., 1999. Airborne laser scanning - an introduction and overview. ISPRS Journal of Photogrammetry and Remote Sensing 54 (2), 68–82.

WGMS, 2008. Global Glacier Changes: Facts and Figures. UNEP; World Glacier Monitoring Service, Zürich, Switzerland.

Würländer, R., Eder, K., Geist, T., 2004. High quality DEMs for glacier monitoring - image matching versus laser scanning. International Archives of Photogrammetry, Remote Sensing and Spatial Information Sciences 35 (B7), 753–758.

Zemp, M., Thibert, E., Huss, M., Stumm, D., Rolstad Denby, C., Nuth, C., Nussbaumer, S. U., Moholdt, G., Mercer, A., Mayer, C., Joerg, P. C., Jansson, P., Hynek, B., Fischer, A., Escher-Vetter, H., Elvehø y, H., Andreassen, L. M., Aug. 2013. Reanalysing glacier mass balance measurement series. The Cryosphere 7 (4), 1227–1245.

Personal declaration

I hereby declare that the submitted thesis is the result of my own, independent, work. All external sources are explicitly acknowledged in the thesis.

Zurich, April 30, 2014

Thierry Bossard